eNeuro

Research Article: New Research

Development

Peripheral Nerve Single-Cell Analysis Identifies Mesenchymal Ligands that Promote Axonal Growth

Jeremy S. Toma,[1] Konstantina Karamboulas,[1,a] Matthew J. Carr,[1,2,a] Adelaida Kolaj,[1,3] Scott A. Yuzwa,[1] Neemat Mahmud,[1,3] Mekayla A. Storer,[1] David R. Kaplan,[1,2,4] and Freda D. Miller[1,2,3,4]

https://doi.org/10.1523/ENEURO.0066-20.2020

[1]Program in Neurosciences and Mental Health, Hospital for Sick Children, 555 University Avenue, Toronto, Ontario M5G 1X8, Canada, [2]Institute of Medical Sciences University of Toronto, Toronto, Ontario M5G 1A8, Canada, [3]Department of Physiology, University of Toronto, Toronto, Ontario M5G 1A8, Canada, and [4]Department of Molecular Genetics, University of Toronto, Toronto, Ontario M5G 1A8, Canada

Abstract

Peripheral nerves provide a supportive growth environment for developing and regenerating axons and are essential for maintenance and repair of many non-neural tissues. This capacity has largely been ascribed to paracrine factors secreted by nerve-resident Schwann cells. Here, we used single-cell transcriptional profiling to identify ligands made by different injured rodent nerve cell types and have combined this with cell-surface mass spectrometry to computationally model potential paracrine interactions with peripheral neurons. These analyses show that peripheral nerves make many ligands predicted to act on peripheral and CNS neurons, including known and previously uncharacterized ligands. While Schwann cells are an important ligand source within injured nerves, more than half of the predicted ligands are made by nerve-resident mesenchymal cells, including the endoneurial cells most closely associated with peripheral axons. At least three of these mesenchymal ligands, ANGPT1, CCL11, and VEGFC, promote growth when locally applied on sympathetic axons. These data therefore identify an unexpected paracrine role for nerve mesenchymal cells and suggest that multiple cell types contribute to creating a highly pro-growth environment for peripheral axons.

Key words: growth factor; nerve; paracrine interactions; regeneration; scRNA-seq; peripheral neurons; neuronal growth; Schwann cell; mesenchymal cell

Significance Statement

This work expands our understanding of the cellular sources of ligands in the injured peripheral nerve that are potentially important for promoting axon growth. Here, we used single-cell RNA sequencing (scRNA-seq) to reveal that Schwann cells and, surprisingly, nerve mesenchymal cells are primary sources of ligands in the injured nerve. We then combined injured nerve scRNA-seq data with proteomic and transcriptomic data from sensory and sympathetic neurons and used a systems-biology/modeling approach to predict novel mesenchymal cell-derived factors that may promote peripheral axon growth. We tested some of these predictions and found three factors, ANGPT1, CCL11, and VEGFC, that promoted outgrowth of cultured sympathetic axons, supporting a potential role for mesenchymal-derived factors in axon growth.

Introduction

Following injury, mammalian peripheral neurons can regenerate and reinnervate their target tissues. Their ability to do so is thought to be a consequence of a peripheral nerve environment that is highly supportive of axonal growth. Support for this idea comes from classic studies with CNS neurons, which normally fail to regenerate following brain or spinal cord injury but will regrow their axons when peripheral

Received February 24, 2020; accepted April 23, 2020; First published April 29, 2020.

The authors declare no competing financial interests.

Author contributions: J.S.T., D.R.K., and F.D.M. designed research; J.S.T., M.J.C., A.K., S.A.Y., and N.M. performed research; J.S.T., K.K., N.M., M.A.S., and F.D.M. analyzed data; J.S.T., K.K., D.R.K., and F.D.M. wrote the paper.

nerve segments are transplanted into the damaged region (David and Aguayo, 1981; for review, see Benowitz et al., 2017). Intriguingly, peripheral nerves are also important for maintenance, repair and regeneration of the non-neural tissues that they innervate. For example, normal peripheral innervation is essential for mammalian hair follicle and hematopoietic stem cells (Brownell et al., 2011; Yamazaki et al., 2011), for cardiac and dermal repair (Mahmoud et al., 2015; Johnston et al., 2013, 2016) and for amphibian limb (for review, see Kumar and Brockes, 2012) and murine digit tip regeneration (Johnston et al., 2016).

The supportive peripheral nerve environment has largely been ascribed to growth factors made by nerve cells (for review, see Terenghi, 1999; Fledrich et al., 2019). These nerve-derived ligands have been particularly well studied with regard to axonal development and regeneration (Chen et al., 2007; Fledrich et al., 2019), although several studies have shown that they are also important for limb and digit tip regeneration (Kumar et al., 2007; Johnston et al., 2016). These growth factors are thought to be Schwann cell derived, since transplantation of Schwann cells alone is enough to promote CNS axon regeneration (for review, see Bunge, 2016) and murine digit tip regeneration (Johnston et al., 2016). In addition to growth factors, the peripheral nerve provides an extracellular matrix environment that is highly conducive to axonal growth, particularly by contrast to the CNS, where known axon growth inhibitors prevail (Chen et al., 2007; Benowitz et al., 2017). This supportive substrate is also thought to derive in part from Schwann cells, which generate a basal lamina and synthesize ECM proteins and cell adhesion molecules (Muir, 2010; Gardiner, 2011).

These studies all indicate that Schwann cells play an important role in establishing a nerve environment that is supportive of axonal growth. However, the nerve is a structurally-complex tissue containing many different cell types, including vasculature-associated cells, immune cells such as tissue-resident macrophages, and mesenchymal cells of both mesodermal and neural crest origin. In this regard, one recent study identified four transcriptionally and spatially-distinct populations of *Pdgfra*-positive mesenchymal cells within the injured peripheral nerve, including endoneurial mesenchymal cells that are tightly associated with Schwann cells and axons (Carr et al., 2019). These nerve mesenchymal cells were shown to directly contribute to the repair and regeneration of mesenchymal target tissues including the digit tip, bone, and dermis. Nerve mesenchymal cells have also been shown to play an essential role in forming bridges over gaps in injured nerves (for review, see Cattin and Lloyd, 2016). Together, these findings raise the possibility that mesenchymal cells might also be important for axonal growth in the peripheral nerve.

Here, we provide support for this concept, using an unbiased systems biology approach to define the sciatic nerve ligand environment. We show, using single-cell profiling, that under both homeostatic and injury conditions, mesenchymal cells and Schwann cells are the predominant sources of peripheral nerve ligands, including known and uncharacterized ligands, and that there is induction of ligand expression in both these cell types following injury. Moreover, using mass spectrometry, transcriptional profiling, and computational modeling, we show that peripheral neurons and CNS retinal ganglion neurons express receptors for many of these ligands. Finally, we validate three of these ligands, ANGPT1, CCL11, and VEGFC, as being synthesized and secreted by *Pdgfra*-positive nerve mesenchymal cells and show that they can promote growth when applied to axons of peripheral sympathetic neurons. Thus, our data support a model where nerve mesenchymal cells and Schwann cells collaborate to establish a generally supportive growth environment in the peripheral nerve.

Materials and Methods

Animals

All animal procedures were performed in accordance with Canadian Council on Animal Care regulations as approved by the Hospital for Sick Children animal care committee. Sprague Dawley rats (purchased from Charles River) used in this study ranged from embryonic day (E)15 to young adult (six weeks old) and CD1 mice (purchased from Charles River) ranged in age from eight to twelve weeks old. All rats and mice were healthy throughout the duration of the study and had free access to chow and water in a 12/12 h light/dark cycle room. In most cases, rats and mice of both sexes were used with the exception of six-week-old male rats for sciatic nerve injury microarray experiments. *Pdgfra*$^{EGFP/+}$ (B6.129S4-Pdgfr$\alpha^{tm11(EGFP)Sor}$/J; JAX stock #007669; Hamilton et al., 2003) mice were obtained from The Jackson Laboratory and were bred and genotyped as recommended by The Jackson Laboratory. Animals that underwent sciatic nerve injury surgeries were housed individually for recovery purposes.

Sciatic nerve resection surgeries

Sciatic nerve resections were performed on young adult male Sprague Dawley rats (microarray analysis), adult CD1 mice (scRNA-seq analysis) or adult *Pdgfra*$^{EGFP/+}$ mice [fluorescence *in situ* hybridization (FISH) and immunostaining]. Before surgery, animals were anesthetized with 2% isoflurane gas and the surgical site was shaved. Animals were kept under anesthesia for the duration of the surgery. To resect the sciatic nerve, an incision was made along the lateral aspect of the mid-thigh of the right hindlimb, the sciatic nerve was then raised, an ~5- to 10-

This work was funded by Canadian Institutes of Health Research (CIHR) and the Canada First Research Excellence Fund "Medicine by Design" (F.D.M. and D.R.K.). J.S.T. and M.A.S. were funded by CIHR fellowships, M.J.C. by a CIHR studentship, and S.A.Y. by a Lap-Chee Tsui Restracomp fellowship during the course of these studies.

[a]K.K. and M.J.C. contributed equally to this work.

S.A. Yuzwa's present address: Department of Laboratory Medicine and Pathobiology, University of Toronto, Toronto, Ontario M5S 1A8, Canada.

Acknowledgements: We thank Dennis Aquino, Jon Krieger, Troy Ketela, and Konstantin Feinberg for advice and technical assistance.

Correspondence should be addressed to Freda D. Miller at fredam@sickkids.ca.

https://doi.org/10.1523/ENEURO.0066-20.2020

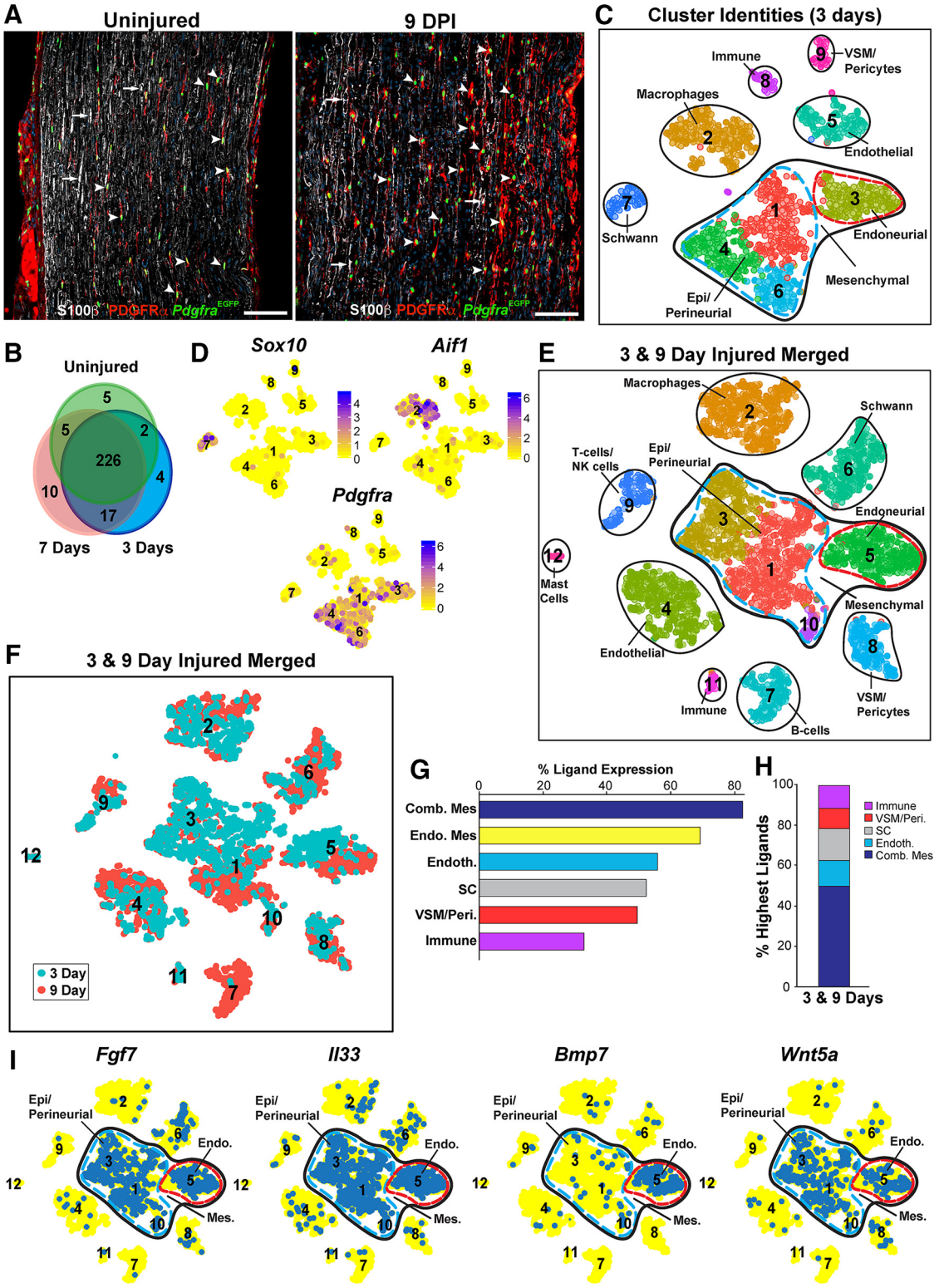

Figure 1. Characterization of ligand expression in the injured sciatic nerve (see also Extended Data Fig. 1-1). ***A***, Images of longitudinal sections of an uninjured adult nerve and a 9 DPI distal sciatic nerve from *Pdgfra*$^{Egfp/+}$ mice analyzed for EGFP (green) and immunoreactivity for PDGFRα (red) and S100β (white). Arrowheads denote endoneurial cells positive for both PDGFRα protein and nuclear *Pdgfra*-EGFP and arrows indicate S100β immunoreactive Schwann cells. Scale bars = 100 μm. ***B***, Venn diagram showing the number of ligands expressed in the uninjured versus 3 and 7 DPI distal sciatic nerves, based on microarray analysis. Ligand mRNAs were defined as expressed if their levels were ≥*Ntf3*. ***C–I***, Characterization of ligand expression in injured distal sciatic nerve scRNA-seq datasets. ***C***, t-SNE cluster visualization of 3 DPI sciatic nerve cell transcriptomes analyzed via the computational

continued

pipeline, with clusters annotated for cell types as identified by marker gene expression. ***D***, t-SNE gene expression overlays on the dataset in ***C*** for the Schwann cell marker *Sox10*, the macrophage marker *Aif1*, and the mesenchymal cell marker *Pdgfra*. Relative transcript expression levels are color coded as per the adjacent color keys. ***E***, t-SNE cluster visualization of the combined 3 and 9 DPI distal sciatic nerve cell transcriptomes with clusters annotated for cell types as identified by marker gene expression. ***F***, t-SNE visualization of the dataset in ***E*** with cells color coded for their dataset of origin. Numbers correspond to cluster numbers in ***E***. ***G***, Bar graph showing the percentage of the 143 injured nerve ligand mRNAs detectably expressed in the combined 3 and 9 DPI sciatic nerve cell types (shown and annotated in ***E***), including *Pdgfra*-positive mesenchymal cells (Comb. Mes), *Pdgfra*-positive endoneurial mesenchymal cells (Endo. Mes), endothelial cells (Endoth.), Schwann cells (SC), VSM/pericyte cells (VSM/Peri.), and immune cells. Ligand mRNAs were considered to be expressed if they were detected in 2% or more of the cell type of interest. ***H***, Stacked bar graph showing the relative percentage of ligand mRNAs expressed at the highest levels in the different injured peripheral nerve cell types shown in ***E***. ***I***, t-SNE gene expression overlays of the combined 3 and 9 DPI sciatic nerve dataset (shown in ***E***) for *Fgf7*, *Il33*, *Bmp7*, and *Wnt5a*. Cells that detectably express the ligand are colored blue and the numbers correspond to the clusters.

mm segment was removed, and the distal nerve ending was carefully tucked away (distally) from the injury site to prevent regeneration. The wound was then closed with 4–0 Polysorb sutures (Covidien). Animals were treated subcutaneously with ketoprofen or meloxicam (~2–5 mg/kg) as well as buprenorphine (0.05 mg/kg) before surgery, along with a postoperative treatment of ketoprofen or meloxicam 24 h after surgery. Mice and rats were housed separately following surgery and remained healthy throughout the postoperative period and were monitored twice daily for 3 d following surgery.

Single-cell isolation and myelin removal for Drop-seq analysis

For preparation of the 3 d postinjury (DPI) nerve scRNA-seq dataset, young adult CD1 mice underwent unilateral surgical resections as described above, and injured distal sciatic nerve segments were collected 3 d following surgery. For the uninjured nerve and neonatal nerve analyses, bilateral sciatic nerve segments were collected from adult and postnatal day (P)2–P4 CD1 mice, respectively. Freshly dissected nerves were digested in a mixture of collagenase Type XI (1 mg/ml, Sigma) and 0.05% Trypsin-EDTA (Thermo Fisher Scientific) for 30 min at 37°C. Enzymatic digestion was halted by diluting the cell suspension with HBSS (Thermo Fisher Scientific). Following centrifugation (1200 rpm for 5 min) and removal of the supernatant, the cell pellet was resuspended in PBS containing 0.5% BSA and passed through a 70-μm cell strainer (BD Biosciences). For datasets purified with myelin removal beads (3 DPI, neonatal and uninjured nerve; as shown in Figs. 1*C*,*E*, 2*C*,*E*; referred to as set 2 for the neonatal analyses, where cells were prepared in two ways), myelin debris was removed from the single-cell suspension using Myelin Removal Beads II and a MidiMACS magnetic separator with LS columns (Miltenyi Biotec), according to the manufacturer's instructions. Following myelin removal, the cell suspension was centrifuged (1200 rpm for 5 min), and the supernatant was removed before resuspending the pellet in 0.22-mm sterile-filtered PBS containing 0.01% BSA. For the second neonatal nerve dataset that was purified using fluorescence-activated cell sorting (FACS), a single-cell suspension of dissociated injured nerve cells was prepared as described above. After passing the cells through a 70-μm cell strainer and resuspending them in PBS containing 0.25% BSA, Hoechst 33258 was added to distinguish nucleated cells from myelin debris, in addition to propidium iodide (PI) to exclude dead cells. The Hoechst^{high} and PI-negative cell fractions were FACS purified using a MoFlo XDP cell sorter (Beckmann Coulter) before proceeding with scRNA-seq analysis. In all cases, cells were then resuspended in PBS containing 0.01% BSA, counted with a hemocytometer, and the solution was adjusted to a final concentration of 140,000 cells/ml and run through the Drop-seq apparatus at the Princess Margaret Genomics Facility. Drop-seq, cDNA amplification, library preparation, sequencing, processing of FASTQ sequencing reads, and read alignment steps were all conducted including minor modifications according to previously published protocols (Macosko et al., 2015). For the 3 DPI nerve scRNA-seq analysis (as shown in Fig. 1*C*), a raw digital gene expression (DGE) matrix was generated from 2500 cell barcodes as described in the Drop-seq Alignment Cookbook (version 1.2, January 2016; http://mccarrolllab.com/dropseq/). Similarly, for the uninjured nerve scRNA-seq analysis (as shown in Fig. 2*C*), a raw DGE matrix was generated from 2000 cell barcodes and used for all further analyses. In the case of the two neonatal nerve datasets (FACS sorted and bead treated), 2500 and 6200 cell barcodes were used to generate the DGE matrices as described above. DGE matrices described here were used for all subsequent analyses. The previously published DGE matrices for the 9-d injured nerve datasets (both FACS and myelin bead treated; GEO:GSE120678) were described in Carr et al. (2019).

Computational analysis of scRNA-seq data

Drop-seq data (DGE matrices) were analyzed used a previously described custom computational pipeline (Yuzwa et al., 2017; Carr et al., 2019; Storer et al., 2020; described in detail in Innes and Bader, 2019). Briefly, data were filtered to remove cells with low unique molecular identifier counts, cell doublets, contaminant red blood cells, and cells that contained high mitochondrial gene content. Genes detected in less than three cells were removed. Cell transcriptomes were then normalized as previously described (Lun et al., 2016) using an algorithm in the scran package in R that corrects for differences in sequencing depth by the use of scaling factors within each cell by pooling random subsets of cells, summing their library sizes, and comparing them with average library size across all cells in the group. This is iteratively performed, and the cell-wise scaling factors can be deconvolved from the set of pool-wise scaling factors. Following

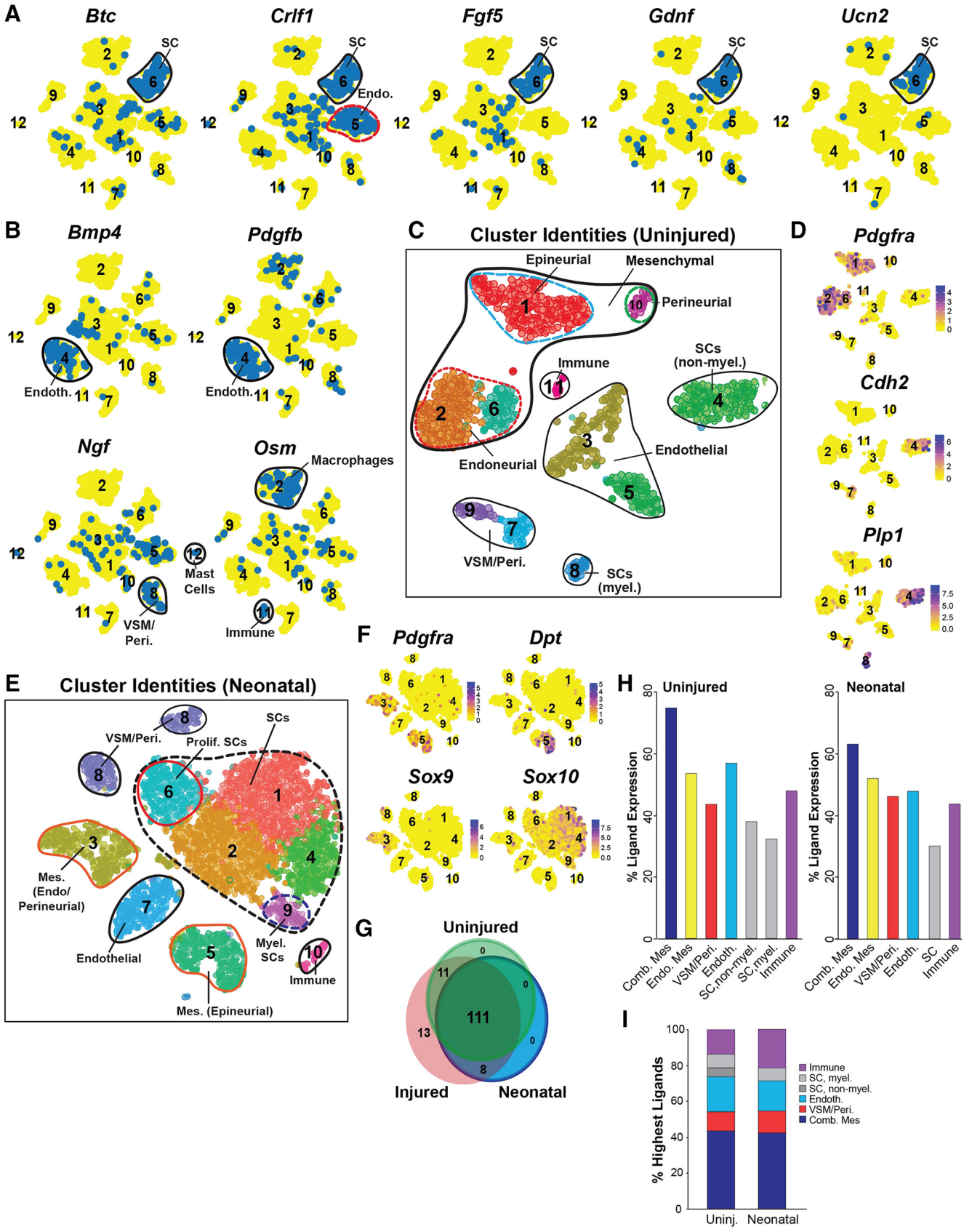

Figure 2. Ligand expression in the injured, uninjured and neonatal sciatic nerves (see also Extended Data Fig. 2-1). ***A***, ***B***, t-SNE gene expression overlays of the combined 3 and 9 DPI sciatic nerve dataset (shown in Fig. 1*E*) for *Btc*, *Crlf1*, *Fgf5*, *Gdnf*, and *Ucn2*

continued

(***A***) and *Bmp4*, *Pdgfb*, *Ngf*, and *Osm* (***B***). Cells that detectably express the ligand are colored blue and the numbers correspond to the clusters. Specific cell types with the highest ligand expression are circled and annotated, including Schwann cells (SC), endoneurial mesenchymal cells (Endo.), endothelial cells (Endoth.), VSM/pericytes (VSM/Peri.), and various types of immune cells. ***C***, t-SNE cluster visualization of uninjured sciatic nerve single-cell transcriptomes annotated for cell types as identified by marker gene expression. ***D***, t-SNE gene expression overlays of the dataset in ***C*** for the mesenchymal cell gene *Pdgfra*, and for the Schwann cell genes *Cdh2* and *Plp1*. Relative transcript expression levels are color coded as per the adjacent color keys. ***E***, t-SNE cluster visualization of neonatal sciatic nerve single-cell transcriptomes annotated for cell types identified by marker gene expression. Mes. = mesenchymal cells. ***F***, t-SNE gene expression overlays of the dataset in ***E*** for the mesenchymal cell genes *Pdgfra*, *Dpt*, and *Sox9,* and the Schwann cell gene *Sox 10*. Relative transcript expression levels are color coded as per the adjacent color key. ***G***, Venn diagram showing overlapping expression of the 143 injured nerve ligand mRNAs in the uninjured, neonatal, and injured nerve scRNA-seq datasets. Ligand mRNAs were considered to be expressed if they were detectable in 2% or more cells in any defined cell type cluster. ***H***, Bar graphs showing the percentage of the 143 injured nerve ligand mRNAs detectably expressed in the uninjured or neonatal sciatic nerve cell types (shown and annotated in ***C***, ***E***), including *Pdgfra*-positive mesenchymal cells (Comb. Mes), *Pdgfra*-positive endoneurial mesenchymal cells (Endo. Mes), endothelial cells (Endoth.), Schwann cells (SC; for the uninjured, also designated as myelinating vs non-myelinating), VSM/pericyte cells (VSM/Peri.), or immune cells. Ligand mRNAs were considered to be expressed if they were detected in 2% or more cells of that particular cell type. ***I***, Stacked bar graphs showing the relative percentages of ligand mRNAs expressed at the highest levels in the different uninjured and neonatal peripheral nerve cell types shown in ***C***, ***E***, respectively.

normalization, DGE matrices were imported into Seurat (v. 1.4.0.16) in R. Principal component (PC) analysis was then undertaken using highly variable genes, and clustering analysis was performed using top PCs. This analysis was conducted using the shared nearest neighbor (SNN) modularity optimization-based clustering algorithm implemented in Seurat (FindClusters function). Clustering was iteratively performed at increasing resolution until a lower limit of ~10–20 differentially expressed genes [calculated by the Seurat FindMarkers function, $p < 0.01$ family-wise error rate (FWER), Holm's method] was reached between the most similar clusters. For conservative analysis of all datasets analyzed, clusters were assigned at the lowest resolution that still distinguished distinct cell types, as defined by established marker genes. As a result, clusters were assigned at a resolution of 0.4 for analysis of all datasets.

For the 3 DPI dataset (2075 total cells), nine clusters were identified with 210 differentially expressed genes between most similar clusters ($p < 0.01$, FWER). Cells were sequenced to an average depth of >70,000 reads/cell. The average number of genes detected per cell was 1027 ± 588, and the average number of transcripts was 2257 ± 2855. For the 3 and 9 DPI nerve combined dataset, cell transcriptomes from the 3 DPI dataset and the myelin bead removal-treated 9 DPI dataset (from Carr et al., 2019; GEO:GSE120678) were merged using the unique cell identifier barcodes from all cells present in all clusters of the two datasets following pipeline processing. The constructed raw DGE matrices of the combined datasets were then re-run through the pipeline for re-clustering, resulting in 5395 total cells. Twelve clusters were identified with 200 differentially expressed genes between most similar clusters ($p < 0.01$, FWER). The uninjured nerve dataset was previously analyzed for *Pdgfra*-positive mesenchymal cells (Carr et al., 2019), but not for other cell types. Reanalysis of this dataset (1841 total cells) identified 11 clusters with 105 differentially expressed genes between the most similar clusters ($p < 0.01$, FWER). For the combined neonatal dataset, cell transcriptomes from both the FAC-sorted (set 1; Extended Data Fig. 2-1*C*) and myelin removal bead-treated (set 2; Extended Data Fig. 2-1*C*) samples were merged using the unique cell identifier barcodes from all cells present in all clusters of the two datasets following pipeline processing. The constructed raw DGE matrices of the combined datasets were then re-run through the pipeline for re-clustering, resulting in 6885 total cells. Ten clusters were identified with 540 differentially expressed genes between most similar clusters ($p < 0.01$, FWER). For the FAC-sorted sample, cells were sequenced to an average depth of >90,000 reads/cell. The average number of genes detected per cell was 1005 ± 728 and the average number of transcripts was 2044 ± 1985. For the bead treated sample, cells were sequenced to an average depth of >43,000 reads/cell. The average number of genes detected per cell was 732 ± 485, and the average number of transcripts was 1231 ± 1095.

For the combined Schwann cell dataset (Fig. 3*A*,*B*), the unique cell identifier barcodes from all cells present in *Sox10*-positive clusters in each of the six described datasets (Figs. 1*E*, 2*C*,*E*; FAC-sorted cells in Carr et al., 2019) were merged. For the combined mesenchymal cell dataset (Fig. 4*A*,*B*), the unique cell identifier barcodes from all cells present in *Pdgfra*-positive clusters in each of the same six datasets were merged. The constructed raw DGE matrices of the combined datasets were then re-run through the pipeline, resulting in 5331 total Schwann cells and 5416 total mesenchymal cells. Batch correction of these combined datasets as well as data shown in Extended Data Figure 2-1*C* was performed using the Harmony batch-effect-correction method (Korsunsky et al., 2019) with Seurat V2. Briefly, gene expression data from the combined datasets were transferred to Seurat, where highly variable genes were then used to carry out principal component analysis. The Harmony iterative algorithm was used to integrate datasets and adjust for dataset specific effects based on the top 20 principal components. Iterative clustering was performed using the FindClusters function in Seurat V2, with clusters being assigned at a resolution of 0.4. This resulted in seven and nine clusters in the combined Schwann cell and mesenchymal cell datasets, respectively. t-Distributed stochastic neighbor embedding (t-SNE) visualizations of batch-

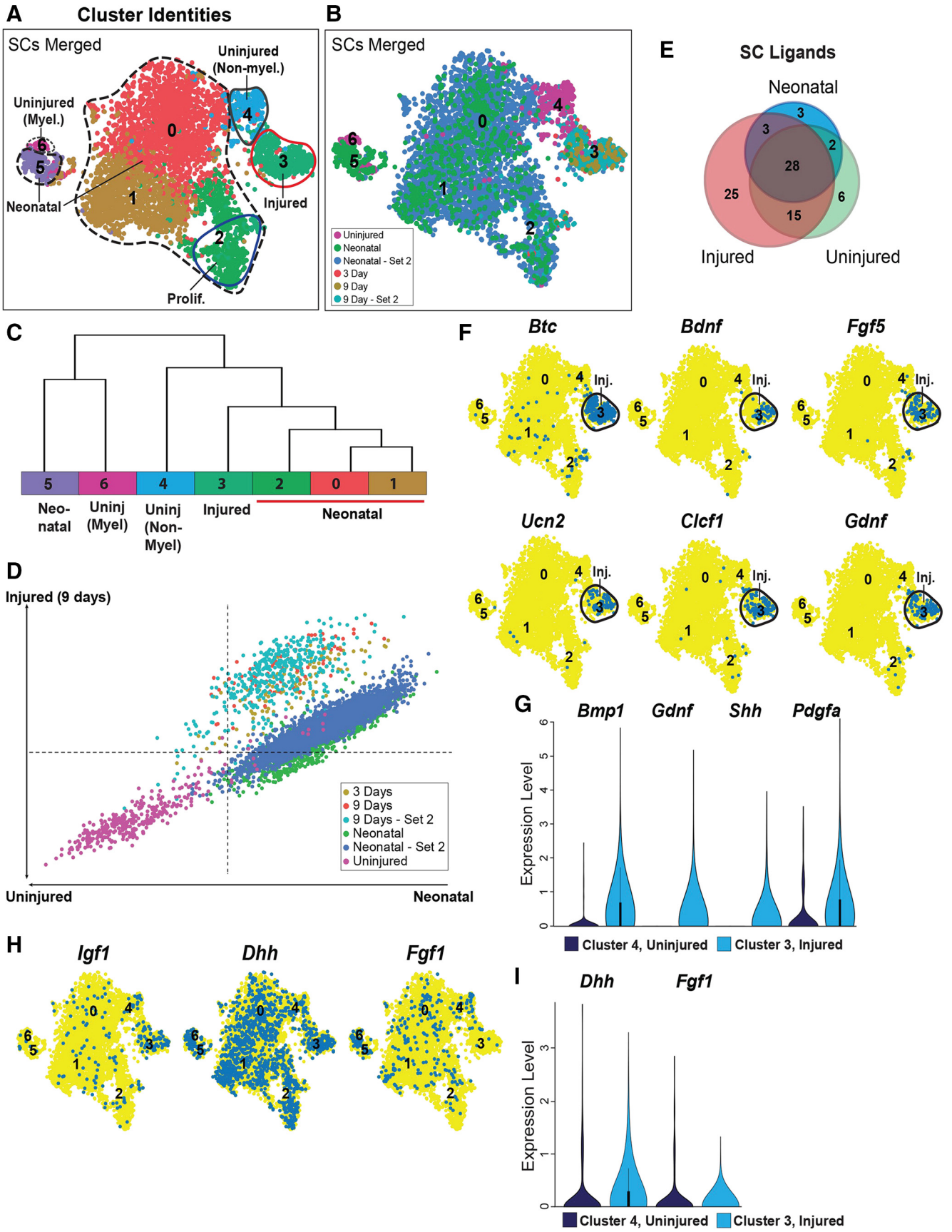

Figure 3. Characterization of ligand expression in sciatic nerve Schwann cells (see also Extended Data Fig. 3-1). Schwann cell

continued

transcriptomes from the injured, uninjured and neonatal nerve datasets (in Figs. 1*E*, 2*C*,*E*; also see Carr et al., 2019) were extracted, combined together, analyzed and batch-corrected using Harmony data integration and clustered in Seurat based on principal components. ***A***, ***B***, t-SNE visualizations of the combined Schwann cells (SCs), showing clusters (***A***) and datasets of origin (***B***). The clusters in ***A*** are also annotated based on marker gene expression (Extended Data Fig. 3-1*A*) and datasets of origin. Neonatal and 9 d refer to the FAC-sorted preparations at these timepoints while neonatal – set 2 and 9 d – set 2 refer to the cells prepared with myelin removal beads. ***C***, A dendrogram showing hierarchical analysis of cell clusters from the combined Schwann cell dataset, with cluster identity numbers, annotations and colors as in ***A***. ***D***, Scatterplot showing differential correlation of single-cell transcriptomes from the combined Schwann cell dataset in ***A*** (individual colors represent different datasets) with bulk transcriptomes from uninjured adult versus neonatal Schwann cells on the *x*-axis and uninjured adult versus 9 DPI on the *y*-axis. ***E***, Venn diagram showing the overlap of ligand mRNAs expressed in neonatal, injured and uninjured Schwann cell clusters from the combined Schwann cell dataset in ***A***. Ligand mRNAs were considered to be expressed if they were detectable in 2% or more cells in any defined cell type cluster. ***F***, t-SNE gene expression overlays of the combined Schwann cell data in ***A*** for *Btc*, *Bdnf*, *Fgf5*, *Ucn2*, *Clcf1*, and *Gdnf*. Cells that detectably express the ligand are colored blue, and the numbers correspond to the clusters. Injured Schwann cell cluster 3 (Inj.) is circled. ***G***, Violin plots showing the relative expression of *Bmp1*, *Gdnf*, *Shh*, and *Pdgfa* in injured Schwann cluster 3 versus uninjured Schwann cell cluster 4 from the dataset in ***A***. ***H***, t-SNE gene expression overlays of the combined Schwann cell data in ***A*** for *Igf1*, *Dhh*, and *Fgf1*. Cells that detectably express the ligand are colored blue and the numbers correspond to the clusters. ***I***, Violin plots showing the relative expression of *Dhh* and *Fgf1* in injured Schwann cell cluster 3 versus uninjured cluster 4 from the dataset in ***A***.

corrected data were generated using the FeaturePlot function in Seurat. t-SNE gene expression overlays displayed in the figures were generated using the FeaturePlot function in Seurat and binary expression overlays were performed using the SubsetCells and TSNEPlot functions in Seurat. These tSNE overlays were further edited using Adobe Illustrator (Adobe Systems Incorporated) as necessary to highlight features of the t-SNE visualization.

Cell types (clusters) were defined based on the expression of the following established marker genes: endothelial cells: *Pecam1*/*Cd31*, *Plvap*, and *Esam*; Schwann lineage cells: *Ngfr*/*p75NTR* and *Sox10*; non-myelinating Schwann cells: *Ngfr*/*p75NTR*, *Cdh2*, *L1cam*, *Ednrb*, *Emp1*, and *Sema3e*; premyelinating Schwann cells: *Pou3f1* and *Egr2*; myelinating Schwann cells: *Mag*, *Mbp*, *Pmp22*, *Mpz*, and *Plp1*; macrophages/monocytes: *Aif1*/*Iba1*; lymphoid immune cells including B cells, T cells, and NK cells: *Ptprcap*, *Trbc2*, and *Cd52*; B cells: *Cd19*; vasculature-associated smooth muscle (VSM) and pericyte cells: *Desmin*, *Mylk*, *Acta2*, and *Rgs5*; mesenchymal cells: *Pdgfra*; epineurial mesenchymal cells: *Pcolce2*, *Dpp4*, *Dpt*, *Ly6c1*, and *Comp*; endoneurial mesenchymal cells: *Etv1*, *Wif1*, *Sox9*, *Osr2*, and *Meox1*; perineurial mesenchymal cells: *Slc2a1*, *Casq2*, and *Msln*; differentiating nerve bridge mesenchymal cells: *Dlk1* and *Mest*; and proliferating cells: *Mki67* and *Top2a*.

In combined datasets, dataset identities were distinguished by using the gg color hue and hcl functions in R. Correlation analysis comparing gene expression between different clusters was performed by averaging the expression of each gene across all cells in the individual clusters to be compared, then Pearson correlation analysis was performed using the Cor function and plotted in R. Genes of interest were then highlighted using Adobe Illustrator (Adobe Systems Incorporated; as in Extended Data Fig. 3-1*B*). Differential correlation of single-cell transcriptomes as shown in Figure 3*D* was performed as described previously (Gerber et al., 2018). Briefly, mock bulk transcriptomes were generated for the 9 DPI Schwann cells (both bead and FAC sorted), the uninjured non-myelinating Schwann cells and the neonatal Schwann cells (both bead and FAC sorted) by determining the mean expression of each gene in the total combined cells in each dataset. Each single-cell transcriptome was then correlated with each of the mock bulk transcriptomes. We then determined the differential correlation of each single cell with the bulk uninjured nerve versus the bulk 9 DPI transcriptomes (*y*-axis) and the differential correlation with the bulk uninjured nerve versus the bulk neonatal nerve transcriptomes (*x*-axis). Violin plots were generated using the VioPlot package in R. Hierarchical clustering of the batch corrected combined Schwann cell data in Figure 3*C* was performed based on the top 20 Principal Component (PC) using the BuildClusterTree and PlotClusterTree functions in Seurat. Node numbers were removed from the plot and cluster descriptions and colors were added for clarity using Adobe Illustrator (Adobe Systems Incorporated). The single cell heatmaps were generated (with scaled expression values) using the DoHeatMap function in Seurat at resolution 0.4.

Ligand mRNA expression and Venn diagram analysis

The expression of ligand mRNAs (Table 1) was characterized from the whole nerve microarray analysis using a custom curated ligand-receptor database (modified from Yuzwa et al., 2016). Extracellular matrix proteins and potential ligands without well-defined, receptor-mediated paracrine roles were excluded. The VennDiagram package in R was used to determine overlapping ligands in the uninjured, 3-d injured, and 7-d injured nerve datasets and was modified to show proportional representation of data using the euler*APE* tool (Micallef and Rodgers, 2014).

The combined 3 and 9 DPI nerve scRNA-seq dataset (Fig. 1*E*) was analyzed to identify the percentage of cells in each cell type expressing the ligand mRNAs identified by the microarray analysis. For this analysis, *Pdgfra*-positive mesenchymal cells were separated into endoneurial cells (cluster 5; Fig. 1*E*) and all other mesenchymal cells. Ligand mRNAs were considered further only if they were detectable in 2% or more cells of at least one cell type. The 143 resultant injured nerve ligands (Table 2) were further analyzed in the other scRNA-seq datasets. Venn diagrams comparing expression of the 143 injured nerve ligands in the various datasets (Figs. 2*G*, 3*E*, 4*C*) were prepared using the VennDiagram package, modified to

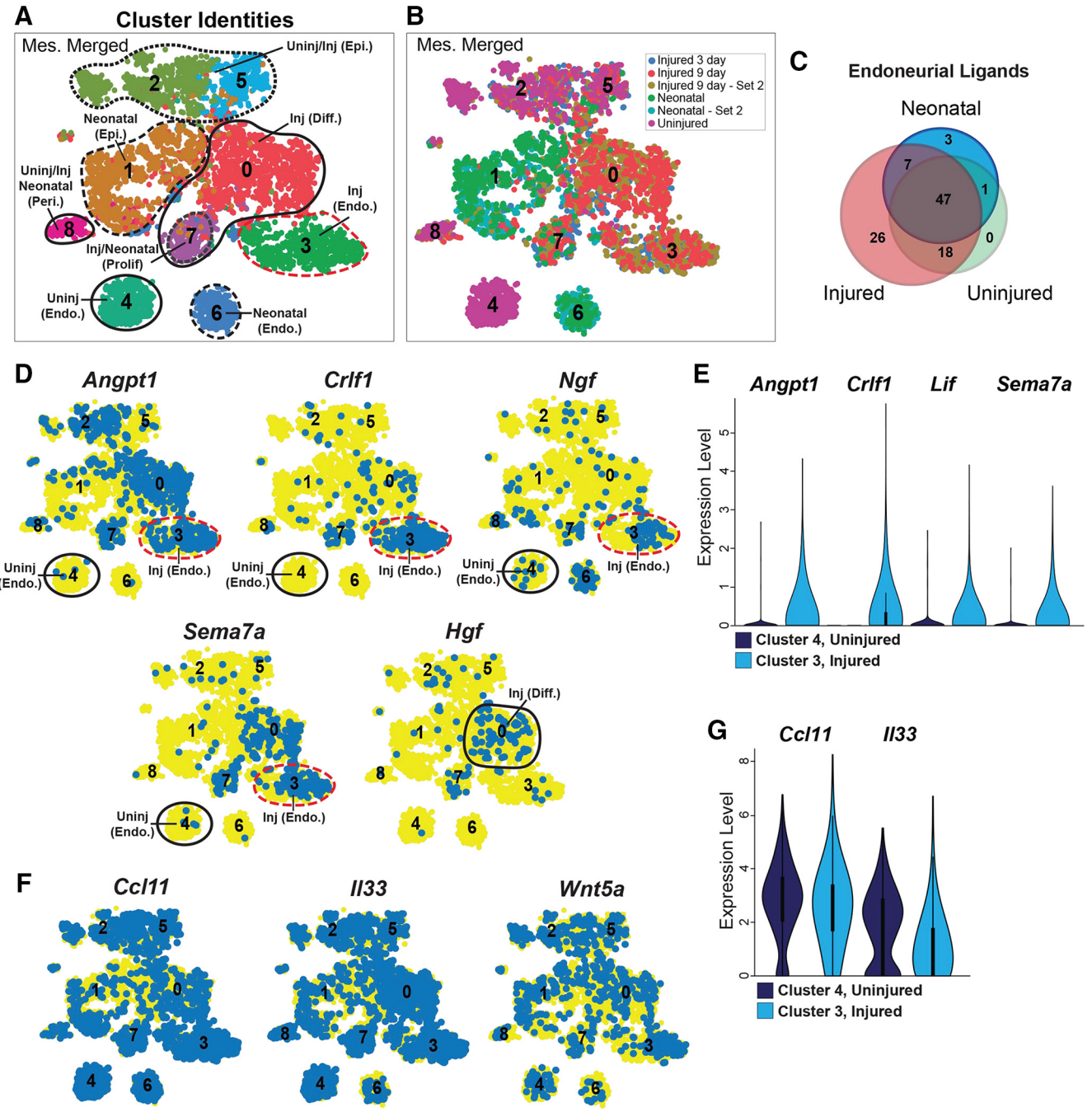

Figure 4. Characterization of ligand expression in sciatic nerve mesenchymal cells (see also Extended Data Fig. 4-1). *Pdgfra*-positive mesenchymal cell transcriptomes from the injured, uninjured and neonatal nerve datasets (in Figs. 1*E*, 2*C*,*E*; also see Carr et al., 2019) were extracted, combined together, analyzed and batch-corrected using Harmony data integration and clustered in Seurat based on principal components. ***A***, ***B***, t-SNE visualizations of the combined mesenchymal cells showing clusters (***A***) and datasets of origin (***B***). The clusters in ***A*** are also annotated based on marker gene expression (Extended Data Fig. 4-1) and datasets of origin. Neonatal and 9 d refer to the FAC-sorted preparations at these timepoints, while neonatal – set 2 and 9 d – set 2 refer to the cells prepared with myelin removal beads. ***C***, Venn diagram showing the overlap of ligand mRNAs expressed in neonatal (cluster 6), injured (cluster 3), and uninjured (cluster 4) nerve endoneurial mesenchymal cells from the combined mesenchymal nerve dataset in ***A***. Ligand mRNAs were considered to be expressed if they were detectable in 2% or more cells in the relevant cluster. ***D***, t-SNE gene expression overlays of the combined mesenchymal cell data in ***A*** for *Angpt1*, *Crlf1*, *Ngf*, *Sema7a*, and *Hgf.* Cells that detectably express the ligand are colored blue, and the numbers correspond to the clusters. Relevant clusters are circled and annotated, including uninjured endoneurial (Uninj Endo.), injured endoneurial (Inj Endo.), and injured differentiating (Inj Diff.) mesenchymal cells. ***E***, Violin plots showing the relative expression of *Angpt1*, *Crlf1*, *Lif*, and *Sema7a* in injured endoneurial mesenchymal cell cluster 3 versus uninjured endoneurial cell cluster 4 from the dataset in ***A***. ***F***, t-SNE gene expression overlays of the combined mesenchymal cell data in ***A*** for *Ccl11*, *Il33*, and *Wnt5a*. Cells that detectably express the ligand are colored blue, and the numbers correspond to the clusters. ***G***, Violin plots showing the relative expression of *Ccl11* and *Il33* in injured endoneurial mesenchymal cell cluster 3 versus uninjured endoneurial cell cluster 4 from the dataset in ***A***.

show proportional representation with the euler*APE* tool (Micallef and Rodgers, 2014).

RNA isolation and microarray analysis

Total RNA was extracted from E15 rat dorsal root ganglion (DRG) sensory neurons and neonatal rat superior cervical ganglion (SCG) sympathetic neurons using the RNeasy Micro kit (QIAGEN) according to manufacturer's instructions. RNA was isolated from the distal rat sciatic nerve following injury (3 and 7 d after resection) and contralateral uninjured sciatic nerve as follows. After harvesting, nerves were flash frozen in liquid nitrogen and stored at −80°C until RNA isolation was performed. Nerve tissue was lysed using a Dounce homogenizer with cooled TRIzol (1 ml/50–100 mg of tissue) followed by passing the lysate through a 23.5-gauge needle. The homogenate was then spun at 12,000 × *g* at 4°C for 10 min, with the clear supernatant transferred to a new tube and allowed to incubate at room temperature for 5 min, 0.2 ml of chloroform was then added per milliliter of homogenate, shaken vigorously for 15 s, incubated 2–3 min at room temperature, and spun at 12,000 × *g* for 15 min at 4°C. The resulting aqueous phase was removed and added to a new tube with equal volume of 70% ethanol before RNA isolation with the RNeasy Micro kit (QIAGEN) according to manufacturer's instructions. Microarray analysis was then performed at the Center for Applied Genomics at the Hospital for Sick Children (Toronto, ON). A total of 250 ng of total RNA was processed using the Affymetrix WT Plus kit to generate cDNA following Bioanalyzer analysis to confirm the quality of the RNA. 5.5 μg of labeled cDNA was hybridized onto Rat Gene 2.0 ST arrays using the Affymetrix FS450_0002 hybridization protocol and scanned using the Affymetrix GeneChip Scanner 3000.

Normalization and differential gene expression analysis of microarray data

Raw probe intensity values were background corrected and then normalized with quantile normalization. Values were transformed into the log2 scale and summarized into probesets using the robust multichip analysis (RMA) algorithm in the oligo Bioconductor package in R. For all of the rat microarray datasets, gene annotation was performed using the "ragene20sttranscriptcluster.db" library in R. Motor neuron microarray data (Kaplan et al., 2014) was obtained from mouse P7 lumbar motor neurons from the GEO database under the accession number GSE52118. For these data, raw probe intensity values were normalized and summarized into probesets as described above, except for the Affymetrix Mouse Genome 430 2.0 Array ($n = 3$ replicates), and gene annotation was performed using the "mouse4302.db" library in R. The Limma Bioconductor package was used to calculate differential gene expression between the sensory neurons (DRGs, $n = 6$ replicates) and sympathetic neurons (SCGs, $n = 4$ replicates). Bayesian statistics were calculated and annotated receptor genes were considered to be differentially expressed if they were ≥2-fold different with $p < 0.05$ false discovery rate (FDR; Benjamini and Hochberg correction).

Cell-surface capture mass spectrometry

Cell-surface mass spectrometry was conducted based on modified published protocols (McDonald et al., 2009; Schiess et al., 2009; Yuzwa et al., 2016). Briefly, 6-cm dishes containing sensory and sympathetic neurons were washed with coupling buffer [1× PBS (pH 6.5) and 0.1% fetal bovine serum (FBS)] following removal of the medium. Cultures were treated with 5 mM $NaIO_4$ in coupling buffer for 30 min at room temperature in the dark and lysed in buffer containing 20 mM Tris-HCl, 150 mM NaCl, 0.0002% NaN_3, 1% NP-40 (pH 7.5), and one complete mini-protease inhibitor tablet (Roche) per 10 ml of lysis buffer. Lysates were passed through 23-gauge needles, protein concentrations determined using the Pierce BCA assay kit (catalog #23227, Thermo Fisher Scientific), and equal amounts of total protein (between 0.9 and 1.5 mg for sensory neurons and <1 mg for sympathetic neurons) were added to 200 μl of Ultralink Hydrazide resin (Pierce) pre-equilibrated with lysis buffer and rotated overnight at room temperature. The unbound protein was removed via centrifugation the following day, washed twice with 8 M urea and three times with 50 mM ammonium bicarbonate (pH 8; ABC). The resin was treated with 50 mM dithiothreitol (DTT; American Bioanalytical) in ABC at 37°C for 60 min, washed once with ABC, and incubated with 65 mM iodacetamide in ABC at room temperature in the dark for 30 min. The resin was washed once with ABC, once with 1.5 M NaCl and three times with ABC and incubated with 40 ng/μl of Trypsin (Worthington) in ABC overnight at 37°C. The following day, the resin was washed three times with 1.5 M NaCl, followed by 80% acetonitrile, methanol, water, and ABC and then incubated with 1300 U/ml of PNGaseF (New England Biolabs) at 37°C overnight in ABC. The following day, the eluted peptides were collected from the resin and the resin washed once with ABC and combined with the eluted peptides. The eluates were lyophilized overnight and prepared for mass spectrometry using C18 reverse-phase ZipTips (EMD Millipore). Peptides were lyophilized and resuspended in 11 μl of 0.1% formic acid following elution from ZipTips. Samples were then analyzed on an Orbitrap analyzer (Q-Exactive, Thermo Fisher) outfitted with a nano-spray source and EASY-nLC nano-LC system (Thermo Fisher); 5 μl of the resuspended peptide mixtures were loaded onto a 75 μm × 50 cm PepMax RSLC EASY-Spray column filled with 2 μM C18 beads (Thermo Fisher) at a pressure of 800 Bar. Peptides were eluted over 60 min at a rate of 250 nl/min using a 0–35% acetonitrile gradient in 0.1% formic acid. Peptides were introduced by nano-electrospray into the Q-Exactive mass spectrometer (Thermo Fisher). The instrument method consisted of one MS full scan (400–1500 m/z) in the Orbitrap mass analyzer with an automatic gain control (AGC) target of 1e6, maximum ion injection time of 120 ms, and a resolution of 70,000 followed by 10 data-dependent MS/MS scans with a resolution of 17,500, an AGC target of 1e6, maximum ion time of 120 ms, and one microscan. The intensity threshold to trigger a MS/MS scan was set to 1.7e4. Fragmentation occurred in the HCD trap with normalized collision energy set to 26. The dynamic exclusion was applied using a

setting of 8 s. Peptide and protein identification was performed using PEAKS version 8 software (Bioinformatics Solutions Inc.). Peptides and proteins were identified at the 0–0.1% FDR level in the sensory neuron dataset and at the 0.8–1% FDR level in the sympathetic neuron dataset. With both sensory and sympathetic neuron culture datasets, data were pooled across the three samples, and we included all proteins where at least a single peptide was detected in at least one of the samples.

Identification of receptors based on the microarray and mass spectroscopy data

Receptors were identified in both the microarray and mass spectrometry data using the ligand-receptor database described in Yuzwa et al. (2016), with modifications. In addition, proteins that were classified as receptors using the PANTHER (http://pantherdb.org) protein classification system, but not necessarily present in the ligand-receptor database, were included. Manual curation of receptors with known signaling functions (such as the Plxn receptors) as well as other genes identified as receptors by Gene Ontology (GO) terms were also included as an update to the previously published version of the ligand-receptor database. Receptor classifications (Fig. 5*B*) were based on GO terms and descriptions provided by websites including GeneCards (http://genecards.org) and UniProt (http://uniprot.org).

Computational modeling and pre-processing of data

To define receptors for generation of ligand-receptor models, gene expression values from the injured nerve and from the motor, sensory, and sympathetic neuron microarrays were first averaged across replicates, and in the case of multiple probes corresponding to the same receptor gene, the highest expressed probe was used (this was following averaging). For rat retinal ganglion cells (RGCs), we analyzed RNA-seq data from Blanco-Suarez et al. (2018) as obtained from the GEO database (accession GEO: GSE108484). Data from control RGCs were used ($n = 3$) and processed as described above for the microarray data. Expression values with fragments per kilobase of transcript per million mapped reads (FPKM) >1 were considered expressed and included for analysis. For the modeling, receptor mRNAs that had expression values exceeding the thresholds as described in the results were included. These receptors and the 143 injured nerve ligands (Table 2) were then analyzed using a custom Python script ("Cellcellinteractnet," Python version 2.7.6) and custom ligand-receptor database (database modified from Yuzwa et al., 2016) to predict ligand-receptor interactions. Models were all constructed from this information using Cytoscape (3.7.0). The Venn diagram comparing predicted interactions in Figure 7*C* was prepared using the VennDiagram package, modified to show proportional representation with the euler*APE* tool (Micallef and Rodgers, 2014).

Sympathetic neuron cultures

SCGs of newborn (P1–P2) Sprague Dawley rats were dissected, dissociated and cells were plated at eight ganglia per 3.5-cm tissue culture-treated dish for microarrays, $\sim 1 \times 10^6$ cells per 6-cm dish for mass spectrometry, or $\sim 1.4 \times 10^5$ cells per 13-mm glass coverslip for immunostaining. Neurons were plated on dishes and coverslips coated with poly-D-lysine and laminin (1 μg/ml laminin; VWR). Neurons were cultured in growth medium composed of UltraCULTURE medium (Lonza), 2 mM L-glutamine (Lonza), 100 U/ml penicillin (Wisent) with 100 μg/ml streptomycin (pen/strep; Wisent), and 50 ng/ml NGF (Cedarlane). Neurons were cultured in growth medium containing 3% heat-inactivated FBS for 3 d with inclusion of 7.2 μM cytosine arabinoside (CA) for the first day, and 3.6 μM CA for the second and third days. Cultures were switched to growth medium alone for an additional 3 d, as described previously (Park et al., 2010; Feinberg et al., 2017).

Sensory neuron cultures

Sensory neurons from E15 rat DRGs were cultured as described (Feinberg et al., 2010, 2017). For immunostaining, neurons were plated at a density of 2×10^5 cells per 13-mm glass coverslip precoated with laminin (VWR), and poly-D-lysine (Sigma-Aldrich). Neurons were plated at a density of 1×10^6 cells per 6-cm dish for proteomics. For microarrays, neurons were plated under both conditions. Initially, cells were plated in a medium #1 containing Neurobasal medium (Invitrogen), GlutaMAX (Invitrogen), 50 ng/ml NGF (Cedarlane), B27 supplement (Invitrogen), and pen/strep. The day after plating, cultures were treated for 2 d in medium #2 composed of Eagles basal medium (Invitrogen), ITS supplement (Sigma), 0.2% BSA (Sigma), 4 mg/ml D-glucose (Sigma), GlutaMAX (Invitrogen), 50 ng/ml NGF (Cedarlane), and pen/strep with 0.8 μM CA to eliminate mitotic non-neuronal cells. Cells were then treated with another cycle of medium #1 for 2 d followed by a final 2-d cycle of medium #2. After the second CA treatment, cultures were grown in medium #1 for two additional days before cell harvest.

Culturing and sorting mesenchymal cells from the sciatic nerve for ELISA analysis

Sciatic nerves were harvested from P4 Sprague Dawley rat pups. Each biological sample included four litters of pups (two litters harvested per day over 2 d). Nerve cells from two litters were dissociated and plated on 6-cm dishes in medium consisting of low-glucose DMEM/F12 (3:1, Invitrogen) and 1% pen/strep (referred to as basal medium) with 10% FBS. In order to isolate PDGFRα-positive mesenchymal cells, 1–2 d after plating, cells were treated with an antibody solution containing basal medium with goat anti-PDGFRα antibody (1:250, R&D Systems, catalog #AF1062) and donkey anti-goat Alexa Fluor 488 secondary (1:500, Thermo Fisher Scientific, catalog #A11055) that was preincubated for 30 min at room temperature. Cells were treated for 1 h at 37°C with the antibody solution before being returned to basal medium with 10% FBS overnight. PDGFRα-positive cells were then isolated using a Mo-Flo XDP sorter (Beckman Coulter). Following the sort, between 4–9 $\times 10^5$ cells were

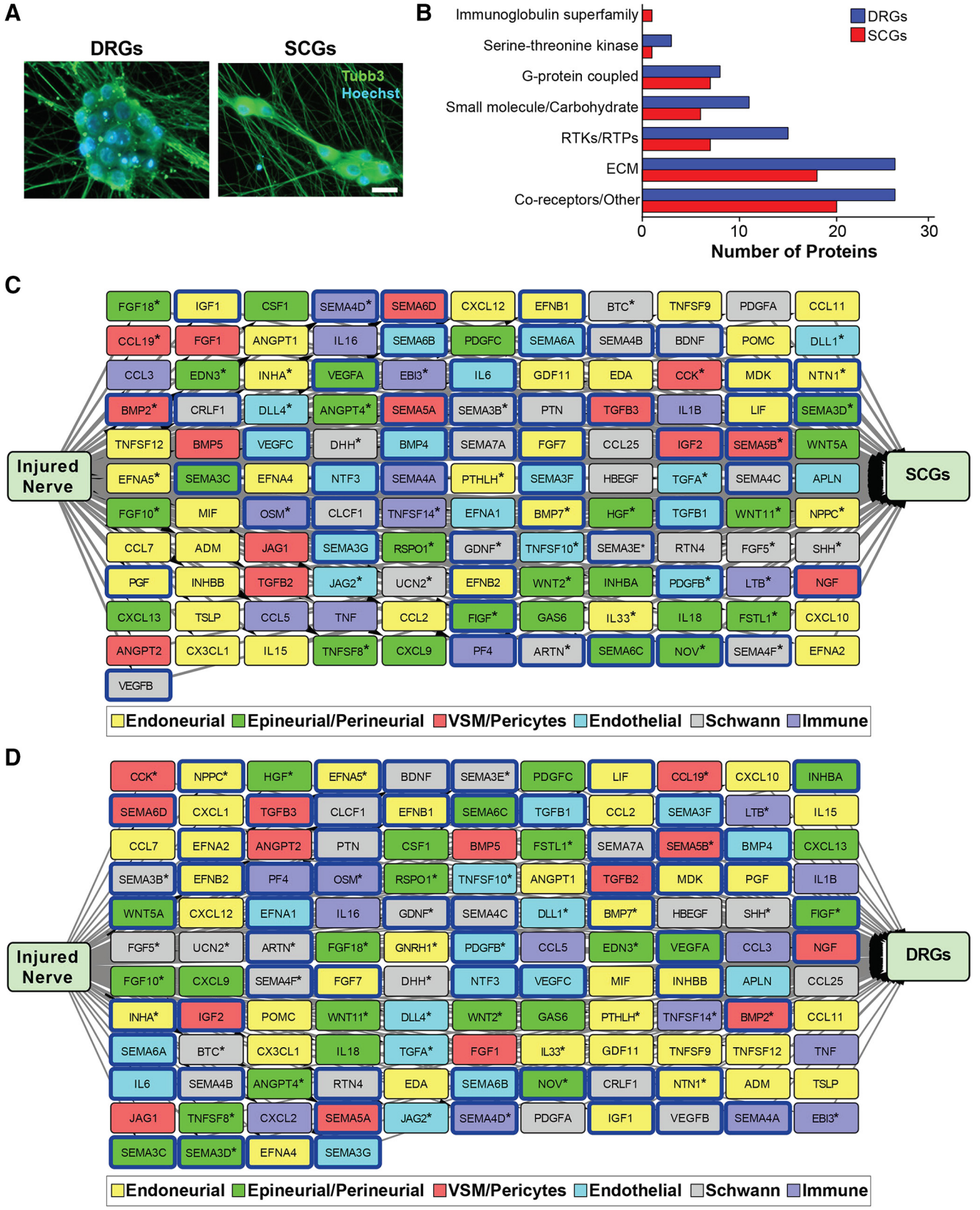

Figure 5. Sensory and sympathetic neuron receptor expression and modeling of their predicted interactions with injured nerve-derived ligands (see also Extended Data Fig. 5-1). ***A***, Images of E15 rat DRG sensory neurons cultured for 9 d (left panel) and neonatal rat SCG sympathetic neurons cultured for 6 d (right panel), immunostained for βIII-tubulin (Tubb3; green). Cells were counterstained with Hoechst 33258 to show cell nuclei (blue). Scale bars = 20 μm. ***B***, Bar graphs showing types of receptor proteins detected on

continued

the surface of sensory and sympathetic neurons following cell-surface capture mass spectrometry. Classification of receptors was based on GO terms identified via the UniProt database (http://uniprot.org) as well as manual curation of all detected cell-surface proteins. RTKs/RTPs = receptor tyrosine kinases and receptor tyrosine phosphatases; ECM = extracellular matrix. ***C***, ***D***, Models showing predicted unidirectional paracrine interaction networks between the 143 injured nerve ligands and receptors expressed by sympathetic (***C***, SCGs) and sensory (***D***, DRGs) neurons, as defined at the transcriptional and proteomics levels. Interactions were predicted by computational modeling using the ligand-receptor database, and then manually curated for well-validated interactions. Nodes represent ligands that are color coded to identify the injured nerve cell type with the highest expression of the ligand mRNA based on the scRNA-seq analysis. Predicted interactions where the receptors were detected at the protein level are indicated by a blue box around the corresponding ligand node. Asterisks indicate ligands that were expressed at 4-fold higher levels in the indicated cell type as compared with all other injured nerve cell types. Arrows indicate directionality of interactions.

re-plated on 6-cm dishes with basal medium and 10% FBS. Approximately 72 h later, medium containing FBS was removed, cells were washed with HBSS, and basal medium without serum was added for conditioning. Cells were treated with cycles of basal medium for conditioning (24–96 h) and basal medium with FBS for a period of 2.5–4 weeks total. Collected conditioned medium was spun down at 1300 rpm for 5 min to removed cell debris and frozen at −80°C until ELISAs were performed. ELISA assays for rat ANGPT1 (catalog #LS-F10827, LSBio), CCL11 (catalog #LS-F11046, LSBio), and VEGFC (catalog #LS-F5482, LS Bio) were performed and results were analyzed according to manufacturer's instructions.

Sympathetic neuron compartment cultures

Campenot cultures were established on 35-mm collagen-coated dishes as previously reported (Campenot et al., 1991); 20 × 20 mm Teflon chambers (Tyler Research) were grease-sealed and assembled on plates where the substratum was corrugated with 20 parallel tracks 200 μm wide using a pin rake (CAMP-PR, Tyler Research), forming lanes for outgrowth. Neonatal SCG sympathetic neurons were enzymatically and mechanically dissociated and plated in the central chamber at a density of three to four ganglia per compartment in 10 ng/ml NGF (Cedarlane, catalog #CLMCNET-001.1), methylcellulose Ultraculture media (Lonza) supplemented with 2 mM L-glutamine (Lonza), and antibiotics [100 U/ml penicillin (Wisent) and 100 µg/ml streptomycin (Wisent)]; 10 μM CA with 3% FBS was added to the cell bodies for 2–3 d as the axons were permitted to extend into the adjacent compartments containing 10 ng/ml NGF. After this period, central and side chambers were washed with fresh medium, medium in the cell body chamber was replaced with 10 ng/ml NGF, and medium on the axonal chambers was replaced with 100 ng/ml candidate ligand and varying amounts of NGF (0.5 ng/ml for experimental compartments, 50 ng/ml for maximum NGF control). Ligands included human recombinant ANGPT1 (Peprotech, catalog #130-06-5UG), murine recombinant Eotaxin (CCL11, Peprotech, catalog #250-01-5UG), and human recombinant VEGFC (Peprotech, catalog #100-20CD). Images of axon outgrowth were obtained at 3d post-ligand addition using a Zeiss AxioObserver Z1 microscope and outgrowth was analyzed using ImageJ software (NIH). To quantify the density of axonal growth in these compartments, a line was drawn perpendicular to the axis of the outgrowth within the furthest 1 mm of outgrowth where axons were maximally defasciculated and the number of axons crossing the line were quantified.

Immunostaining, imaging, and analysis of cultures

Immunostaining of cultured cells was performed on glass coverslips and tissue culture dishes. Cells were fixed for ~10 min in 4% paraformaldehyde in PBS solution and washed three times (10 min per wash) in PBS before treatment with the primary antibody solution, which contained the antibody, 10% normal donkey or normal goat blocking serum (Jackson ImmunoResearch), and 0.3% Triton X-100 (Fisher) in PBS. After 1–2 h of incubation at room temperature, cells were washed three times (10 min per wash) with PBS. Cells were then incubated in a secondary antibody solution containing antibodies diluted 1:500 in 0.3% Triton X-100 (Fisher) in PBS. After 1 h, cells were then washed three times (10 min per wash) in PBS with Hoechst 33258 (Sigma) added in one of the washes to label nuclei. For glass slides, coverslips were mounted with PermaFluor mounting media (Thermo Fisher Scientific). For tissue culture dishes, mounting medium was added directly on to the cells, and coverslips were placed on top of this. Cells were imaged using either a Zeiss AxioImager M2 microscope with an X-Cite 120 LED light source and a C11440 Hamamatsu camera using Zen acquisition software in the case of glass coverslips, or with a Zeiss AxioObserver Z1 microscope with Zen software in the case of tissue culture dishes. To quantify cells, multiple regions per glass coverslip or dish were imaged and cells were counted. For purified sensory and sympathetic neuron culture quantifications, S100β-positive and βIII-tubulin-positive cells were counted in four regions per coverslip across two coverslips per biological replicate and summed before calculating percent positive immunoreactive cells. Fibronectin-positive cells were counted in three regions over two sympathetic neuron replicates. Total cell counts per biological replicate ranged from ~100 to ~600. In cases where cells in dishes were counted, between three and eight regions per dish were used. Images were then processed using Photoshop software (Adobe Systems Incorporated), where brightness and contrast were edited as appropriate.

Immunostaining of sections

Adult *Pdgfra*$^{EGFP/+}$ mice underwent unilateral sciatic nerve injury and injured distal sciatic nerve and uninjured

Table 1: Ligand mRNAs expressed in uninjured, 3 DPI, and 7 DPI sciatic nerves using global transcriptomic analysis

Uninjured (238)	3 DPI (249)	7 DPI (258)	Uninjured, 3 DPI, and 7 DPI intersect (226)
Adipoq	Adipoq	Adipoq	Adipoq
Adm	Adm	Adm	Adm
Agt	Agt	Agt	Agt
Angpt1	Angpt1	Angpt1	Angpt1
Angpt2	Angpt2	Angpt2	Angpt2
Angpt4	Angpt4	Angpt4	Angpt4
Apln	Apln	Apln	Apln
Artn	Areg^{++}	Areg^{++}	Artn
Avp	Artn	Artn	Avp
Bdnf	Avp	Avp	Bdnf
Bmp1	Bdnf	Bdnf	Bmp1
Bmp2	Bmp1	Bmp1	Bmp2
Bmp4	Bmp2	Bmp2	Bmp4
Bmp5	Bmp4	Bmp4	Bmp5
Bmp6	Bmp5	Bmp5	Bmp6
Bmp7	Bmp6	Bmp6	Bmp7
Btc	Bmp7	Bmp7	Btc
Cck	Btc	Btc	Cck
Ccl11	Cck	Btla^{+}	Ccl11
Ccl19	Ccl11	Calca^{+}	Ccl19
Ccl2	Ccl17**	Cck	Ccl2
Ccl21	Ccl19	Ccl11	Ccl21
Ccl22	Ccl2	Ccl19	Ccl22
Ccl24	Ccl20^{++}	Ccl2	Ccl24
Ccl25	Ccl21	Ccl20^{++}	Ccl25
Ccl27	Ccl22	Ccl21	Ccl27
Ccl3	Ccl24	Ccl22	Ccl3
Ccl5	Ccl25	Ccl24	Ccl5
Ccl7	Ccl27	Ccl25	Ccl7
Clcf1	Ccl3	Ccl27	Clcf1
Clu	Ccl5	Ccl3	Clu
Cmtm8	Ccl7	Ccl5	Cmtm8
Cntf	Cga^{++}	Ccl7	Cntf
Cntn1	Clcf1	Cga^{++}	Cntn1
Cntn2	Clu	Clcf1	Cntn2
Copa	Cmtm8	Clu	Copa
Crlf1	Cntf	Cmtm8	Crlf1
Csf1	Cntn1	Cntf	Csf1
Cst3	Cntn2	Cntn1	Cst3
Ctf1	Copa	Cntn2	Ctf1
Ctgf	Crlf1	Copa	Ctgf
Cx3cl1	Csf1	Crlf1	Cx3cl1
Cxcl1	Cst3	Csf1	Cxcl1
Cxcl10	Ctf1	Cst3	Cxcl10
Cxcl12	Ctgf	Ctf1	Cxcl12
Cxcl13	Cx3cl1	Ctgf	Cxcl13
Cxcl16	Cxcl1	Cx3cl1	Cxcl16
Cxcl2	Cxcl10	Cxcl1	Cxcl2
Cxcl9	Cxcl12	Cxcl10	Cxcl9
Dhh	Cxcl13	Cxcl11^{+}	Dhh
Dll1	Cxcl16	Cxcl12	Dll1
Dll4	Cxcl2	Cxcl13	Dll4
Ebi3	Cxcl9	Cxcl16	Ebi3
Eda	Dhh	Cxcl2	Eda
Edn3	Dll1	Cxcl9	Edn3
Efna1	Dll4	Dhh	Efna1
Efna2	Ebi3	Dll1	Efna2
Efna4	Eda	Dll4	Efna4
Efna5	Edn3	Ebi3	Efna5

(Continued)

Table 1: Continued

Uninjured (238)	3 DPI (249)	7 DPI (258)	Uninjured, 3 DPI, and 7 DPI intersect (226)
Efnb1	Efna1	Eda	Efnb1
Efnb2	Efna2	Edn3	Efnb2
Efnb3	Efna4	Efna1	Efnb3
Epo	Efna5	Efna2	Epo
Esm1	Efnb1	Efna4	Esm1
Fgf1	Efnb2	Efna5	Fgf1
Fgf10	Efnb3	Efnb1	Fgf17
Fgf17	Epo	Efnb2	Fgf18
Fgf18	Esm1	Efnb3	Fgf19
Fgf19	Fgf1	Epo	Fgf2
Fgf2	Fgf17	Esm1	Fgf4
Fgf4	Fgf18	Fgf1	Fgf5
Fgf5	Fgf19	Fgf10	Fgf7
Fgf7	Fgf2	Fgf17	Figf
Figf	Fgf4	Fgf18	Fjx1
Fjx1	Fgf5	Fgf19	Flt3lg
Flt3lg	Fgf7	Fgf2	Fstl1
Fstl1	Figf	Fgf23^{+}	Gal
Gal	Fjx1	Fgf4	Gap43
Gap43	Flt3lg	Fgf5	Gas6
Gas6	Fstl1	Fgf7	Gdf10
Gdf10	Gal	Figf	Gdf11
Gdf11	Gap43	Fjx1	Gdf9
Gdf9	Gas6	Flt3lg	Gdnf
Gdnf	Gdf10	Fstl1	Ghrh
Ghrh	Gdf11	Gal	Gip
Gip	Gdf5^{++}	Gap43	Gmfb
Gmfb	Gdf6**	Gas6	Gmfg
Gmfg	Gdf9	Gdf10	Gnrh1
Gnrh1	Gdnf	Gdf11	Gpi
Gpi	Gh1**	Gdf5^{++}	Grp
Grp	Ghrh	Gdf9	Habp2
Guca2a	Gip	Gdnf	Hbegf
Habp2	Gmfb	Ghrh	Hcrt
Hbegf	Gmfg	Gip	Hdgf
Hcrt	Gnrh1	Gmfb	Hdgfrp3
Hdgf	Gpi	Gmfg	Hgf
Hdgfrp3	Grp	Gnrh1	Hmgb1
Hgf	Habp2	Gpi	Ifna4
Hmgb1	Hbegf	Grp	Igf1
Ifna1	Hcrt	Guca2a	Igf2
Ifna4	Hdgf	Habp2	Igfbpl1
Igf1	Hdgfrp3	Hbegf	Ihh
Igf2	Hgf	Hcrt	Il13
Igfbpl1	Hmgb1	Hdgf	Il15
Ihh	Ifna4	Hdgfrp3	Il16
Il13	Igf1	Hgf	Il17b
Il15	Igf2	Hmgb1	Il18
Il16	Igfbpl1	Ifna1	Il19
Il17b	Ihh	Ifna4	Il23a
Il18	Il12a^{++}	Igf1	Il25
Il19	Il13	Igf2	Il33
Il21*	Il15	Igfbpl1	Inha
Il23a	Il16	Ihh	Inhba
Il25	Il17b	Il12a^{++}	Inhbb
Il33	Il18	Il13	Insl3
Inha	Il19	Il15	Jag1
Inhba	Il23a	Il16	Jag2
Inhbb	Il25	Il17b	Kiss1
Insl3	Il27**	Il18	Kitlg

(Continued)

Table 1: Continued

Uninjured (238)	3 DPI (249)	7 DPI (258)	Uninjured, 3 DPI, and 7 DPI intersect (226)
Jag1	Il33	Il19	Lgals3
Jag2	Il6^{++}	Il1b^{+}	Lif
Kiss1	Inha	Il23a	Lrsam1
Kitlg	Inhba	Il25	Ltb
Lgals3	Inhbb	Il33	Mdk
Lgi1	Inhbe^{++}	Il6^{++}	Metrn
Lif	Insl3	Inha	Mif
Lrrc4	Jag1	Inhba	Mln
Lrsam1	Jag2	Inhbb	Nampt
Ltb	Kiss1	Inhbe^{++}	Nenf
Mdk	Kitlg	Insl3	Ngf
Metrn	Lgals3	Jag1	Nodal
Mif	Lgi1	Jag2	Nov
Mln	Lif	Kiss1	Npb
Mst1*	Lrsam1	Kitlg	Npff
Nampt	Ltb	Lgals3	Nppb
Nenf	Mdk	Lif	Nppc
Ngf	Metrn	Lrrc4	Nrtn
Nodal	Mif	Lrsam1	Ntf3
Nov	Mln	Ltb	Ntf4
Npb	Mmp12^{++}	Mdk	Ntn1
Npff	Mmp9^{++}	Metrn	Osm
Nppb	Nampt	Mif	Oxt
Nppc	Nell2^{++}	Mln	Pcsk1n
Nrtn	Nenf	Mmp12^{++}	Pdap1
Ntf3	Ngf	Mmp9^{++}	Pdgfa
Ntf4	Nodal	Nampt	Pdgfb
Ntn1	Nov	Nell2^{++}	Pdgfc
Osm	Npb	Nenf	Pf4
Oxt	Npff	Ngf	Pgf
Pcsk1n	Nppb	Nodal	Plg
Pdap1	Nppc	Nov	Pnoc
Pdgfa	Nrtn	Npb	Prdx2
Pdgfb	Ntf3	Npff	Prdx6
Pdgfc	Ntf4	Nppb	Prlh
Pf4	Ntn1	Nppc	Proc
Pgf	Osm	Nrg1^{+}	Prok1
Plg	Oxt	Nrtn	Prok2
Pnoc	Pcsk1n	Ntf3	Psip1
Prdx2	Pdap1	Ntf4	Pspn
Prdx6	Pdgfa	Ntn1	Pth2
Prlh	Pdgfb	Osm	Pthlh
Proc	Pdgfc	Oxt	Ptn
Prok1	Pf4	Pcsk1n	Rabep1
Prok2	Pgf	Pdap1	Rln3
Psip1	Plg	Pdgfa	Rspo1
Pspn	Pnoc	Pdgfb	Rtn1
Pth2	Ppy^{++}	Pdgfc	Rtn4
Pthlh	Prdx2	Pf4	S100b
Ptn	Prdx6	Pgf	Scgb3a1
Rabep1	Prlh	Plg	Scrn1
Rln3	Proc	Pnoc	Sct
Rspo1	Prok1	Pomc^{+}	Sema3a
Rspo3	Prok2	Ppbp^{+}	Sema3b
Rspo4*	Psip1	Ppy^{++}	Sema3c
Rtn1	Pspn	Prdx2	Sema3d
Rtn4	Pth2	Prdx6	Sema3e
S100b	Pthlh	Prlh	Sema3f
Scg3*	Ptn	Proc	Sema3g
Scgb3a1	Rabep1	Prok1	Sema4a

(Continued)

Table 1: Continued

Uninjured (238)	3 DPI (249)	7 DPI (258)	Uninjured, 3 DPI, and 7 DPI intersect (226)
Scrn1	Rln3	Prok2	Sema4b
Sct	Rspo1	Psip1	Sema4c
Sema3a	Rtn1	Pspn	Sema4d
Sema3b	Rtn4	Pth2	Sema4g
Sema3c	S100b	Pthlh	Sema5a
Sema3d	Scgb3a1	Ptn	Sema5b
Sema3e	Scrn1	Rabep1	Sema6a
Sema3f	Sct	Rln3	Sema6b
Sema3g	Sema3a	Rspo1	Sema6c
Sema4a	Sema3b	Rspo3	Sema6d
Sema4b	Sema3c	Rtn1	Sema7a
Sema4c	Sema3d	Rtn4	Serpinh1
Sema4d	Sema3e	S100b	Sfrp1
Sema4g	Sema3f	Scgb3a1	Sfrp2
Sema5a	Sema3g	Scrn1	Sfrp4
Sema5b	Sema4a	Sct	Sfrp5
Sema6a	Sema4b	Sema3a	Shh
Sema6b	Sema4c	Sema3b	Smoc1
Sema6c	Sema4d	Sema3c	Sost
Sema6d	Sema4f^{++}	Sema3d	Sparc
Sema7a	Sema4g	Sema3e	Sparcl1
Serpinh1	Sema5a	Sema3f	Spp1
Sez6	Sema5b	Sema3g	Sst
Sfrp1	Sema6a	Sema4a	Tgfa
Sfrp2	Sema6b	Sema4b	Tgfb1
Sfrp4	Sema6c	Sema4c	Tgfb2
Sfrp5	Sema6d	Sema4d	Tgfb3
Shh	Sema7a	Sema4f^{++}	Thpo
Smoc1	Serpinh1	Sema4g	Timp2
Sost	Sez6	Sema5a	Tnf
Sparc	Sfrp1	Sema5b	Tnfrsf11b
Sparcl1	Sfrp2	Sema6a	Tnfsf10
Spp1	Sfrp4	Sema6b	Tnfsf11
Sst	Sfrp5	Sema6c	Tnfsf12
Tgfa	Shh	Sema6d	Tnfsf13
Tgfb1	Smoc1	Sema7a	Tnfsf14
Tgfb2	Sost	Serpinh1	Tnfsf15
Tgfb3	Sparc	Sfrp1	Tymp
Thpo	Sparcl1	Sfrp2	Ucn2
Timp2	Spp1	Sfrp4	Ucn3
Tnf	Sst	Sfrp5	Vegfa
Tnfrsf11a*	Tgfa	Shh	Vegfb
Tnfrsf11b	Tgfb1	Smoc1	Vegfc
Tnfsf10	Tgfb2	Sost	Wnt2
Tnfsf11	Tgfb3	Sparc	Wnt5a
Tnfsf12	Thpo	Sparcl1	Wnt11
Tnfsf13	Timp2	Spp1	Xcl1
Tnfsf14	Tnf	Sst	
Tnfsf15	Tnfrsf11b	Tdgf1^{+}	
Tymp	Tnfsf10	Tgfa	
Ucn2	Tnfsf11	Tgfb1	
Ucn3	Tnfsf12	Tgfb2	
Vegfa	Tnfsf13	Tgfb3	
Vegfb	Tnfsf13b^{++}	Thpo	
Vegfc	Tnfsf14	Timp2	
Wnt2	Tnfsf15	Tnf	
Wnt5a	Tnfsf8^{++}	Tnfrsf11b	
Wnt11	Tnfsf9^{++}	Tnfsf10	
Xcl1	Tslp^{++}	Tnfsf11	
	Tymp	Tnfsf12	

(Continued)

Table 1: Continued

Uninjured (238)	3 DPI (249)	7 DPI (258)	Uninjured, 3 DPI, and 7 DPI intersect (226)
	Ucn2	Tnfsf13	
	Ucn3	Tnfsf13b^{++}	
	Vegfa	Tnfsf14	
	Vegfb	Tnfsf15	
	Vegfc	Tnfsf8^{++}	
	Wnt2	Tnfsf9^{++}	
	Wnt5a	Tslp^{++}	
	Wnt7a^{++}	Tymp	
	Wnt11	Ucn2	
	Xcl1	Ucn3	
		Vegfa	
		Vegfb	
		Vegfc	
		Wnt1^{+}	
		Wnt2	
		Wnt5a	
		Wnt7a^{++}	
		Wnt11	
		Xcl1	

Ligands identified in 3 DPI, 7 DPI, and uninjured rat sciatic nerves based on microarray analysis and our curated ligand-receptor database (modified from Yuzwa et al., 2016). Ligands were considered expressed if their expression levels exceeded that of *Ntf3* mRNA. Ligands expressed only in the uninjured nerve are indicated by one asterisk, only in the 3 DPI nerve by two asterisks, and only in the 7 DPI nerve by one plus sign. Ligands expressed in the 3 and 7 DPI nerves but not in the uninjured nerve are indicated by two plus signs. Also shown in a separate column are ligands expressed in all populations (intersect).
* uninjured only.
** 3 DPI only.
$^{+}$ 7 DPI only.
$^{++}$ 3 DPI and 7 DPI intersect.

contralateral sciatic nerve tissue was harvested at 9 DPI. Nerves were fixed overnight in 4% paraformaldehyde at 4°C, then cryoprotected overnight in 30% sucrose at 4°C. Nerves were then cryosectioned longitudinally at 12 μm and immunostained for PDGFRα, S100β and counterstained with Hoechst 33258 (Sigma). Images were acquired with a 20× objective lens on a Zeiss AxioImager M2 microscope with a light source, camera, and software setup as described above.

Antibodies

The following primary antibodies were used in this study at the indicated dilutions: rabbit anti-Fibronectin (1:500; Sigma; catalog #F3648), goat anti-PDGFRα (1:250 for cultures and 1:500 for sections; R&D Systems, catalog #AF1062), rabbit anti-S100β (1:500; Dako; catalog #Z0311), and mouse anti-βIII-tubulin (1:1000; BioLegend; catalog #801202). The following secondary antibodies were used in this study (all from Thermo Fisher Scientific and used at a dilution of 1:500, or two drops/ml in the case of the ReadyProbe): donkey anti-goat IgG Alexa Fluor 647 (catalog #A21447), donkey anti-mouse IgG Alexa Fluor 488 (catalog #A21202), donkey anti-mouse IgG ReadyProbes Alexa Fluor 488 (catalog #R37114), donkey anti-rabbit IgG Alexa Fluor 488 (catalog #A21206), and donkey anti-rabbit IgG Alexa Fluor 555 (catalog #A31572).

FISH

Single molecule FISH was performed on 9 DPI adult *Pdgfra*$^{EGFP/+}$ nerve sections with probes targeting *Vegfc* (catalog #492701), *Ccl11* (catalog #464031), and *Angpt1* (catalog #449271) mRNAs using the RNAscope kit (Advanced Cell Diagnostics), according to the manufacturer's instructions. Briefly, freshly dissected nerves were fixed overnight in 4% PFA at 4°C and cryopreserved in 30% sucrose overnight (at 4°C) under RNase-free conditions using RNase-free reagents. Nerves were cryosectioned sagittally at a thickness of 14 μm. Sections were washed with ethanol, followed by tissue pretreatment (1:10 dilution) for 20 min, probe hybridization, and signal amplification. Positive signal was identified as red punctate dots. Digital images were acquired with a Quorum Spinning-Disk confocal microscope system using Volocity acquisition software (PerkinElmer). Z-stack confocal images were taken with an optical slick thickness of 0.3 μm, and projected Z-stacked images are shown. The scrambled probe provided with the RNAscope kit was used as a negative control.

Statistical analyses

With the exception of analyses related to the microarray and scRNA-seq data, all statistics were performed using GraphPad Prism 8 (GraphPad Software). Standard deviation values are given for the genes and transcripts per cell values for the scRNA-seq data. Scatter plots show standard error of the mean. Statistical significance was considered reached at $p < 0.05$. All statistical tests and conditions are described in the text. Graphs were generated in both GraphPad Prism 8 and Excel (Microsoft).

Data/software accessibility

Raw scRNA-seq and microarray datasets have been deposited in the GEO database under the ID codes GEO: GSE147285 and GSE146958. The Cellcellinteractnet code, the updated ligand-receptor database, and the raw proteomics data are available on request.

Results

Defining growth factors made within the injured and uninjured peripheral nerve

We hypothesized that peripheral nerves promote axon growth in part due to ligand secretion by resident nerve *Pdgfra*-positive mesenchymal cells. To test this idea, we analyzed the sciatic nerve, which contains axons from sensory, sympathetic and motor neurons. Initially, we confirmed that *Pdgfr*α-positive mesenchymal cells are found within the nerve endoneurium where axons are located. To do this, we analyzed control and injured sciatic nerve sections from mice carrying a transgene where EGFP is driven by *Pdgfra* regulatory sequences, and which thus tags *Pdgfra*-positive mesenchymal cells (*Pdgfra*$^{Egfp/+}$ mice; Hamilton et al., 2003). We resected sciatic nerves from these mice, and at 9 DPI immunostained for the PDGFRα protein product and for the Schwann cell marker S100β. For comparison, we performed a similar analysis of the contralateral uninjured sciatic nerve. This

Table 2: Gene abundance analysis of ligand mRNAs in the combined 3 and 9 DPI nerve scRNA-seq dataset

	Gene abundance (%)						
Gene	Epineurial/ perineurial	Endoneurial	Combined mesenchymal	VSM/ pericytes	Endothelial cells	Schwann cells	Immune
Adm**	11.6	34.2	17.4	2.8	BT	BT	BT
Agt*	2.2	10.4	4.2	13.2	BT	BT	BT
Angpt1**	17.3	23.7	18.9	21.1	2.1	BT	BT
Angpt2*	3.2	BT	2.6	29.0	18.5	BT	BT
Angpt4**	2.6	BT	2.0	BT	BT	BT	BT
Apln*	2.0	6.0	3.0	BT	11.2	BT	BT
Artn	BT	BT	BT	BT	BT	3.3	BT
Bdnf*	2.6	BT	2.3	2.2	BT	9.5	BT
Bmp1**	53.1	35.7	48.7	14.8	10.8	50.6	2.7
Bmp2*	BT	3.0	2.1	24.6	3.3	BT	BT
Bmp4*	2.8	BT	2.3	BT	16.6	BT	BT
Bmp5*	BT	3.8	BT	11.7	BT	BT	BT
Bmp7**	2.2	31.1	9.5	BT	BT	BT	BT
Btc*	BT	2.0	2.0	BT	BT	60.4	BT
Cck	BT	BT	BT	5.0	BT	BT	BT
Ccl11**	29.4	87.0	44.0	34.1	7.5	6.2	4.7
Ccl19	BT	BT	BT	2.5	BT	BT	BT
Ccl2**	27.0	81.5	40.9	21.1	12.9	13.8	15.2
Ccl24	BT	BT	BT	BT	BT	BT	2.4
Ccl25	BT	BT	BT	BT	BT	2.2	BT
Ccl3*	3.0	4.2	3.3	3.2	2.3	3.1	13.7
Ccl5*	3.0	2.8	2.9	BT	BT	BT	6.4
Ccl7**	21.8	78.0	36.1	10.4	7.7	6.6	7.7
Ccl9**	11.8	75.0	27.9	4.1	6.1	5.9	22.5
Clcf1*	3.7	4.5	3.9	BT	4.3	16.0	BT
Crlf1*	3.2	25.9	9.0	BT	BT	35.2	BT
Csf1**	32.3	31.2	32.0	13.9	11.7	11.6	3.3
Ctgf**	25.7	36.9	28.5	25.6	33.3	3.5	2.2
Cx3cl1**	4.0	14.4	6.7	BT	5.3	BT	BT
Cxcl1**	27.4	59.3	35.5	38.2	29.0	11.7	9.5
Cxcl10**	2.6	9.8	4.4	3.2	4.1	6.6	2.0
Cxcl12**	46.6	52.6	48.1	33.8	44.0	5.9	5.0
Cxcl13**	6.7	BT	5.1	BT	BT	BT	BT
Cxcl16*	6.3	4.2	5.7	2.8	3.7	BT	15.7
Cxcl2*	12.3	22.9	15.0	7.3	10.4	7.2	22.9
Cxcl9**	5.3	2.7	4.6	BT	4.6	BT	BT
Dhh	BT	BT	BT	BT	6.3	30.1	BT
Dll1	BT	BT	BT	BT	6.4	BT	BT
Dll4	BT	BT	BT	BT	10.0	BT	BT
Ebi3	BT	BT	BT	BT	BT	BT	2.5
Eda**	6.0	9.7	7.0	BT	BT	3.7	BT
Edn3**	3.1	BT	2.3	BT	BT	BT	BT
Efna1*	3.4	8.0	4.5	BT	24.9	BT	BT
Efna2**	3.3	3.8	3.4	2.5	BT	3.5	BT
Efna4**	4.8	6.2	5.2	3.2	BT	4.0	BT
Efna5**	5.1	6.7	5.5	BT	BT	BT	BT
Efnb1**	22.5	39.2	26.8	9.5	11.4	11.4	2.3
Efnb2**	13.0	42.4	20.4	4.1	16.4	4.0	BT
Fgf1*	7.1	4.8	6.5	9.8	BT	2.2	BT
Fgf10**	7.5	BT	5.8	BT	BT	BT	BT
Fgf18**	8.5	BT	6.8	BT	BT	BT	BT
Fgf5	BT	BT	BT	BT	BT	19.4	BT
Fgf7**	26.1	37.7	29.1	3.2	BT	12.5	BT
Figf**	15.8	11.2	14.6	BT	BT	BT	BT
Fstl1**	96.8	96.5	96.7	85.8	56.5	33.4	19.6
Gas6**	44.3	2.3	35.9	13.6	22.5	2.2	6.2
Gdf10**	24.5	4.7	19.5	BT	3.3	2.0	BT
Gdf11**	4.3	10.4	5.9	10.1	3.4	3.9	BT
Gdnf	BT	BT	BT	BT	BT	21.8	BT
Gmfb**	23.4	34.6	26.3	10.7	17.5	27.9	11.6

(Continued)

Table 2: Continued

	Gene abundance (%)						
Gene	Epineurial/ perineurial	Endoneurial	Combined mesenchymal	VSM/ pericytes	Endothelial cells	Schwann cells	Immune
Gmfg	BT	BT	BT	BT	5.7	BT	17.9
Gnrh1**	BT	2.3	BT	BT	BT	BT	BT
Grp	BT	BT	BT	BT	3.4	BT	BT
Hbegf*	6.5	5.2	6.2	10.7	19.2	43.9	BT
Hgf**	4.0	BT	3.1	BT	BT	BT	BT
Igf1**	76.6	84.3	78.6	15.8	31.7	16.7	13.8
Igf2*	15.5	8.2	13.6	16.4	6.1	2.4	BT
Il15**	2.2	9.0	3.9	BT	7.4	BT	BT
Il16*	BT	3.0	BT	BT	2.3	BT	7.9
Il18**	6.4	5.3	6.1	BT	BT	BT	2.5
Il1b*	5.6	7.3	6.1	5.0	5.7	5.0	18.6
Il33**	39.1	63.3	45.3	2.5	3.6	6.4	2.2
Il6*	7.2	7.0	7.1	12.6	15.2	BT	BT
Inha**	BT	2.0	BT	BT	BT	BT	BT
Inhba**	12.6	11.9	12.4	9.8	BT	BT	1.9
Inhbb**	BT	12.7	4.5	BT	9.2	BT	BT
Jag1*	20.3	17.2	19.5	33.1	17.8	8.4	2.8
Jag2	BT	BT	BT	BT	8.4	BT	BT
Lif**	2.6	13.2	5.3	BT	BT	5.9	BT
Ltb	BT	BT	BT	BT	BT	BT	12.2
Mdk**	39.0	51.1	42.1	9.1	4.0	25.1	BT
Metrn*	7.1	14.5	9.0	8.5	3.0	57.8	2.6
Mif**	32.7	40.2	34.6	26.5	31.4	29.5	26.0
Nenf**	54.7	59.1	55.8	42.6	29.4	50.8	8.4
Ngf*	2.4	6.7	3.5	10.4	BT	BT	BT
Nov**	25.0	11.4	21.5	6.0	5.4	5.0	BT
Nppc**	2.2	5.3	3.0	BT	BT	BT	BT
Ntf3*	3.4	BT	2.9	4.4	4.8	BT	BT
Ntn1**	19.2	25.5	20.8	BT	6.0	4.6	BT
Osm	BT	BT	BT	BT	BT	BT	8.3
Pdgfa*	12.1	7.8	11.0	49.5	6.8	50.6	5.7
Pdgfb	BT	BT	BT	2.5	22.3	BT	2.4
Pdgfc**	7.2	BT	5.8	6.0	4.3	BT	BT
Pf4*	2.3	4.3	2.8	BT	BT	BT	10.0
Pgf**	2.0	12.2	4.6	7.6	BT	BT	BT
Pomc**	BT	3.3	BT	BT	3.3	2.2	BT
Pthlh**	10.4	13.7	11.2	BT	BT	2.4	BT
Ptn*	35.9	10.4	29.4	2.2	19.9	52.5	BT
Rspo1**	2.2	BT	BT	BT	BT	BT	BT
Rspo3**	6.0	BT	4.7	BT	2.4	BT	BT
Rtn4*	57.9	68.3	60.5	51.7	47.1	73.6	28.3
Sema3b*	7.7	12.4	8.9	BT	BT	53.8	BT
Sema3c**	35.4	9.0	28.7	BT	BT	25.1	BT
Sema3d**	9.6	2.0	7.6	BT	BT	BT	BT
Sema3e*	2.0	BT	BT	BT	BT	31.0	BT
Sema3f*	2.3	4.5	2.9	2.8	14.5	2.9	BT
Sema3g*	BT	3.0	BT	BT	11.8	9.0	BT
Sema4a*	BT	3.7	2.0	BT	BT	BT	6.9
Sema4b*	2.0	3.2	2.3	3.5	BT	7.7	BT
Sema4c*	8.4	12.0	9.3	6.3	10.2	16.0	BT
Sema4d	BT	BT	BT	BT	BT	BT	14.5
Sema4f	BT	BT	BT	BT	BT	18.3	BT
Sema5a*	4.3	3.5	4.1	13.2	BT	BT	BT
Sema5b	BT	BT	BT	10.4	BT	BT	BT
Sema6a*	4.0	14.5	6.7	BT	35.6	9.4	BT
Sema6b*	3.1	7.0	4.1	BT	18.1	BT	BT
Sema6c**	7.2	4.0	6.4	BT	BT	2.0	BT
Sema6d*	5.9	11.7	7.3	18.9	9.5	16.7	BT
Sema7a*	7.5	19.5	10.5	BT	17.4	20.0	BT
Sfrp1**	42.3	31.9	39.6	4.1	3.4	8.8	BT

(Continued)

Table 2: Continued

Gene	Gene abundance (%)						
	Epineurial/ perineurial	Endoneurial	Combined mesenchymal	VSM/ pericytes	Endothelial cells	Schwann cells	Immune
Sfrp2**	29.6	6.5	23.8	2.2	3.3	BT	2.4
Sfrp4**	61.5	51.9	59.1	8.5	9.4	11.0	6.3
Sfrp5**	8.8	3.2	7.4	BT	2.1	8.1	BT
Shh	BT	BT	BT	BT	BT	12.8	BT
Tgfa	BT	BT	BT	BT	2.6	BT	BT
Tgfb1*	6.5	12.0	7.9	6.0	13.4	10.3	12.4
Tgfb2*	13.3	2.7	10.6	16.4	5.1	6.2	BT
Tgfb3*	26.3	8.7	21.8	27.4	2.3	4.6	BT
Tnf*	BT	2.2	BT	BT	BT	BT	7.7
Tnfrsf11b**	6.6	BT	5.0	BT	BT	BT	BT
Tnfsf10	BT	BT	BT	BT	22.8	1.1	BT
Tnfsf12**	15.0	16.7	15.4	11.4	9.1	6.8	7.3
Tnfsf14	BT	BT	BT	BT	BT	BT	2.3
Tnfsf8**	3.8	2.0	3.3	BT	BT	BT	BT
Tnfsf9**	2.8	5.8	3.6	5.4	BT	BT	BT
Tslp**	2.5	4.8	3.1	2.8	2.4	BT	BT
Ucn2	BT	BT	BT	BT	BT	15.0	BT
Vegfa**	28.2	18.7	25.8	3.8	4.1	2.6	7.0
Vegfb*	7.1	7.0	7.0	7.3	6.0	8.4	3.3
Vegfc*	2.0	BT	BT	BT	5.5	BT	BT
Wnt11**	2.7	BT	2.2	BT	BT	BT	BT
Wnt2**	6.5	BT	5.3	BT	BT	BT	BT
Wnt5a**	15.9	14.4	15.5	4.4	BT	BT	BT

The combined 3 and 9 DPI scRNA-seq dataset (Fig. 1*E*) was analyzed for the percentage of cells within the defined nerve cell types that expressed ligand mRNAs as identified by microarray analysis (Table 1). Ligand mRNAs were only considered to be detected if they were expressed in at least 2% of cells within at least one cell type. BT = below threshold and indicates that <2% of cells detectably expressed the ligand mRNA. Ligands annotated with one asterisk in the left-most column were expressed in ≥2% *Pdgfra*-positive mesenchymal cells and two asterisks indicate ligands with the highest expression in either the epineurial/perineurial or endoneurial *Pdgfra*-positive mesenchymal cells.

* >2% expression in *Pdgfra*-positive cells.

** >2% expression and highest expression in *Pdgfra*-positive cells.

analysis identified many *Pdgfra*-EGFP-positive, PDGFRα protein-positive cells within the endoneurium of both the control and injured nerves (Fig. 1*A*), consistent with a similar recent analysis in Carr et al. (2019).

Having confirmed the presence of many mesenchymal cells in the endoneurium, we obtained an overview of ligands expressed in the sciatic nerve by performing global transcriptomic analysis of rat sciatic nerves that were either uninjured or that were injured by resection 3 or 7 d earlier. In all cases, we isolated total RNA from four independent biological replicates of the distal nerve segment and analyzed samples on Affymetrix GeneChip Rat Gene 2.0 ST Arrays. To define ligand mRNAs, we used a curated database of secreted ligands and their cognate receptors (Yuzwa et al., 2016), establishing an expression cutoff by considering only mRNAs expressed at similar or higher levels than neurotrophin 3 (*Ntf3*) mRNA, which is expressed in and important for peripheral nerves. *Ntf3* mRNA was expressed in the top 67.6%, 70.3%, and 71.2% of mRNAs in control, 3-d injured, and 7-d injured distal nerves, respectively. This analysis identified 238, 249, and 258 ligand mRNAs in the uninjured, 3-d injured, and 7-d injured nerves, respectively (Fig. 1*B*; Table 1). Most (226) were detected in all three conditions, but 31 ligand mRNAs were found only in the injured nerves, including *Areg*, *Ccl20*, *Il6*, and *Wnt7a* and five ligands were detected only in the control nerve, including *Il21* (Table 1).

Single-cell profiling defines similarities between peripheral nerves at 3 and 9 DPI

The microarray analysis defined the global nerve ligand environment. To ask which nerve cells express these ligands, we performed single-cell RNA sequencing (scRNA-seq), initially analyzing the distal sciatic nerve 3 d following a nerve transection. To do this, we dissociated the distal transected sciatic nerve, removed myelin debris with myelin-removal beads, and sequenced cells using high-throughput, droplet-based scRNA-seq (for details of all sequencing runs, see Materials and Methods). To analyze these individual transcriptomes, we then used a pipeline that incorporates extensive low-level data quality analysis with visualization and clustering methods that use evidence-based parameter selection (Innes and Bader, 2019), as previously described (Yuzwa et al., 2017; Carr et al., 2019; Storer et al., 2020). Genes with high variance were then used to compute principal components as inputs for projecting cells in two dimensions using t-SNE followed by graph-based clustering (Butler et al., 2018) with a range of resolution parameters.

This analysis defined nine distinct clusters containing 2075 cells in the 3-d injured sciatic nerve dataset (Fig. 1*C*). To assign cell types to these different clusters, we used well-characterized marker genes (for all cell type-specific marker genes used, see Materials and Methods; Fig. 1*D*; Extended Data Fig. 1-1*A*). This approach

Table 3: Gene abundance of injured nerve ligand mRNAs in the uninjured nerve scRNA-seq dataset

	Gene abundance (%)						
Gene	Epineurial/ perineurial	Endoneurial	VSM/ pericytes	Endothelial	Schwann (non-myelinating)	Schwann (myelinating)	Immune
Adm**	14.4	8.4	BT	3.6	BT	BT	2.9
Agt**	2.9	BT	BT	BT	BT	BT	2.9
Angpt1*	12.2	BT	12.4	BT	BT	BT	BT
Angpt2*	2.2	BT	21.1	13.6	BT	6.0	BT
Angpt4**	6.2	BT	BT	BT	BT	BT	2.9
Apln	BT	BT	BT	7.1	BT	BT	BT
Bdnf	BT	BT	3.1	BT	BT	BT	BT
Bmp1**	42.0	16.1	6.8	6.2	4.6	4.8	BT
Bmp2*	3.5	BT	15.5	BT	BT	BT	11.4
Bmp4**	18.6	6.5	BT	17.6	BT	BT	BT
Bmp5*	2.4	6.8	8.1	BT	BT	BT	BT
Bmp7**	3.1	11.9	BT	BT	BT	BT	BT
Cck	BT	BT	3.1	BT	BT	BT	BT
Ccl11**	35.8	88.3	22.4	9.0	5.3	3.6	2.9
Ccl19**	6.2	BT	5.0	BT	BT	BT	BT
Ccl2*	2.2	16.1	4.3	BT	BT	BT	28.6
Ccl3	BT	BT	BT	BT	BT	BT	11.4
Ccl5	BT	BT	BT	BT	BT	BT	11.4
Ccl7**	6.0	35.5	2.5	5.0	2.7	3.6	8.6
Ccl9**	BT	16.6	BT	BT	BT	2.4	14.3
Clcf1	BT	BT	BT	4.0	BT	BT	2.9
Csf1**	31.9	10.0	4.3	15.2	8.8	2.4	8.6
Ctgf*	16.6	2.1	10.6	28.8	BT	BT	BT
Cx3cl1	BT	BT	BT	11.2	BT	2.4	BT
Cxcl1**	17.5	52.3	18.6	15.0	11.5	6.0	8.6
Cxcl10	BT	BT	BT	BT	BT	BT	5.7
Cxcl12*	34.3	60.0	39.8	78.1	13.4	3.6	2.9
Cxcl13**	16.2	BT	BT	BT	BT	BT	BT
Cxcl16**	10.0	BT	BT	3.3	BT	BT	2.9
Cxcl2	BT	BT	BT	BT	BT	BT	8.6
Cxcl9	BT	BT	BT	3.8	BT	BT	BT
Dhh	BT	BT	BT	3.8	13.4	28.9	BT
Dll1	BT	BT	BT	10.0	BT	BT	BT
Dll4	BT	BT	BT	18.1	BT	BT	BT
Eda**	5.1	7.7	BT	BT	3.4	2.4	2.9
Edn3**	8.4	BT	BT	BT	BT	BT	BT
Efna1*	4.2	4.0	3.7	30.2	BT	BT	BT
Efna2	BT	BT	BT	BT	BT	BT	2.9
Efna5**	4.4	BT	BT	BT	BT	BT	BT
Efnb1**	9.5	14.3	2.5	10.5	6.1	3.6	2.9
Efnb2*	3.5	11.0	4.3	15.7	BT	BT	BT
Fgf1*	4.9	BT	10.6	BT	10.3	26.5	2.9
Fgf10**	9.1	BT	BT	BT	BT	BT	BT
Fgf18**	8.4	BT	BT	BT	BT	BT	BT
Fgf7**	28.8	6.3	2.5	2.4	BT	8.4	BT
Figf**	12.8	BT	BT	3.1	BT	BT	BT
Fstl1**	90.9	75.5	47.2	34.5	29.8	10.8	8.6
Gas6**	61.5	9.3	18.0	49.8	3.8	6.0	2.9
Gdf10**	39.4	4.0	BT	3.1	BT	2.4	2.9
Gdf11*	BT	4.2	4.3	BT	BT	BT	2.9
Gmfb*	14.2	8.6	5.6	10.5	7.6	15.7	5.7
Gmfg	BT	BT	BT	3.1	BT	BT	28.6
Hbegf*	BT	2.3	12.4	17.4	25.2	8.4	5.7
Igf1**	56.9	43.9	8.1	17.6	2.7	BT	BT
Igf2*	3.5	8.6	7.5	14.3	BT	BT	BT
Il15*	BT	4.7	BT	5.0	BT	BT	BT
Il16	BT	BT	BT	3.1	BT	8.4	25.7
Il18**	7.1	3.7	BT	BT	BT	BT	BT
Il1b	BT	BT	BT	BT	BT	BT	8.6
Il33**	29.4	71.5	BT	5.0	3.4	2.4	2.9

(Continued)

Table 3: Continued

	Gene abundance (%)						
Gene	Epineurial/ perineurial	Endoneurial	VSM/ pericytes	Endothelial	Schwann (non-myelinating)	Schwann (myelinating)	Immune
Il6*	2.4	2.8	4.3	5.2	BT	BT	BT
Inha**	2.0	BT	BT	BT	BT	BT	BT
Inhba	BT	BT	8.1	BT	BT	BT	BT
Jag1*	12.4	4.2	20.5	19.3	BT	BT	BT
Jag2	BT	BT	BT	9.5	BT	BT	BT
Lif**	BT	3.0	BT	BT	BT	BT	2.9
Ltb	BT	BT	BT	BT	BT	BT	11.4
Mdk**	8.2	16.4	BT	BT	3.4	BT	2.9
Metrn*	2.7	BT	2.5	BT	14.5	12.0	2.9
Mif*	14.8	14.7	19.3	31.0	13.7	18.1	31.4
Nenf**	54.2	48.6	28.0	31.0	26.7	19.3	17.1
Ngf*	BT	2.6	11.2	BT	BT	BT	BT
Nov**	19.2	7.9	6.8	5.0	7.3	15.7	BT
Nppc**	BT	2.6	BT	BT	BT	BT	BT
Ntf3*	4.0	BT	11.8	5.7	BT	BT	BT
Ntn1**	31.2	12.6	BT	6.7	BT	BT	BT
Osm	BT	BT	BT	BT	BT	BT	8.6
Pdgfa*	7.3	BT	32.9	9.8	14.1	16.9	5.7
Pdgfb	BT	BT	3.1	28.1	BT	BT	BT
Pdgfc**	3.3	BT	BT	BT	BT	BT	2.9
Pgf*	2.4	4.7	7.5	BT	BT	BT	BT
Pomc	BT	BT	BT	5.0	BT	BT	2.9
Pthlh**	12.6	7.2	BT	BT	BT	BT	BT
Ptn*	7.7	4.0	BT	45.7	56.5	BT	5.7
Rspo1**	8.4	BT	BT	BT	BT	BT	BT
Rtn4**	37.6	33.4	21.7	33.8	24.0	21.7	11.4
Sema3b*	15.5	32.7	3.1	3.1	44.3	56.6	BT
Sema3c**	38.1	9.1	2.5	3.6	9.2	2.4	BT
Sema3d**	13.7	BT	BT	BT	BT	BT	BT
Sema3e*	3.5	BT	BT	BT	14.5	BT	BT
Sema3f	BT	BT	2.5	12.6	BT	BT	BT
Sema3g*	BT	3.0	BT	18.8	2.7	2.4	BT
Sema4a	BT	BT	BT	BT	BT	BT	5.7
Sema4b**	2.0	2.1	BT	BT	BT	BT	BT
Sema4c*	6.6	6.3	BT	11.2	5.7	22.9	BT
Sema4d	BT	BT	BT	BT	2.3	BT	8.6
Sema5a*	2.7	3.5	6.8	BT	BT	9.6	BT
Sema6a*	2.7	18.7	BT	26.2	2.7	2.4	2.9
Sema6b*	2.0	2.8	BT	12.4	BT	BT	2.9
Sema6c*	BT	3.3	BT	BT	BT	7.2	BT
Sema6d*	3.3	3.5	8.1	9.5	25.2	13.3	BT
Sema7a	BT	BT	BT	28.8	8.4	BT	2.9
Sfrp1**	45.4	15.0	2.5	4.0	6.9	BT	BT
Sfrp2**	45.1	5.1	BT	5.2	3.8	6.0	5.7
Sfrp4**	61.7	8.6	3.1	9.8	5.3	6.0	8.6
Sfrp5*	18.8	5.8	3.7	4.5	26.0	31.3	5.7
Tgfa	BT	BT	BT	4.0	BT	BT	BT
Tgfb1*	2.0	3.3	BT	7.9	BT	BT	17.1
Tgfb2**	8.2	2.8	5.6	6.0	BT	BT	BT
Tgfb3**	16.8	2.3	16.1	3.1	BT	BT	BT
Tnf	BT	BT	BT	BT	BT	BT	11.4
Tnfsf10	BT	BT	BT	18.6	BT	BT	BT
Tnfsf12**	13.3	17.8	6.2	12.6	9.9	9.6	5.7
Tnfsf14	BT	BT	BT	BT	BT	BT	8.6
Tnfsf9*	BT	4.0	BT	BT	5.7	BT	BT
Tslp**	3.5	BT	BT	BT	BT	BT	2.9
Vegfa**	14.2	7.9	8.1	6.2	BT	2.4	2.9
Vegfb*	5.5	4.7	6.2	5.7	3.4	7.2	BT
Vegfc*	3.3	BT	BT	6.2	BT	BT	BT

(Continued)

Table 3: Continued

	Gene abundance (%)						
Gene	Epineurial/ perineurial	Endoneurial	VSM/ pericytes	Endothelial	Schwann (non-myelinating)	Schwann (myelinating)	Immune
Wnt11**	6.6	BT	BT	BT	BT	BT	2.9
Wnt2**	6.9	BT	BT	BT	BT	BT	BT
Wnt5a**	17.5	10.3	BT	BT	BT	BT	BT

The uninjured nerve scRNA-seq dataset (Fig. 2*C*) was analyzed to determine the percentage of cells within a given cell type that detectably expressed (≥2%) the 143 injured nerve ligand mRNAs (Table 2). Cell populations were defined as for the injured nerve analysis except that Schwann cells were divided into myelinating (cluster 8) and non-myelinating (cluster 4) cells. BT = below threshold and indicates that <2% of cells detectably expressed the ligand mRNA. Ligands annotated with one asterisk in the leftmost column were expressed in ≥2% *Pdgfra*-positive mesenchymal cells and two asterisks indicate ligands with the highest expression in either the epineurial/perineurial or endoneurial *Pdgfra*-positive mesenchymal cells.

* >2% expression in *Pdgfra*-positive cells.

** >2% expression and highest expression in *Pdgfra*-positive cells.

identified *Pecam1*/*Cd31*-positive endothelial cells, *Sox10*-positive Schwann cells, *Aif1*/*Iba1*-positive macrophages, *Trbc2*-positive immune cells, and *Rgs5*-positive VSM and pericyte cells. As previously seen in the 9-d injured sciatic nerve (Carr et al., 2019), we also identified distinct populations of *Pdgfra*-positive nerve mesenchymal cells, including *Dpp4*-positive epineurial cells (clusters 1, 4, and 6) and *Wif1*-positive endoneurial cells (cluster 3).

We next asked whether distal sciatic nerve cells were similar at 3 and 9 d following a transection, taking advantage of a recently published 9 DPI scRNA-seq analysis where nerve cells were also isolated using myelin beads (Carr et al., 2019). To do this, we extracted the relevant raw transcriptomes from the previously published 9 DPI dataset, combined them with the 3 DPI raw transcriptomes we had generated, and put this combined 5395 cell dataset through our computational pipeline, which corrects for any differences in sequencing depth and library size. As seen with the 3 DPI dataset alone, marker gene analysis (Fig. 1*E*; Extended Data Fig. 1-1*B*,*C*) identified clusters containing endothelial cells, VSM/pericyte cells, Schwann cells, macrophages, immune cells, and *Pdgfra*-positive mesenchymal cells. These mesenchymal cells included *Etv1*-positive endoneurial cells (cluster 5), *Pcolce2*-positive epineurial cells (cluster 3), *Msln*-positive perineurial cells (cluster 10), and differentiating nerve bridge cells enriched for *Dlk1* (cluster 1; Fig. 1*E*; Extended Data Fig. 1-1*B*,*C*). Analysis of the dataset of origin (Fig. 1*F*) showed that all cell type clusters were comprised of intermingled 3 and 9 DPI cells except for cluster 7, which included *Cd19*-positive B cells that came almost exclusively (99.4%) from the 9 DPI time point (Extended Data Fig. 1-1*B*). Similar results were obtained following batch correction. Thus, 3- and 9-d distal transected sciatic nerve cells are transcriptionally similar, although there is an increased proportion of B cells at 9 d.

Schwann cells, mesenchymal cells, vasculature, and immune cells make distinct contributions to the peripheral nerve ligand environment

To understand how the different cell types contributed to the injured nerve environment, we analyzed the combined 3- and 9-d scRNA-seq dataset for expression of ligands identified in the microarray analysis (Fig. 1*B*; Table 1), excluding extracellular matrix proteins and ligands without well-defined, receptor-mediated paracrine roles. This analysis identified 143 ligands that were detectably expressed in ≥2% of at least one nerve cell type (Table 2), including many well-known nerve ligands such as the neurotrophins NGF, BDNF, and NT3, the Ret family ligands GDNF, Artemin and Neurturin, DHH, and various Semaphorin and FGF family members. Notably, *Pdgfra*-positive mesenchymal cells detectably expressed more ligand mRNAs than any other nerve cell type (118/143, or 82.5%; Fig. 1*G*; Table 2). Of these, 71 were expressed, proportionately, in more mesenchymal cells than any other cell type (Fig. 1*H*; Table 2), and some were highly mesenchymally enriched, including *Adm*, *Bmp7*, *Cxcl13*, *Fgf7*, *Fgf10*, *Gdf10*, *Hgf*, *Il33*, *Ntn1*, *Pthlh*, and *Wnt5a* (Fig. 1*I*; Extended Data Fig. 1-1*D*). A total of 39 of these mesenchymal ligands were most highly expressed in the endoneurial mesenchymal cells that are closely apposed to Schwann cells and axons (Fig. 1*G*; Table 2).

Schwann cells were a second major source of injured nerve ligands, detectably expressing 74 ligand mRNAs (Fig. 1*G*,*H*; Table 2). A total of 23 of these were expressed in more Schwann cells than any other cell type, including *Artn*, *Bdnf*, *Btc*, *Clcf1*, *Crlf1*, *Dhh*, *Fgf5*, *Gdnf*, *Hbegf*, *Sema3e*, *Sema4f*, *Shh*, and *Ucn2* (Fig. 2*A*; Extended Data Fig. 2-1*A*; Table 2). Of the other cell types, endothelial and VSM/pericyte cells expressed 18 and 15 ligand mRNAs, respectively, at the highest levels (Fig. 1*G*,*H*; Table 2). These included *Bmp4* and *Pdgfb* mRNAs in endothelial cells and *Bmp2* and *Ngf* in VSM/pericytes (Fig. 2*B*). The immune cells expressed 16 ligand mRNAs in the highest proportions including well-characterized immune ligands like *Osm* and *Tnf* (Figs. 1*G*,*H*, 2*B*; Table 2). Thus, ligands known to be important for axon growth and tissue regeneration are expressed by diverse nerve cell populations after injury.

Single-cell transcriptional profiling of uninjured and developing nerves

We asked whether this cellular profile of ligand expression was exclusive to the injured nerve by analyzing single-cell transcriptional datasets of the uninjured and developing sciatic nerves. For the uninjured nerve, we used a dataset that was previously analyzed for *Pdgfra*-positive mesenchymal cells (Carr et al., 2019), but not for other cell types. Analysis of the entire 1841 uninjured

Table 4: Gene abundance of injured nerve ligand mRNAs in the neonatal nerve scRNA-seq dataset

	Gene abundance (%)					
Gene	Epineurial	Endoneurial/perineurial	VSM/pericytes	Endothelial	Schwann cells	Immune cells
Adm**	5.1	4.7	BT	3.0	BT	BT
Agt*	2.5	BT	12.2	BT	BT	BT
Angpt1*	5.1	BT	11.1	BT	BT	BT
Angpt2*	5.5	BT	18.1	6.9	2.0	BT
Apln	BT	BT	BT	29.0	BT	BT
Bdnf	BT	BT	3.6	BT	BT	BT
Bmp1**	34.2	21.5	10.9	11.0	10.8	BT
Bmp2	BT	BT	6.7	3.4	BT	8.7
Bmp4*	3.4	BT	BT	6.9	BT	BT
Bmp5	BT	BT	13.4	BT	BT	BT
Bmp7**	BT	3.9	BT	BT	BT	BT
Ccl11**	9.4	49.8	20.0	BT	BT	2.6
Ccl2*	BT	10.0	9.9	BT	BT	20.0
Ccl24	BT	BT	BT	BT	BT	27.0
Ccl3	BT	BT	BT	BT	BT	16.5
Ccl5	BT	BT	BT	BT	BT	2.6
Ccl7**	3.4	18.5	2.7	BT	BT	14.8
Ccl9	BT	BT	BT	BT	BT	28.7
Clcf1	BT	BT	BT	2.3	BT	BT
Csf1**	15.2	4.3	4.8	4.1	2.4	BT
Ctgf*	7.1	4.0	7.4	7.4	BT	BT
Cxcl1*	BT	12.4	20.6	2.5	BT	2.6
Cxcl10	BT	BT	BT	BT	2.6	BT
Cxcl12**	18.9	37.2	23.1	33.8	BT	BT
Cxcl16	BT	BT	BT	4.2	BT	11.3
Cxcl2	BT	BT	BT	BT	BT	4.3
Cxcl9**	BT	2.1	BT	BT	BT	BT
Dhh	BT	BT	2.3	7.1	25.6	3.5
Dll1	BT	BT	BT	5.3	BT	BT
Dll4	BT	BT	BT	15.2	BT	BT
Ebi3	BT	BT	BT	BT	BT	13.0
Eda**	7.1	9.0	BT	BT	4.4	BT
Edn3**	4.1	3.5	BT	BT	BT	BT
Efna1*	3.1	4.3	BT	34.0	BT	BT
Efna2**	2.9	3.3	BT	BT	2.9	BT
Efna4**	2.6	3.6	BT	BT	BT	BT
Efna5**	6.0	4.0	BT	BT	2.3	BT
Efnb1**	18.3	30.6	6.3	9.7	9.1	2.6
Efnb2**	5.4	15.1	4.8	16.3	BT	BT
Fgf1**	5.1	5.6	3.6	BT	5.4	3.5
Fgf10**	5.7	BT	BT	BT	BT	BT
Fgf18**	7.8	BT	BT	BT	BT	BT
Fgf7**	21.0	10.3	BT	BT	BT	BT
Figf**	3.8	4.8	BT	BT	BT	BT
Fstl1**	96.0	92.2	72.9	59.3	43.0	11.3
Gas6*	22.4	14.3	7.4	24.6	BT	45.2
Gdf10**	8.4	BT	BT	BT	BT	BT
Gdf11**	BT	6.6	3.8	2.7	BT	BT
Gmfb**	9.5	17.6	6.1	13.8	14.1	9.6
Gmfg	BT	BT	BT	6.4	BT	36.5
Grp	BT	BT	BT	2.1	BT	BT
Hbegf*	BT	2.5	14.3	15.0	19.2	3.5
Igf1**	56.0	52.0	4.6	16.6	2.0	40.0
Igf2**	92.3	89.5	54.0	69.7	11.1	25.2
Il15	BT	BT	BT	BT	BT	4.3
Il16	BT	BT	BT	4.6	BT	12.2
Il18	BT	BT	BT	BT	BT	9.6
Il1b	BT	BT	BT	BT	BT	3.5
Il33**	13.7	16.1	BT	BT	BT	BT

(Continued)

Table 4: Continued

	Gene abundance (%)					
Gene	Epineurial	Endoneurial/perineurial	VSM/pericytes	Endothelial	Schwann cells	Immune cells
Inha**	2.6	BT	BT	BT	BT	BT
Inhba**	4.1	BT	BT	BT	BT	BT
Inhbb	BT	BT	8.0	BT	BT	BT
Jag1**	18.4	19.1	15.5	11.0	BT	BT
Jag2	BT	BT	BT	7.1	BT	BT
Ltb	BT	BT	BT	BT	BT	2.6
Mdk**	52.3	68.1	20.2	8.8	20.9	8.7
Metrn*	3.4	8.7	10.5	5.0	43.2	10.4
Mif*	17.5	26.4	28.8	26.0	32.8	26.1
Nenf**	54.3	54.6	39.7	28.8	24.5	BT
Ngf**	BT	8.7	8.0	BT	BT	0.0
Nov**	23.8	4.3	3.8	3.4	2.8	3.5
Nppc**	BT	6.1	BT	BT	BT	BT
Ntf3	BT	BT	2.3	BT	BT	BT
Ntn1**	22.2	10.0	BT	BT	BT	BT
Osm	BT	BT	BT	BT	BT	3.5
Pdgfa*	3.4	3.6	30.5	3.0	17.8	BT
Pdgfb	BT	BT	2.9	21.9	BT	BT
Pdgfc	BT	BT	3.2	BT	2.2	2.6
Pf4	BT	BT	BT	BT	BT	61.7
Pgf	BT	BT	3.8	BT	BT	BT
Pthlh**	7.1	4.0	BT	BT	BT	BT
Ptn*	29.3	13.9	6.5	15.9	43.4	4.3
Rspo1**	7.8	6.5	BT	BT	BT	BT
Rtn4*	31.0	38.2	35.7	40.4	26.8	38.3
Sema3b*	5.4	6.5	2.3	2.8	34.7	7.8
Sema3c**	51.7	19.2	BT	BT	7.1	3.5
Sema3d**	10.4	15.9	BT	BT	BT	BT
Sema3f*	2.6	BT	BT	2.8	BT	BT
Sema3g	BT	BT	BT	9.6	7.5	BT
Sema4a	BT	BT	BT	BT	BT	10.4
Sema4b	BT	BT	BT	BT	BT	3.5
Sema4c*	5.1	5.7	2.7	8.1	8.5	5.2
Sema4d	BT	BT	BT	BT	BT	7.8
Sema5a*	5.4	5.5	12.4	BT	BT	BT
Sema5b*	4.4	8.6	14.1	BT	2.6	BT
Sema6a*	4.4	7.9	BT	22.8	4.5	BT
Sema6b	BT	BT	BT	2.5	BT	BT
Sema6c**	4.9	3.3	2.5	BT	BT	BT
Sema6d*	2.0	3.0	4.4	6.4	16.7	8.7
Sema7a	BT	BT	2.1	17.3	2.0	BT
Sfrp1**	50.5	48.5	2.9	4.1	28.0	3.5
Sfrp2**	17.2	BT	BT	BT	BT	BT
Sfrp4**	43.7	5.5	BT	BT	BT	2.6
Sfrp5**	5.4	30.7	BT	BT	8.1	2.6
Tgfb1	BT	BT	BT	10.3	BT	20.9
Tgfb2*	12.1	2.7	18.3	9.9	BT	BT
Tgfb3**	21.5	8.3	10.9	BT	BT	BT
Tnf	BT	BT	BT	BT	BT	6.1
Tnfrsf11b*	2.9	BT	BT	3.9	BT	BT
Tnfsf10	BT	BT	BT	6.4	BT	BT
Tnfsf12**	8.0	10.8	5.5	6.5	3.2	4.3
Tnfsf9	BT	BT	BT	BT	BT	4.3
Tslp	BT	BT	2.7	2.8	BT	3.5
Vegfa**	16.0	3.6	3.8	3.2	BT	BT
Vegfb**	4.0	7.7	6.3	5.5	4.3	6.1
Vegfc	BT	BT	BT	8.5	BT	BT

(Continued)

Table 4: Continued

	Gene abundance (%)					
Gene	Epineurial	Endoneurial/perineurial	VSM/pericytes	Endothelial	Schwann cells	Immune cells
Wnt11	BT	BT	2.7	BT	BT	BT
Wnt2**	7.5	BT	BT	BT	BT	BT
Wnt5a**	17.0	6.8	BT	BT	BT	BT

The neonatal nerve scRNA-seq dataset (Fig. 2*E*) was analyzed to determine the percentage of cells within a given cell type that detectably expressed (≥2%) the 143 injured nerve ligand mRNAs (Table 2). Cell populations were defined as for the injured nerve analysis. BT = below threshold and indicates that <2% of cells detectably expressed the ligand mRNA. Ligands annotated with one asterisk in the leftmost column were expressed in ≥2% *Pdgfra*-positive mesenchymal cells and two asterisks indicate ligands with the highest expression in either the epineurial/perineurial or endoneurial *Pdgfra*-positive mesenchymal cells.
* >2% expression in *Pdgfra*-positive cells.
** >2% expression and highest expression in *Pdgfra*-positive cells.

nerve cell dataset (Fig. 2*C*,*D*; Extended Data Fig. 2-1*B*) identified clusters comprised of epineurial, perineurial, and endoneurial mesenchymal cells, as well as VSM/pericyte cells, endothelial cells, and a small population (1.9%) of immune cells. There were also two *Sox10*-positive Schwann cell populations; non-myelinating cells expressing *Ngfr/p75NTR*, *Cdh2*, and *L1cam*, and myelinating Schwann cells expressing high levels of *Mbp*, *Pmp22*, and *Plp*. This latter population was likely relatively reduced in numbers because myelin removal beads were used when isolating the nerve cells. There were very few proliferating cells, as indicated by expression of cell cycle genes like *Top2a* and *Ki67* (Extended Data Fig. 2-1*B*).

For the developing neonatal nerve, we generated a new dataset, sequencing P2–P4 sciatic nerve cells after isolating them using either flow cytometry or myelin removal beads in two separate preparations. We combined raw transcriptomes from both preparations and analyzed them together. This analysis, which included 6885 total cells, identified 10 clusters containing intermingled cells from both preparations (Fig. 2*E*; Extended Data Fig. 2-1*C*, *D*). This intermingling was unaffected by batch correction (Extended Data Fig. 2-1*C*). Cell type-specific marker genes identified endothelial cells, VSM/pericyte cells, macrophages, and epineurial, endoneurial, and perineurial mesenchymal cells (Fig. 2*E*,*F*; Extended Data Fig. 2-1*D*). At this age, there were five *Sox10*-positive Schwann cell clusters, with one cluster (6) containing proliferative Schwann cells and another (9) myelinating Schwann cells expressing high levels of *Mag*, *Mbp*, *Mpz*, and *Pmp22* (Fig. 2*E*,*F*).

Analysis of ligand mRNA expression in these datasets showed that cells in the uninjured and developing sciatic nerves expressed many but not all injured nerve ligands. Specifically, of 143 total ligands, 122 and 119 were detectably expressed in uninjured and neonatal nerves, respectively, and 111 were shared in all three conditions (Fig. 2*G*; Tables 3, 4). These ligand mRNAs were contributed by all of the different cell types in the uninjured and neonatal nerves (Fig. 2*H*,*I*). However, the pattern of ligand expression differed from the injured nerve (compare Figs. 2*I*, 1*H*), with endoneurial mesenchymal cells and Schwann cells contributing relatively fewer ligands in the developing and uninjured nerves (endoneurial cells, 11% and 27% in the uninjured vs injured nerves; Schwann cells, 5% and 16% in the uninjured vs injured nerves). Moreover, 13 injured nerve ligands were not detectably expressed in the neonatal or uninjured nerves (*Artn*, *Btc*, *Ccl25*, *Crlf1*, *Fgf5*, *Gdnf*, *Gnrh1*, *Hgf*, *Rspo3*, *Sema4f*, *Shh*, *Tnfsf8*, and *Ucn2*; Tables 3, 4). Notably, all of these were injured nerve Schwann cell or mesenchymal cell ligands (Table 2). Thus, multiple cell types contribute to the sciatic nerve ligand environment in all conditions, but mesenchymal and Schwann cells become relatively more important following injury.

Injured Schwann cells acquire a unique transcriptional phenotype following injury including upregulation of many growth factor genes

To ask about the apparent injury-associated increase in ligand expression, we analyzed the Schwann cells and *Pdgfra*-positive mesenchymal cells in more detail. We first combined transcriptomes from all Schwann cell clusters in the neonatal, uninjured, 3 DPI, and 9 DPI nerve datasets [cluster 6 (Fig. 1*E*), clusters 4 and 8 (Fig. 2*C*), clusters 1, 2, 4, 6, and 9 (Fig. 2*E*)]. We augmented this combined dataset by including Schwann cells from the FAC-sorted 9 DPI dataset from Carr et al. (2019). Once this combined dataset was put through the pipeline, we used the Harmony batch correction method (Korsunsky et al., 2019) to correct for any technical variation. Analysis of this combined dataset indicated that injured nerve Schwann cells were distinct from both developing and adult uninjured Schwann cells. Specifically, the combined dataset included 5331 Schwann cells in seven clusters (Fig. 3*A*,*B*). The differentiating neonatal Schwann cells were present in clusters 0, 1, and 2 with proliferating cells in cluster 2 (Fig. 3*A*,*B*; Extended Data Fig. 3-1*A*). Adult and neonatal myelinating Schwann cells were present in clusters 5 and 6, while the adult uninjured non-myelinating Schwann cells were in cluster 4. By contrast, almost all injured nerve Schwann cells were present in cluster 3.

To better understand these clusters, we performed hierarchical and correlation analyses of average gene expression (Fig. 3*C*). These analyses confirmed that the injured Schwann cells were distinct from the other populations, and indicated that they were more similar to the differentiating neonatal cells ($r = 0.88$ for the comparison between clusters 3 and 0) than to the adult non-myelinating Schwann cells ($r = 0.76$ for the comparison between clusters 3 and 4). To understand these similarities and differences at an individual cell level, we performed single-cell correlation analysis. As comparators for the analysis, we determined average gene expression for uninjured non-myelinating versus neonatal non-myelinating Schwann

Table 5: Gene abundance of injured nerve ligand mRNAs in the combined injured, uninjured and neonatal Schwann cell scRNA-seq dataset

	Gene abundance (%)				Fold change
Gene	Neonatal	Uninjured (myelinating)	Uninjured (non-myelinating)	Injured	Injured:uninjured (non-myel.)
Angpt2	2.0	6.4	BT (0.4)	BT (1.7)	4.1
Artn	BT (0.0)	BT (0.0)	BT (0.0)	3.1*	>3.1
Bdnf	BT (0.0)	BT (0.0)	BT (0.0)	9.3*	>9.3
Bmp1	10.9	3.8	4.9	46.1*	9.3
Btc	BT (0.8)	BT (0.0)	BT (0.0)	58.8*	>58.8
Ccl11	BT (0.8)	3.8	4.5	5.6*	1.2
Ccl2	BT (0.7)	BT (0.0)	BT (1.6)	12.7*	7.7
Ccl3	BT (0.0)	BT (0.0)	BT (0.0)	3.9*	>3.9
Ccl7	BT (0.2)	2.6	2.9	6.1*	2.1
Ccl9	BT (0.0)	2.6	BT (0.4)	6.6*	16.1
Clcf1	BT (0.2)	BT (0.0)	BT (0.0)	18.6*	>18.6
Crlf1	BT (1.3)	BT (0.0)	2.5	30.5*	12.4
Csf1	2.4	BT (1.3)	9.1	9.7*	1.1
Ctgf	BT (0.1)	BT (0.0)	BT (0.0)	3.4*	>3.4
Cx3cl1	BT (0.0)	2.6	BT (0.0)	BT (0.2)	-
Cxcl1	BT (1.4)	6.4	11.9	10.7	0.9
Cxcl10	2.6	BT (0.0)	BT (0.4)	5.9*	14.4
Cxcl12	BT (1.4)	2.6	12.3	5.4	0.4
Cxcl2	BT (0.1)	BT (0.0)	BT (0.0)	7.1*	>7.1
Dhh	25.3	28.2	11.9	26.8	2.2
Eda	4.4	2.6	3.7	2.9	0.8
Efna2	2.8	BT (1.3)	BT (0.8)	3.2*	3.9
Efna4	BT (1.0)	BT (1.3)	BT (0.0)	4.9*	>4.9
Efna5	2.2	BT (0.0)	BT (0.0)	BT (0.3)	-
Efnb1	8.9	2.6	7.0	10.0*	1.4
Efnb2	BT (0.6)	BT (0.0)	BT (0.4)	3.9*	9.5
Fgf1	5.4	28.2	10.7	BT (1.5)	0.1
Fgf5	BT (0.0)	BT (0.0)	BT (0.0)	18.3*	>18.3
Fgf7	BT (1.3)	9.0	BT (0.8)	12.9*	15.7
Fstl1	42.6	9.0	30.9	29.0	0.9
Gas6	BT (0.6)	6.4	2.9	2.5	0.9
Gdf11	BT (1.2)	BT (0.0)	BT (0.4)	3.1*	7.4
Gdnf	BT (0.0)	BT (0.0)	BT (0.0)	20.5*	>20.5
Gmfb	14.2	16.7	7.0	21.9*	3.1
Hbegf	19.0	9.0	26.7	39.0*	1.5
Igf1	2.1	BT (1.3)	3.3	15.4*	4.7
Igf2	11.2	BT (1.3)	BT (1.2)	3.6	2.9
Il16	BT (0.7)	7.7	BT (0.4)	BT (0.3)	0.8
Il18	BT (0.3)	BT (0.0)	2.1	BT (0.5)	0.2
Il1b	BT (0.0)	BT (0.0)	BT (0.0)	3.7*	>3.7
Il33	BT (0.2)	2.6	2.9	4.2*	1.5
Jag1	BT (0.9)	BT (1.3)	BT (1.2)	6.9*	5.6
Lif	BT (0.0)	BT (0.0)	BT (0.0)	4.9*	>4.9
Mdk	20.6	BT (1.3)	3.3	25.3*	7.7
Metrn	42.8	11.5	14.0	53.6*	3.8
Mif	32.5	17.9	11.9	26.1	2.2
Nenf	24.3	19.2	27.2	47.3*	1.7
Nov	2.7	14.1	7.8	4.2	0.5
Ntn1	BT (0.6)	BT (0.0)	BT (0.8)	3.2*	3.9
Pdgfa	17.5	15.4	15.6	47.5*	3.0
Pdgfb	BT (0.2)	BT (0.0)	BT (0.0)	2.2*	>2.2
Pdgfc	2.2	BT (1.3)	BT (1.2)	BT (1.0)	0.8
Ptn	42.9	BT (0.0)	57.2	47.3	0.8
Rtn4	26.7	21.8	24.3	70.7*	2.9
Sema3b	34.4	56.4	43.2	51.4	1.2
Sema3c	7.1	BT (1.3)	9.5	19.5*	2.1
Sema3e	BT (1.0)	BT (0.0)	14.4	29.2*	2.0
Sema3f	BT (0.4)	BT (0.0)	2.1	2.9*	1.4
Sema3g	7.5	2.6	BT (1.6)	8.1*	4.9
Sema4b	BT (0.4)	BT (0.0)	BT (0.8)	7.1*	8.6

(Continued)

Table 5: Continued

	Gene abundance (%)				Fold change
Gene	Neonatal	Uninjured (myelinating)	Uninjured (non-myelinating)	Injured	Injured:uninjured (non-myel.)
Sema4c	8.5	21.8	5.3	15.4	2.9
Sema4d	BT (0.9)	BT (0.0)	2.1	BT (1.0)	0.5
Sema4f	BT (0.0)	BT (0.0)	BT (0.0)	17.1*	>17.1
Sema5a	BT (0.9)	10.3	BT (0.0)	BT (1.9)	>1.9
Sema5b	2.6	BT (0.0)	BT (0.0)	BT (0.2)	-
Sema6a	4.5	2.6	2.9	8.0*	2.8
Sema6c	BT (1.3)	7.7	BT (1.2)	2.0	1.6
Sema6d	16.5	11.5	25.5	14.1	0.6
Sema7a	2.1	BT (0.0)	9.5	17.1*	1.8
Sfrp1	27.6	BT (0.0)	7.0	8.0	1.1
Sfrp2	BT (0.4)	5.1	3.7	2.0	0.5
Sfrp4	BT (1.3)	6.4	4.9	8.8*	1.8
Sfrp5	8.1	30.8	28.0	5.1	0.2
Shh	BT (0.0)	BT (0.0)	BT (0.0)	12.0*	>12.0
Tgfb1	BT (0.9)	BT (1.3)	BT (0.8)	9.8*	11.9
Tgfb2	BT (0.6)	BT (0.0)	BT (0.8)	6.1*	7.4
Tgfb3	BT (1.8)	BT (1.3)	BT (1.6)	4.2*	2.6
Tnfsf12	3.2	9.0	9.5	6.3	0.7
Tnfsf9	BT (0.6)	BT (1.3)	5.3	BT (0.7)	0.1
Ucn2	BT (0.1)	BT (0.0)	BT (0.0)	14.1*	>14.1
Vegfa	BT (1.1)	2.6	BT (0.8)	2.4	2.9
Vegfb	4.2	7.7	3.3	7.5	2.3

The combined Schwann cell scRNA-seq dataset (Fig. 3*A*,*B*) was analyzed to determine the percentage of cells within the different Schwann cell clusters that detectably expressed (≥2%) the 143 injured nerve ligand mRNAs (Table 2). Also shown is the difference, expressed as fold change, in the percentage of positive cells in the injured versus uninjured, non-myelinating Schwann cell clusters. BT = below threshold and indicates that <2% of cells detectably expressed the ligand mRNA. Also shown are the absolute values, since these were used to determine the fold changes. Neonatal includes cells in clusters 0, 1, 2, and 5, uninjured myelinating includes cluster 6 cells, uninjured non-myelinating includes cluster 4 cells, and injured includes cluster 3 cells. Asterisks indicate ligand mRNAs with the highest expression in the injured Schwann cell cluster.
*Injured, highest expression.

cells and for uninjured non-myelinating versus 9 DPI Schwann cells. We then compared each single-cell transcriptome with the averaged bulk transcriptomes using Pearson's correlation and used the resultant correlation coefficients to assign a two-dimensional coordinate to each cell. This analysis (Fig. 3*D*) showed that (1) virtually all 3 and 9 DPI Schwann cells were more similar to the neonatal Schwann cells than to the uninjured non-myelinating cells, (2) most neonatal Schwann cells were more similar to the injured cells than to the uninjured non-myelinating cells, and (3) despite these similarities, there was very little direct overlap between the injured and neonatal cells.

These data indicate that following nerve injury Schwann cells become more like neonatal Schwann cells, but that they are nonetheless distinct. In this regard, it has been reported that this unique injury state might involve acquisition of mesenchymal-like characteristics (Arthur-Farraj et al., 2017; Clements et al., 2017). To explore this idea further, we compared injured nerve Schwann cells and *Pdgfra*-positive mesenchymal cells from the combined 3 and 9 DPI nerve dataset (Fig. 1*E*). Correlation analysis showed that the injured Schwann cells were very distinct from both endoneurial and epineurial cells in the injured nerve (Extended Data Fig. 3-1*B*; $r = 0.74$–0.78). Thus, after injury, Schwann cells acquire a unique transcriptional profile that is similar but not identical to neonatal Schwann cells.

We asked about ligand gene expression in this combined dataset. This analysis showed that nerve injury led to upregulation of a subset of ligand mRNAs in Schwann cells. Specifically, in the combined Schwann cell dataset, 82 of the 143 injured nerve ligands were detectably expressed, but only 28 of these were common to the neonatal, uninjured, and injured Schwann cells (Fig. 3*E*; Table 5). Notably, 36 ligand mRNAs were expressed in ≥3-fold more injured versus uninjured non-myelinating cells (Table 5), with some almost exclusive to the injured cells, including *Artn*, *Bdnf*, *Btc*, *Ccl2*, *Ccl3*, *Clcf1*, *Crlf1*, *Cxcl2*, *Fgf5*, *Gdnf*, *Lif*, *Sema4f*, *Shh*, *Tgfb1*, and *Ucn2* mRNAs (Fig. 3*F*,*G*; Extended Data Fig. 3-1*C*). Other ligand mRNAs were also upregulated following injury but were still expressed by other Schwann cell populations, such as *Bmp1*, *Fgf7*, *Igf1*, and *Pdgfa* (Fig. 3*G*,*H*; Extended Data Fig. 3-1*D*). By contrast, some ligand mRNAs were expressed to some degree in all or most Schwann cell populations, including, for example, *Dhh*, *Mdk*, and *Fgf1* (Fig. 3*H*,*I*; Extended Data Fig. 3-1*D*). Thus, injured nerve Schwann cells acquire a unique, development-like transcriptional state that includes upregulation of growth factors implicated in nerve development, nerve regeneration, and tissue repair, including, for example, GDNF (Trupp et al., 1995; Naveilhan et al., 1997), BDNF (Lindsay, 1988; Leibrock et al., 1989), and PDGFα (Johnston et al., 2016).

Upregulation of ligands in endoneurial mesenchymal cells following nerve injury

We performed a similar analysis of nerve mesenchymal cells, combining transcriptomes from the neonatal,

Table 6: Gene abundance of injured nerve ligand mRNAs in the combined injured, uninjured and neonatal mesenchymal cell scRNA-seq dataset

	Gene abundance (%)								
	Neonatal		Inj/uninjured	Injured/ uninjured/ neonatal	Uninjured	Injured		Neonatal/ injured	Fold change Injured: uninjured endoneurial
Gene	Epineurial	Endoneurial	Epineurial	Perineurial	Endoneurial	Endoneurial	Differentiating	Proliferating	
Adm	5.2	4.8	17.3	17.0	9.0	35.1	7.6	10.1	3.9
Agt	BT (1.7)	BT (0.5)	3.3	BT (0.0)	BT (1.9)	10.7	BT (1.7)	3.9	5.6
Angpt1	3.7	BT (0.5)	11.6	5.2	BT (0.7)	23.9	24.6	20.8	33.6
Angpt2	3.4	BT (0.0)	2.0	BT (1.3)	BT (0.5)	BT (1.0)	5.1	2.9	2.0
Angpt4	BT (0.5)	BT (0.0)	4.9	BT (1.3)	BT (0.2)	BT (0.4)	2.0	2.6	1.7
Apln	BT (0.7)	2.1	BT (0.5)	BT (0.7)	BT (0.7)	5.3	BT (1.9)	6.5	7.5
Bdnf	BT (0.6)	BT (1.1)	BT (0.2)	BT (0.7)	BT (0.0)	BT (1.9)	5.2	BT (1.6)	>1.9
Bmp1	34.3	12.7	51.4	52.9	16.4	37.2	52.3	47.6	2.3
Bmp2	BT (0.2)	BT (0.0)	2.9	BT (0.7)	BT (0.9)	3.1	BT (0.7)	3.9	3.3
Bmp4	2.6	2.6	11.7	BT (0.7)	6.6	BT (1.0)	BT (0.3)	BT (1.0)	0.1
Bmp5	BT (0.4)	BT (1.6)	BT (1.8)	BT (1.3)	6.6	4.0	BT (1.1)	BT (1.6)	0.6
Bmp7	BT (1.7)	6.3	BT (1.5)	8.5	12.1	30.1	BT (1.2)	5.9	2.5
Btc	BT (0.4)	BT (0.0)	BT (1.1)	BT (0.0)	BT (0.2)	BT (1.6)	BT (1.5)	4.6	6.9
Ccl11	18.0	70.9	42.6	19.0	89.3	85.9	21.4	40.4	1.0
Ccl19	BT (0.1)	BT (0.0)	4.9	BT (0.0)	BT (0.0)	BT (0.0)	BT (0.5)	BT (0.0)	-
Ccl2	BT (0.7)	19.8	14.4	10.5	16.1	81.6	25.6	49.5	5.1
Ccl3	BT (0.1)	BT (0.0)	2.0	2.0	BT (0.0)	5.2	5.8	3.6	>5.2
Ccl5	BT (0.2)	BT (0.0)	2.2	BT (1.3)	BT (0.2)	3.0	2.5	3.3	12.7
Ccl7	6.0	29.1	12.7	10.5	36.0	77.3	23.8	44.6	2.1
Ccl9	BT (0.2)	2.9	5.2	2.6	16.8	72.1	12.0	26.1	4.3
Clcf1	BT (0.8)	BT (0.5)	BT (1.6)	BT (1.3)	BT (0.9)	4.4	5.0	5.2	4.6
Crlf1	BT (0.2)	BT (0.0)	BT (1.1)	5.2	BT (0.0)	26.1	3.4	11.1	>26.1
Csf1	12.2	3.4	40.9	11.8	10.9	31.0	24.0	30.9	2.8
Ctgf	7.3	BT (1.9)	18.9	19.0	2.4	37.2	29.2	25.4	15.7
Cx3cl1	BT (0.0)	BT (0.8)	BT (0.9)	BT (0.7)	BT (1.7)	14.3	8.6	4.2	8.6
Cxcl1	1.9	23.3	20.1	17.6	53.1	60.7	35.9	37.8	1.1
Cxcl10	BT (0.4)	BT (1.3)	BT (0.9)	BT (0.7)	BT (1.7)	9.6	3.5	6.5	5.8
Cxcl12	17.3	63.2	42.8	10.5	61.1	52.9	50.2	48.5	0.9
Cxcl13	BT (0.0)	BT (0.3)	17.6	BT (0.0)	BT (1.2)	BT (0.4)	BT (1.0)	BT (0.7)	0.3
Cxcl16	BT (0.8)	BT (1.3)	10.3	3.9	BT (1.7)	5.1	8.2	4.6	3.0
Cxcl2	BT (0.1)	BT (1.3)	7.1	6.5	BT (0.5)	24.7	12.8	20.2	52.2
Cxcl9	BT (1.0)	BT (1.9)	BT (1.4)	BT (0.0)	BT (0.5)	2.2	7.6	7.5	4.6
Dhh	BT (1.3)	2.4	BT (0.0)	BT (0.7)	BT (0.2)	BT (0.5)	BT (0.8)	2.3	2.3
Eda	8.2	10.6	4.0	19.6	7.8	9.4	7.7	7.5	1.2
Edn3	5.3	BT (0.5)	6.6	6.5	BT (1.7)	BT (0.3)	BT (1.6)	BT (1.0)	0.2
Efna1	4.1	3.7	3.2	5.9	4.0	7.8	3.9	4.2	1.9
Efna2	3.6	3.7	2.4	BT (1.3)	BT (1.2)	4.4	4.9	5.2	3.7
Efna4	4.2	BT (1.9)	2.5	6.5	BT (0.7)	6.1	9.0	3.9	8.6
Efna5	6.1	4.2	4.7	11.1	BT (1.2)	5.2	2.0	4.9	4.4
Efnb1	27.0	25.9	9.5	39.2	14.2	37.8	31.7	32.6	2.7
Efnb2	9.5	17.2	3.4	23.5	10.9	41.9	19.7	20.5	3.8
Fgf1	7.0	3.7	5.7	15.7	BT (0.9)	4.6	9.9	7.2	4.9
Fgf10	4.0	BT (0.0)	13.6	BT (0.0)	BT (0.0)	BT (0.7)	3.9	BT (1.6)	-
Fgf18	6.6	BT (0.0)	11.7	4.6	BT (1.9)	BT (1.5)	5.9	6.2	0.8
Fgf5	BT (1.9)	BT (0.0)	BT (0.5)	BT (0.0)	BT (0.2)	BT (0.1)	2.1	2.0	0.6
Fgf7	21.3	4.0	27.8	23.5	6.6	35.9	24.2	25.1	5.4
Figf	6.1	BT (0.8)	21.2	5.9	2.1	9.7	10.2	15.6	4.5
Fstl1	96.2	92.3	96.9	86.3	76.1	94.7	96.1	90.6	1.2
Gas6	26.6	BT (0.5)	51.4	88.2	9.7	11.1	38.7	20.5	1.1
Gdf10	5.0	BT (0.3)	42.0	3.3	4.3	4.5	17.8	12.1	1.1
Gdf11	4.0	7.1	BT (1.6)	3.3	4.3	9.8	5.3	4.6	2.3
Gmfb	13.7	18.3	15.2	28.1	9.2	34.4	25.9	30.6	3.7
Gnrh1	BT (0.8)	BT (0.8)	BT (1.9)	3.3	BT (0.5)	2.2	BT (1.5)	BT (1.6)	4.6
Hbegf	2.3	2.1	BT (1.4)	BT (1.3)	2.4	4.9	9.3	13.4	2.1
Hgf	BT (0.4)	BT (0.0)	BT (1.2)	BT (0.7)	BT (0.2)	BT (0.8)	6.0	6.2	3.5

(Continued)

Table 6: Continued

	Gene abundance (%)								
	Neonatal		Inj/uninjured	Injured/ uninjured/ neonatal	Uninjured	Injured		Neonatal/ injured	Fold change Injured: uninjured endoneurial
Gene	Epineurial	Endoneurial	Epineurial	Perineurial	Endoneurial	Endoneurial	Differentiating	Proliferating	endoneurial
Igf1	44.2	82.8	75.8	17.6	45.0	85.1	84.1	63.8	1.9
Igf2	91.9	92.3	4.7	20.9	8.8	9.0	26.1	25.1	1.0
Il15	BT (0.6)	BT (1.3)	BT (1.4)	9.8	4.7	9.3	4.2	2.6	2.0
Il16	BT (0.4)	BT (0.5)	2.2	BT (0.7)	BT (1.2)	3.1	BT (1.3)	BT (1.0)	2.7
Il18	BT (0.3)	BT (0.3)	9.4	BT (0.7)	4.0	5.5	5.2	5.2	1.4
Il1b	BT (0.0)	BT (0.0)	2.3	BT (0.7)	BT (0.0)	7.4	5.9	7.2	>7.4
Il33	17.2	13.8	32.7	56.2	72.7	63.7	40.8	44.6	0.9
Il6	BT (0.2)	2.1	3.7	BT (0.0)	2.8	8.1	10.0	8.8	2.8
Inha	2.0	BT (1.3)	BT (1.9)	2.0	BT (1.2)	2.3	2.3	2.3	2.0
Inhba	3.4	BT (0.5)	2.1	6.5	BT (1.4)	12.8	15.8	23.5	9.0
Inhbb	BT (0.0)	BT (0.0)	BT (1.3)	2.6	BT (0.0)	12.8	BT (1.6)	2.3	>12.8
Jag1	22.3	13.8	13.4	25.5	4.5	16.7	23.4	23.1	3.7
Lif	BT (1.3)	BT (1.1)	2.4	BT (0.0)	3.1	11.6	2.1	6.2	3.8
Mdk	58.8	70.9	16.1	30.1	16.4	54.6	65.9	45.6	3.3
Metrn	5.2	10.3	3.1	5.9	BT (1.2)	13.3	5.1	23.5	11.2
Mif	21.1	30.4	18.6	15.0	14.9	42.2	42.5	54.7	2.8
Nenf	54.7	62.7	55.7	49.0	49.8	59.7	60.5	59.6	1.2
Ngf	2.3	13.5	BT (1.2)	8.5	2.6	7.7	BT (1.7)	6.8	2.9
Nov	16.7	5.6	30.0	BT (0.7)	8.1	9.7	17.6	22.5	1.2
Nppc	2.1	7.7	BT (0.3)	BT (0.0)	2.6	6.3	8.3	4.2	2.4
Ntf3	BT (1.3)	BT (0.5)	4.6	BT (0.0)	BT (0.7)	BT (1.4)	5.3	3.6	1.9
Ntn1	21.7	BT (0.5)	24.8	61.4	12.8	25.0	11.1	18.6	2.0
Pdgfa	4.0	2.6	6.5	9.8	BT (1.7)	7.9	11.0	25.1	4.8
Pdgfc	BT (0.7)	BT (0.3)	6.0	BT (0.0)	BT (0.2)	BT (1.4)	7.2	8.1	5.8
Pf4	BT (0.8)	BT (1.1)	2.0	BT (1.3)	BT (0.0)	4.0	3.7	4.9	>4.0
Pgf	BT (1.4)	BT (1.1)	2.0	3.3	5.0	12.7	2.5	3.9	2.6
Pomc	BT (0.3)	BT (1.1)	BT (0.9)	BT (0.7)	BT (1.4)	3.1	BT (1.2)	BT (1.3)	2.2
Pthlh	5.7	6.3	9.8	20.3	7.6	13.8	13.4	11.1	1.8
Ptn	21.1	21.7	15.5	2.6	4.0	11.1	56.8	45.6	2.7
Rspo1	11.5	BT (0.0)	3.2	20.9	BT (1.2)	BT (0.5)	BT (0.5)	BT (0.3)	0.5
Rspo3	BT (0.4)	BT (0.0)	3.1	BT (1.3)	BT (0.0)	BT (0.7)	11.6	6.2	-
Rtn4	35.1	36.2	47.9	43.8	33.9	68.6	60.5	72.3	2.0
Sema3b	5.2	9.3	14.0	11.1	33.4	11.3	5.0	6.5	0.3
Sema3c	43.0	14.8	50.5	18.3	9.2	8.6	23.0	27.7	0.9
Sema3d	18.0	3.7	11.4	45.1	BT (0.7)	BT (1.8)	6.3	7.8	2.5
Sema3e	BT (0.7)	BT (0.3)	3.7	BT (0.0)	BT (0.2)	BT (0.1)	BT (1.0)	2.9	0.6
Sema3f	2.2	BT (0.5)	BT (1.1)	2.6	BT (0.7)	4.5	2.0	3.3	6.3
Sema3g	BT (0.3)	BT (1.3)	BT (0.6)	BT (0.0)	3.1	2.7	BT (1.0)	2.0	0.9
Sema4a	BT (0.8)	BT (1.9)	BT (0.6)	4.6	BT (1.7)	3.3	BT (1.3)	BT (1.6)	2.0
Sema4b	BT (1.7)	BT (0.3)	BT (1.5)	2.0	2.1	2.9	2.6	2.3	1.3
Sema4c	5.8	5.8	5.9	13.1	6.4	11.7	9.3	10.1	1.8
Sema5a	4.7	7.4	BT (1.8)	4.6	3.6	3.6	6.1	5.9	1.0
Sema5b	5.6	9.5	BT (0.2)	BT (0.0)	BT (1.2)	BT (1.1)	BT (1.6)	5.2	0.9
Sema6a	6.2	9.8	3.1	7.8	19.0	14.6	3.2	7.5	0.8
Sema6b	BT (0.1)	BT (0.3)	2.5	BT (0.0)	2.8	7.1	BT (1.3)	7.8	2.5
Sema6c	4.3	4.8	5.4	BT (1.3)	3.3	3.4	8.0	6.2	1.0
Sema6d	2.2	3.2	3.7	7.8	3.6	11.2	3.7	9.4	3.2
Sema7a	BT (0.3)	BT (0.5)	BT (1.3)	BT (0.7)	BT (0.9)	19.4	11.0	21.5	20.5
Sfrp1	60.0	29.1	40.0	54.2	15.2	32.9	50.0	32.6	2.2
Sfrp2	11.4	BT (0.3)	47.8	3.9	5.5	7.1	21.7	18.6	1.3
Sfrp4	33.6	BT (1.9)	72.4	32.7	9.0	50.7	56.8	39.1	5.6
Sfrp5	26.7	2.6	2.6	94.8	5.9	2.6	6.3	10.4	0.4
Tgfb1	BT (0.6)	BT (0.3)	2.4	3.3	3.3	11.1	10.0	15.3	3.3
Tgfb2	10.3	BT (1.1)	10.5	3.3	2.8	3.7	17.0	12.1	1.3
Tgfb3	20.6	3.4	16.8	19.0	2.4	9.0	36.1	19.2	3.8
Tnf	BT (0.0)	BT (0.3)	BT (1.7)	BT (0.7)	BT (0.0)	2.5	BT (0.7)	2.6	>2.5

(Continued)

Table 6: Continued

	Gene abundance (%)								
	Neonatal		Inj/uninjured	Injured/ uninjured/ neonatal	Uninjured	Injured		Neonatal/ injured	Fold change Injured: uninjured endoneurial
Gene	Epineurial	Endoneurial	Epineurial	Perineurial	Endoneurial	Endoneurial	Differentiating	Proliferating	
Tnfrsf11b	BT (1.9)	BT (0.0)	4.6	8.5	BT (0.5)	BT (0.7)	4.4	10.7	1.4
Tnfsf10	BT (0.0)	BT (0.0)	BT (0.4)	2.0	BT (1.7)	BT (0.7)	BT (0.2)	BT (1.0)	0.4
Tnfsf12	9.6	11.6	15.7	15.0	17.8	17.3	14.6	14.7	1.0
Tnfsf8	BT (0.3)	BT (0.0)	BT (0.8)	10.5	BT (0.0)	2.2	5.7	3.3	>2.2
Tnfsf9	BT (0.5)	BT (1.6)	BT (1.4)	BT (1.3)	4.0	5.9	4.5	7.2	1.5
Tslp	BT (1.2)	2.4	4.0	2.6	BT (0.2)	4.8	BT (1.2)	2.9	20.2
Vegfa	11.0	4.8	25.0	3.9	8.3	18.2	29.6	27.0	2.2
Vegfb	5.2	9.0	5.4	9.8	4.7	7.1	8.3	11.4	1.5
Vegfc	BT (0.7)	BT (0.0)	2.2	BT (0.7)	BT (0.2)	BT (0.7)	2.2	5.5	2.9
Wnt11	BT (1.2)	BT (0.0)	6.2	BT (0.0)	BT (0.5)	BT (0.5)	BT (0.9)	2.9	1.2
Wnt2	6.0	BT (0.3)	9.1	BT (0.0)	BT (0.2)	BT (1.5)	4.6	4.9	6.3
Wnt5a	15.5	4.0	19.1	7.8	10.4	13.9	13.0	14.0	1.3

The combined mesenchymal cell dataset (Fig. 4*A*,*B*) was analyzed to determine the percentage of cells within the different mesenchymal cell clusters that detectably expressed (≥2%) the 143 injured nerve ligand mRNAs (Table 2). Also shown is the difference, expressed as fold change, in the percentage of positive cells in the injured versus uninjured endoneurial mesenchymal cells. BT = below threshold and indicates that <2% of cells detectably expressed the ligand mRNA. Also shown are the absolute values, since these were used to determine the fold changes. Neonatal epineurial includes cluster 1 cells, neonatal endoneurial includes cluster 6 cells, inj/uninjured epineurial includes clusters 2 and 5 cells, neonatal/uninjured/injured perineurial includes cluster 8 cells, uninjured endoneurial includes cluster 4 cells, injured endoneurial includes cluster 3 cells, injured differentiating includes cluster 0 cells, and neonatal/injured proliferating includes cluster 7 cells.

uninjured and injured nerve *Pdgfra*-positive clusters [clusters 1, 3, 5, and 10 (Fig. 1*E*), clusters 1, 2, 6, and 10 (Fig. 2*C*), clusters 3 and 5 (Fig. 2*E*)], as well as the *Pdgfra*-positive mesenchymal transcriptomes of the FAC-sorted 9 DPI cells from Carr et al. (2019). Once this combined dataset was put through the pipeline, we used Harmony batch correction (Korsunsky et al., 2019) to correct for any technical variation. Analysis of this combined dataset showed that, as published previously (Carr et al., 2019), some mesenchymal populations were transcriptionally altered by injury, while others were largely unaffected. Specifically, the combined dataset included 5416 cells in nine *Pdgfra*-positive clusters (Fig. 4*A*,*B*). The injured and uninjured epineurial cells were coclustered, as were the injured, uninjured, and neonatal perineurial cells (Fig. 4*A*,*B*; Extended Data Fig. 4-1). By contrast, the uninjured, injured, and neonatal endoneurial cells were all segregated from each other. The other segregated clusters included neonatal epineurial cells (cluster 1) and the injured nerve differentiating bridge cells (cluster 0).

We used this combined dataset to ask about injury-induced ligand induction in mesenchymal cells. This analysis indicated that the endoneurial mesenchymal cells were largely responsible for this induction. Specifically, 102 of the 143 injured nerve ligands were detectably expressed in endoneurial mesenchymal cells (Fig. 4*C*), and, of these, 49 were expressed in at least 3-fold more injured versus uninjured cells, with 26 detectably expressed only in the injured cells (Table 6). These upregulated ligand mRNAs included *Angpt1*, *Ccl9*, *Crlf1*, *Cxcl2*, *Inhbb*, *Lif*, *Sema7a*, and *Ngf* (Fig. 4*D*,*E*; Table 6). In addition to this endoneurial cell response, some ligands were highest in the injured bridge cells, such as *Bdnf*, *Cxcl9*, and *Hgf* (Fig. 4*D*; Table 6). By contrast, many ligand mRNAs were expressed to a greater or lesser degree in all nerve mesenchymal cell populations regardless of nerve injury, including for example *Adm*, *Bmp1*, *Ccl11*, *Cxcl12*, *Il33*, *Pthlh*, *Fgf18*, *Pdgfa*, *Tgfb3*, *Vegfa*, and *Wnt5a* (Fig. 4*F*,*G*). Thus, injury induces expression of many ligand mRNAs in endoneurial mesenchymal cells, but many ligands are also expressed under homeostatic conditions in uninjured nerve mesenchymal cells.

Identification of growth factor receptors on peripheral sympathetic and sensory neurons

To determine which of these ligands are likely to be important for axonal growth, we characterized growth factor receptors on sensory and sympathetic neurons which project their axons via the sciatic nerve. To do this, we coupled cell-surface proteomics and transcriptome profiling on purified neuronal cultures. For sensory neurons, we cultured E15 rat DRG neurons for 9 d in medium containing NGF. Immunostaining showed that these cultures were comprised of relatively pure βIII-tubulin-positive neurons with 2–3% contaminating S100β-positive Schwann cells (Fig. 5*A*; Extended Data Fig. 5-1*A*). For sympathetic neurons, we isolated cells from the neonatal rat SCG and cultured them for 6 d in NGF. These cultures contained βIII-tubulin-positive neurons and low percentages of Fibronectin-positive fibroblasts and S100β-positive Schwann cells (Fig. 5*A*; Extended Data Fig. 5-1*A*).

Initially, we characterized the neuronal cell-surface proteomes, taking advantage of the fact that many cell-surface proteins are glycosylated. Specifically, we performed periodate oxidation of cell-surface glycans, bound modified proteins on a hydrazide resin after cell lysis, digested the bound proteins with trypsin and PNGase F, and identified peptides by mass spectrometry. For each sample, we analyzed three independent biological replicates. This

Table 7: Proteins identified in sensory (DRG) and sympathetic (SCG) neurons using mass spectrometry

Sensory neurons (608)	Sympathetic neurons (271)	Sensory and sympathetic intersect (219)
Abca1	11/3R	Abca1
Abca5	Abca1	Ache
Abca7	AceIII	Acp2
Ache	Ache	Adam22
Acp2	Acp2	Adam23
Actb	Adam22	Adgre5
Actg1	Adam23	Adgrl1
Acvr2a	Adgre1	Adgrl2
Adam10	Adgre5	Ahsg
Adam11	Adgrl1	Alcam
Adam19	Adgrl2	Ano6
Adam22	Ahsg	Aplp1
Adam23	Alcam	Apmap
Adam9	Alk	Asah1
Adcy6	Angpt2	Atp1b1
Adcy9	Ano6	Atp6ap1
Adgrb3	Anpep	B3glct
Adgre5	Aplp1	Bcam
Adgrl1	Apmap	Bgn
Adgrl2	Asah1	Bmpr2
Adgrl3	Aspm	Bsg
Agrn	Atp1b1	Bst2
Ahsg	Atp6ap1	Cacna2d1
Alcam	B3glct	Cadm1
Alpl	Bcam	Cadm2
Alpl1	Bgn	Cadm4
Ano6	Bmpr2	CatL
Aplp1	Bsg	Cd151
Aplp2	Bst2	Cd200
Apmap	Cacna2d1	Cd276
Arse	Cadm1	Cd320
Asah1	Cadm2	Cd47
Asph	Cadm4	Cd59
Astn2	CatL	Cd63
Atg9a	Cd151	Cdh2
Atp1a1	Cd200	Celsr3
Atp1b1	Cd276	Chl1
Atp1b3	Cd320	Clmp
Atp5a1	Cd47	Clu
Atp6ap1	Cd59	Cntn1
Atraid	Cd63	Cntn2
Atrn	Cdh17	Cntnap1
Atrnl1	Cdh2	Col1a1
Avil	Cdig2	Col5a2
B3gat3	Cdk5r2	Colgalt1
B3glct	Celsr3	Cpd
Bace1	Chl1	Cpe
Bcam	Clmp	Ctsa
Bgn	Clu	Ctsc
Bmper	Cnnm2	Ctsd
Bmpr2	Cntn1	Ctsl
Brinp1	Cntn2	Ctsz
Brinp2	Cntnap1	Dpp10
Bscl2	Col1a1	Dpp6
Bsg	Col2a1	Ece1
Bst2	Col5a2	Efna5
Btd	Colgalt1	Efnb2
C11orf24	Cp	Emb
Cacna1b	Cpd	Enpp4

(Continued)

Table 7: Continued

Sensory neurons (608)	Sympathetic neurons (271)	Sensory and sympathetic intersect (219)
Cacna1c	Cpe	Entpd2
Cacna2d1	Cst3	Ephb2
Cacna2d2	Ctsa	Ero1a
Cacng8	Ctsc	Fam234b
Cadm1	Ctsd	Fn1
Cadm2	Ctsl	Gaa
Cadm3	Ctsz	Gabbr1
Cadm4	Cyp4f17	Gba
Calm1	Cyp4f40	Gdpd5
Calm2	Dbh	Ggt7
Calu	Dio1	Glg1
Cant1	Dkk3	Gns
Car11	Dopey1	Gpc1
Casc4	Dpp10	Grik3
Casd1	Dpp6	Grm7
CatL	Ece1	Hexa
Cd151	Ecel1	Hs2st1
Cd164	Efna5	Hsp90b1
Cd200	Efnb2	Hyou1
Cd24	Emb	Icam1
Cd276	Enpp4	Igf2r
Cd320	Entpd2	Iglon5
Cd44	Ephb2	Igsf3
Cd47	Ero1a	Il6st
Cd55	F2r	Impad1
Cd59	Fam234b	Insr
Cd63	Fcrl2	Islr2
Cd81	Fn1	Itga1
Cdh18	Folr2	Itga3
Cdh2	Gaa	Itga5
Cdh4	Gabbr1	Itga6
Celsr2	Gba	Itgam
Celsr3	Gdpd5	Itgav
Cemip	Gfra2	Itgb1
Chl1	Ggt7	L1cam
Chpf2	Glg1	Lamb1
Chst3	Gnas	Lamc1
Clcn5	Gns	Lamp1
Clcn6	Gpc1	Ldlr
Clmp	Grik3	Lgals3bp
Clptm1	Grm7	Lnpep
Clu	H2-Q10	LOC100912445
Cntfr	H2-Q7	LOC679087
Cntn1	Hexa	Lrp1
Cntn2	Hs2st1	Lrp11
Cntn3	Hsp90b1	Lrrc8b
Cntn4	Hyou1	Lsamp
Cntn6	Icam1	Ly6h
Cntnap1	Igf2r	Man2a2
Cntnap4	Iglon5	Mcam
Col12a1	Igsf3	Mcoln1
Col18a1	Il6st	Mdga1
Col1a1	Impad1	Megf8
Col5a1	Insr	Megf9
Col5a2	Islr2	Mmp15
Colgalt1	Itga1	Ncam1
Colgalt2	Itga3	Ncam2
Cpd	Itga5	Ncstn
Cpe	Itga6	Negr1
Cpm	Itga8	Nell1

(Continued)

Table 7: Continued

Sensory neurons (608)	Sympathetic neurons (271)	Sensory and sympathetic intersect (219)
Cr1l	Itgam	Neo1
Creld1	Itgav	Nfasc
Crtac1	Itgb1	Npc1
Csmd1	L1cam	Nptn
Csmd2	Lama1	Nrcam
Cspg5	Lamb1	Nrp1
Ctsa	Lamc1	Nrxn1
Ctsc	Lamp1	Nrxn3
Ctsd	Ldlr	Ntrk1
Ctsl	Lgals3bp	Olfm1
Ctsz	Lnpep	Ostm1
Cxadr	LOC100912445	P2rx4
Daf1	LOC286987	P4htm
Dchs1	LOC679087	Panx1
Dgcr2	Lrp1	Pcdh1
Disp2	Lrp11	Pcdh17
Dnase2	Lrrc8b	Pcdh9
Dpp10	Lsamp	Pcdhgc3
Dpp6	Ly6h	Pcyox1
Dpp7	Man2a2	pE4_antigen
Dpysl2	Mcam	Plbd2
Dpysl3	Mcoln1	Pld3
Ece1	Mdga1	Plod1
Ece2	Megf8	Plod3
Edem3	Megf9	Plxna1
Edil3	Mlnr	Plxna3
Eef1a1	Mmp15	Plxna4
Efna1	Mrc1	Plxnb1
Efna3	Mtor	Plxnb2
Efna5	Ncam1	Plxnc1
Efnb1	Ncam2	Ppt1
Efnb2	Ncstn	Prnp
Efnb3	Negr1	Ptk7
Elfn1	Nell1	Ptprg
Elfn2	Neo1	Pttg1ip
Emb	Nfasc	PVR
Enpp4	Nkain3	Pvrl1
Enpp5	Npc1	Pvrl2
Entpd2	Nptn	Rbm12b
Epdr1	Nrcam	Ret
Epha2	Nrp1	rt1-E
Ephb2	Nrxn1	Scarb2
Ero1a	Nrxn3	Scn2b
Extl3	Nt5e	Scn3a
F11r	Ntng1	Scn9a
F2rl2	Ntrk1	Sdk2
Fam189b	Olfm1	Sel1l
Fam234b	Ostm1	Sema4c
Fat1	P2rx4	Sema4d
Fat3	P4htm	Sez6l2
Fat4	Panx1	Sgce
Fbn2	Pcdh1	Slc12a7
Fkbp10	Pcdh17	Slc2a1
Fkbp9	Pcdh9	Slc2a13
Flrt1	Pcdhgc3	Slc2a3
Fn1	Pcyox1	Slc39a6
Foxred2	pE4_antigen	Slc44a2
Fras1	Plbd2	Slc6a15
Fstl1	Pld3	Slco3a1
Gaa	Plod1	Slit1

(Continued)

Table 7: Continued

Sensory neurons (608)	Sympathetic neurons (271)	Sensory and sympathetic intersect (219)
Gabbr1	Plod3	Slit2
Gabbr2	Plxna1	Sorcs2
Gabra2	Plxna3	Sort1
Gabrb3	Plxna4	Spock2
Galnt9	Plxnb1	Ssr2
Gapdh	Plxnb2	Stt3a
Gapdh-ps2	Plxnc1	Stt3b
Gba	Pon1	Suco
Gdpd5	Ppt1	Sulf2
Gfra3	Prnp	Sv2a
Ggh	Ptk7	Sv2b
Ggt5	Ptprg	Sv2c
Ggt7	Ptprm	Tage4
Gla	Pttg1ip	Tenm3
Glg1	PVR	Tenm4
Gnao1	Pvrl1	Tfrc
Gnptab	Pvrl2	Thbs1
Gns	Rbm12b	Thsd7a
Gpc1	Ret	Thy1
Gpm6b	RGD1560108	Timp1
Gpr158	RT1-A2b	Tm9sf3
Gria2	RT1-Ak	Tmed4
Grik3	RT1-Aw2	Tmed7
Grin1	rt1-E	Tmed9
Grm7	RT1.A1	Tmeff1
Grn	Rt1.L	Tmem106b
Hexa	Scarb2	Tmem132a
Hist1h2ba	Scn2b	Tmem63b
Hist1h2bd	Scn3a	Tmem63c
Hist1h2bh	Scn9a	Tmem87a
Hist1h2bk	Scube1	Tmem87b
Hist1h2bl	Sdk2	Tpp1
Hist1h2bo	Sel1l	Trpv2
Hist1h2bq	Sema4c	Tspan3
Hist2h2be	Sema4d	Tspan6
Hist3h2ba	Sez6l2	Tspan8
Hist3h2bb	Sgce	Ttyh3
Hnrnpa1	Slc12a7	Unc5b
Hs2st1	Slc2a1	Unc5c
Hs6st1	Slc2a13	Vwa7
Hsp70	Slc2a3	
Hsp90ab1	Slc39a6	
Hsp90b1	Slc44a2	
Hspa13	Slc6a15	
Hspa2	Slc6a2	
Hspa8	Slco3a1	
Hyou1	Slit1	
Icam1	Slit2	
Icam5	Sorcs1	
Ids	Sorcs2	
Idua	Sorcs3	
Ifnar1	Sort1	
Igf1r	Spock2	
Igf2r	Ssr2	
Igfbpl1	Stab1	
Iglon5	Stt3a	
Igsf3	Stt3b	
Ikbip	Suco	
Il1rapl1	Sulf2	
Il6st	Sv2a	

(Continued)

Table 7: Continued

Sensory neurons (608)	Sympathetic neurons (271)	Sensory and sympathetic intersect (219)
Impad1	Sv2b	
Insr	Sv2c	
Islr2	Tage4	
Itfg1	Tenm3	
Itga1	Tenm4	
Itga3	Tfrc	
Itga4	Thbs1	
Itga5	Thsd7a	
Itga6	Thy1	
Itga7	Timp1	
Itga9	Tll2	
Itgal	Tm9sf3	
Itgam	Tmed4	
Itgav	Tmed7	
Itgb1	Tmed9	
Itgb8	Tmeff1	
Jag1	Tmem106b	
Jkamp	Tmem132a	
Kcnc4	Tmem63b	
Kdelc2	Tmem63c	
Kiaa0319	Tmem87a	
Kirrel3	Tmem87b	
L1cam	Tpp1	
Lama4	Trpv2	
Lama5	TSLC1	
Lamb1	Tspan3	
Lamc1	Tspan6	
Lamp1	Tspan8	
Lamp2	Ttyh3	
Ldlr	Unc5b	
Lgals3bp	Unc5c	
Lgi2	Vwa7	
Lifr		
Lingo1		
Lingo2		
Lman2l		
Lnpep		
LOC100294508		
LOC100359563		
LOC100360413		
LOC100360548		
LOC100364116		
LOC100909441		
LOC100909911		
LOC100911252		
LOC100912445		
LOC100912446		
LOC102549061		
LOC102549957		
LOC314016		
LOC679087		
LOC685186		
Lphn3		
Lppr1		
Lrfn1		
Lrfn4		
Lrfn5		
Lrig2		
Lrp1		
Lrp11		

(Continued)

Table 7: Continued

Sensory neurons (608)	Sympathetic neurons (271)	Sensory and sympathetic intersect (219)
Lrp3		
Lrp8		
Lrrc8a		
Lrrc8b		
Lrrn1		
Lsamp		
Ly6h		
M6pr		
Man2a2		
Man2b1		
Mcam		
Mcoln1		
Mdga1		
Mdga2		
Megf8		
Sensory neurons (608)		
Megf9		
Mfge8		
Mme		
Mmp15		
Mpz		
Mpzl1		
Mrc2		
Mst1r		
Myh7b		
Naglu		
Ncam1		
Ncam2		
Ncan		
Ncln		
Ncstn		
Negr1		
Nell1		
Neo1		
Neu1		
Nfasc		
Nid2		
NKCC1		
Nomo1		
Npc1		
Npr3		
Nptn		
Nptx1		
Nptx2		
Nptxr		
Nrcam		
Nrp1		
Nrxn1		
Nrxn2		
Nrxn3		
Ntm		
Ntng2		
Ntrk1		
Ntrk2		
Olfm1		
Ostm1		
P2rx3		
P2rx4		

(Continued)

Table 7: Continued

Sensory neurons (608)	Sympathetic neurons (271)	Sensory and sympathetic intersect (219)
P3h1		
P3h4		
P4ha1		
P4htm		
Panx1		
Pcdh1		
Pcdh17		
Pcdh19		
Pcdh7		
Pcdh9		
Pcdha6		
Pcdha8		
Pcdhb2		
Pcdhb3		
Pcdhga11		
Pcdhga3		
Pcdhga5		
Pcdhga7		
Pcdhgb4		
Pcdhgb5		
Pcdhgb6		
Pcdhgb7		
Pcdhgb8		
Pcdhgc3		
Pcsk2		
Pcyox1		
pE4_antigen		
Pgap1		
Piezo2		
Pigs		
Pigt		
Pla2g15		
Plaur		
Plbd2		
Pld3		
Plod1		
Plod2		
Plod3		
Plxdc2		
Plxna1		
Plxna2		
Plxna3		
Plxna4		
Plxnb1		
Plxnb2		
Plxnc1		
Plxnd1		
Pm20d1		
Podxl		
Podxl2		
Pofut2		
Pol		
Pomgnt2		
Postn		
Ppia		
Ppib		
Ppil1		
Ppt1		
Prdx2		
Prnp		

(Continued)

Table 7: Continued

Sensory neurons (608)	Sympathetic neurons (271)	Sensory and sympathetic intersect (219)
Prph		
Psap		
Ptger2		
Sensory Neurons (608)		
Ptgfrn		
Ptk7		
Ptprf		
Ptprg		
Ptprn		
Ptpro2		
Ptprs		
Pttg1ip		
PVR		
Pvrl1		
Pvrl2		
Pxdn		
Qpct		
ratASCT1		
Rbm12b		
Rcn1		
Ret		
RGD1562725		
RGD1563124		
RGD1563349		
RGD1565368		
Rgma		
Ror2		
Rps16		
Rps20		
Rps27a		
Rps27a-ps6		
rt1-E		
Rtn4r		
Rtn4rl1		
Scarb2		
Scg3		
Scn10a		
Scn2b		
Scn3a		
Scn7a		
Scn9a		
Sdk2		
Sel1l		
Sema3c		
Sema3f		
Sema3g		
Sema4b		
Sema4c		
Sema4d		
Sema4f		
Sema6a		
Sema6d		
Sema7a		
Serpinh1		
Sez6l2		
Sgcb		
Sgce		
Shisa7		

(Continued)

Table 7: Continued

Sensory neurons (608)	Sympathetic neurons (271)	Sensory and sympathetic intersect (219)
Siae		
Sil1		
Sirpa		
Slc12a2		
Slc12a4		
Slc12a7		
Slc12a9		
Slc1a2		
Slc1a4		
Slc22a23		
Slc24a2		
Slc24a3		
Slc25a31		
Slc25a4		
Slc25a5		
Slc2a1		
Slc2a13		
Slc2a3		
Slc35a5		
Slc38a2		
Slc39a10		
Slc39a14		
Slc39a6		
Slc39a8		
Slc3a2		
Slc44a1		
Slc44a2		
Slc46a1		
Slc4a1		
Slc52a2		
Slc6a15		
Slc6a17		
Slc6a8		
Slc7a1		
Slc8a1		
Slco3a1		
Slit1		
Slit2		
Slitrk2		
Slitrk3		
Sorcs2		
Sort1		
Spock2		
Spock3		
Sppl2a		
Sppl2b		
Ssr2		
St8sia1		
St8sia3		
Stt3a		
Stt3b		
Sensory neurons (608)		
Suco		
Sulf2		
Sun1		
Sun2		
Sv2a		
Sv2b		

(Continued)

Table 7: Continued

Sensory neurons (608)	Sympathetic neurons (271)	Sensory and sympathetic intersect (219)
Sv2c		
Syp		
Sypl1		
Tage4		
Tapbp		
Tctn1		
Tctn2		
Tenm2		
Tenm3		
Tenm4		
Tfrc		
Tgfb2		
Tgfbr3		
Thbs1		
Thsd7a		
Thsd7b		
Thy1		
Timp1		
Tm2d1		
Tm9sf3		
Tmed4		
Tmed7		
Tmed9		
Tmeff1		
Tmem106b		
Tmem132a		
Tmem132c		
Tmem132e		
Tmem158		
Tmem181		
Tmem2		
Tmem200c		
Tmem231		
Tmem255a		
Tmem63b		
Tmem63c		
Tmem87a		
Tmem87b		
Tmem9b		
Tmtc4		
Tmx3		
Tor1aip2		
Tor2a		
Tpbg		
Tpcn1		
Tpp1		
Trhde		
Trpv2		
Tspan13		
Tspan3		
Tspan6		
Tspan7		
Tspan8		
Ttyh3		
Tuba1a		
Tuba1b		
Tuba1c		
Tuba3a		
Tubb2a		
Tubb2b		

(Continued)

Table 7: Continued

Sensory neurons (608)	Sympathetic neurons (271)	Sensory and sympathetic intersect (219)
Tubb3		
Tubb4b		
Tubb5		
Txndc15		
Uba52		
Ubb		
Ubc		
Uggt1		
Unc5b		
Unc5c		
Ust		
Vstm2a		
Vstm5		
Vwa7		
Wbscr17		
Ywhag		
Ywhah		
Z043_117466		

Gene symbols of proteins identified using cell-surface capture mass spectrometry on sensory neurons (column 1), sympathetic neurons (column 2), and both neuron types (column 3; intersect). Total numbers of proteins are indicated. Proteins included in this list were annotated by the terms "cell membrane" and/or "secreted" by the UniProtKB database (http://uniprot.org) and were verified by manual curation.

analysis identified 608 and 271 unique proteins on sensory and sympathetic neurons, respectively, with 219 of these common to both populations (Extended Data Fig. 5-1*B*; Table 7). The lower number of unique proteins on sympathetic neurons is likely due to decreased protein that was isolated (samples averaged ≈1100 vs 300 μg/ml for sensory vs sympathetic neurons). PANTHER classification identified most of these proteins as receptors, transporters and hydrolases, indicating appropriate enrichment for cell-surface proteins (Extended Data Fig. 5-1*C*). We then used the ligand-receptor database and manual curation to identify 102 proteins as receptors of various types, including G-protein-coupled receptors, receptor tyrosine kinases and phosphatases, cytokine receptors, and ligand-gated ion channels (Fig. 5*B*; Table 8). Among these were well-characterized receptors found on both types of neurons such as TrkA (encoded by *Ntrk1*), BMP receptor 2, RET, gp130 (encoded by *Il6st*), and IGF2 receptor, receptors identified only on sensory neurons such as GFRα3 and receptors identified only on sympathetic neurons such as ALK and GFRα2.

Cell-surface proteomics is relatively insensitive, and it ha5s previously been shown that more sensitive transcriptomic profiling can also be used to identify biologically relevant paracrine interactions (Johnston et al., 2016; Yuzwa et al., 2016; Voronova et al., 2017). We therefore complemented the proteomics by analyzing six and four independent biological replicates of cultured DRG and SCG RNA, respectively, on Affymetrix GeneChip Rat Gene 2.0 ST Arrays. To analyze these data, we defined an expression cutoff based on the proteomics data. Specifically, we identified the cell-surface receptor

Table 8: Receptors identified on sensory (DRG) and sympathetic (SCG) neurons using mass spectrometry and microarrays

Mass spectrometry		
DRGs (42)	SCGs (13)	DRGs and SCGs (47)
Acvr2a	Adgre1	Adgre5
Adgrb3	Alk	Adgrl1
Adgrl3	F2r	Adgrl2
Cd44	Fcrl2	Bcam
Celsr2	Folr2	Bmpr2
Cntfr	Gfra2	Cd320
Epha3	Itga8	Cd63
F2rl2	Mrc1	Celsr3
Gabra2	Mlnr	Ephb2
Gabrb3	Ntng1	Gabbr1
Gfra3	Ptprm	Grik3
Gpr158	Sorcs1	Grm7
Gria2	Sorcs3	Icam1
Grin1		Igf2r
Ifnar1		Il6st
Igf1r		Insr
Itfg1		Itga1
Itga4		Itga3
Itga7		Itga5
Itga9		Itga6
Itgal		Itgam
Itgb8		Itgav
Lifr		Itgb1
Lingo1		Ldlr
Mrc2		Lrp1
Mst1r		Mcam
Npr3		Neo1
Ntng2		Nptn
Ntrk2		Nrp1
P2rx3		Ntrk1
Plaur		P2rx4
Plxna2		Plxna1
Plxnd1		Plxna3
Ptger2		Plxna4
Ptprf		Plxnb1
Ptprn		Plxnb2
Ptprs		Plxnc1
Ror2		Ptprg
Rtn4r		PVR
Rtn4rl1		Pvrl1
Sirpa		Pvrl2
Tgfbr3		Ret
		Sorcs2
		Sort1
		Spock2
		Unc5b
		Unc5c
Microarrays		
DRGs (321)	SCGs (297)	
Acvr1	Acvr1	
Acvr1b	Acvr1b	
Acvr1c	Acvr2a	
Acvr2a	Acvr2b	
Acvr2b	Acvrl1	
Acvrl1	Adcyap1r1	
Adcyap1r1	Adipor1	
Adipor1	Adipor2	
Adipor2	Adora2a	
Adora2a	Adra1b	

(Continued)

Table 8: Continued

Microarrays	
DRGs (321)	SCGs (297)
Adra1a	Adrb2
Adra1b	Ager
Adrb2	Alk
Ager	Amfr
Alk	Aplnr
Amfr	Avpr1a
Amhr2	Avpr2
Aplnr	Axl
Ar	Bdkrb2
Avpr1a	Bmpr1a
Avpr2	Bmpr1b
Axl	Bmpr2
Bdkrb2	C3ar1
Bmpr1a	C5ar1
Bmpr1b	Calcrl
Bmpr2	Cckar
Btn1a1	Cckbr
C3ar1	Ccr10
C5ar1	Ccr4
Calcr	Ccr7
Calcrl	Ccr8
Cckar	Cd14
Cckbr	Cd27
Ccr10	Cd33
Ccr4	Cd4
Ccr7	Cd44
Ccr8	Cd5l
Cd14	Cd7
Cd27	Cd74
Cd33	Cntfr
Cd4	Crhr1
Cd40	Crhr2
Cd44	Crlf1
Cd5l	Crlf2
Cd7	Csf1r
Cd74	Csf2ra
Cntfr	Csf2rb
Crhr1	Csf3r
Crhr2	Ctf1
Crlf1	Cx3cr1
Crlf2	Cxcr1
Csf1r	Cxcr3
Csf2ra	Cxcr4
Csf2rb	Dcc
Csf3r	Ddr1
Ctf1	Derl1
Cx3cr1	Dip2a
Cxcr1	Edar
Cxcr2	Ednra
Cxcr3	Ednrb
Cxcr4	Egfr
Cxcr5	Eng
Dcc	Epha1
Ddr1	Epha2
Derl1	Epha3
Dip2a	Epha4
Edar	Epha5
Ednra	Epha7
Ednrb	Ephb1
Egfr	Ephb2
Eng	Ephb3

(Continued)

Table 8: Continued

Microarrays	
DRGs (321)	SCGs (297)
Epha1	Ephb4
Epha2	Epor
Epha3	Eps15l1
Epha4	Erbb2
Epha5	Erbb3
Epha7	Esr2
Ephb1	F2r
Ephb2	F2rl1
Ephb3	F2rl2
Ephb4	F2rl3
Epor	Fas
Eps15l1	Fgfr1
Erbb2	Fgfr2
Erbb3	Fgfr3
Erbb4	Fgfr4
Esr2	Fgfrl1
F2r	Flt1
F2rl1	Flt3
F2rl2	Flt4
F2rl3	Folr1
Fas	Fshr
Fgfr1	Fzd1
Fgfr2	Fzd2
Fgfr3	Fzd4
Fgfr4	Fzd5
Fgfrl1	Fzd9
Flt1	Gabbr1
Flt3	Galr1
Flt4	Galr2
Folr1	Gcgr
Fshr	Gfra2
Fzd1	Gfra3
Fzd2	Gfra4
Fzd4	Ghr
Fzd5	Ghrhr
Fzd9	Ghsr
Gabbr1	Gipr
Galr1	Glp1r
Galr2	Gosr1
Gcgr	Grik5
Gfra2	Grin2a
Gfra3	Grin2b
Gfra4	Grin2c
Ghr	Grin2d
Ghrhr	Gucy2c
Ghsr	Hcrtr1
Gipr	Hcrtr2
Glp1r	Hnf4a
Glp2r	Hpn
Gnrhr	Ifnar1
Gosr1	Ifnar2
Grik5	Ifngr1
Grin2a	Ifngr2
Grin2b	Igf1r
Grin2c	Igf2r
Grin2d	Igfbp1
Gucy2c	Igfbp2
Hcrtr1	Igfbp3
Hcrtr2	Igfbp4
Hnf4a	Igfbp5
Hpn	Igfbp6

(Continued)

Table 8: Continued

Microarrays	
DRGs (321)	SCGs (297)
Ifnar1	Igfbp7
Ifnar2	Il10ra
Ifngr1	Il10rb
Ifngr2	Il12rb1
Igf1r	Il15ra
Igf2r	Il17ra
Igfbp1	Il17rc
Igfbp2	Il18r1
Igfbp3	Il18rap
Igfbp4	Il1r1
Igfbp5	Il1r2
Igfbp6	Il1rap
Igfbp7	Il1rl1
Il10ra	Il1rl2
Il10rb	Il20rb
Il12rb1	Il21r
Il12rb2	Il22ra1
Il13ra2	Il22ra2
Il15ra	Il27ra
Il17ra	Il2ra
Il17rb	Il2rb
Il17rc	Il2rg
Il18r1	Il3ra
Il18rap	Il4r
Il1r1	Il6r
Il1r2	Il6st
Il1rap	Il7r
Il1rl1	Insr
Il1rl2	Irs1
Il20rb	Itga2
Il21r	Itga2b
Il22ra1	Itga5
Il22ra2	Itga9
Il27ra	Itgal
Il2ra	Itgav
Il2rb	Itgb1
Il2rg	Itgb2
Il3ra	Itgb3
Il4r	Itgb5
Il6r	Itgb6
Il6st	Itgb8
Il7r	Itpr3
Il9r	Kit
Insr	Ldlr
Irs1	Lgals3bp
Itga2	Lgr5
Itga2b	Lifr
Itga5	Lingo1
Itga9	Loxl2
Itgal	Lrp1
Itgav	Lrp2
Itgb1	Lrp5
Itgb2	Lrp6
Itgb3	Lsr
Itgb5	Ltbr
Itgb6	Marco
Itgb8	Mc1r
Itpr3	Mc2r
Kdr	Mc3r
Kit	Mc4r
Ldlr	Mc5r

(Continued)

Table 8: Continued

Microarrays	
DRGs (321)	SCGs (297)
Lgals3bp	Mchr1
Lgr5	Met
Lifr	Mpl
Lingo1	Mst1r
Loxl2	Ncoa3
Lrp1	Ncor1
Lrp2	Neo1
Lrp5	Ngfr
Lrp6	Notch1
Lsr	Notch2
Ltbr	Notch3
Marco	Npffr1
Mc1r	Npffr2
Mc2r	Npr1
Mc3r	Npr2
Mc4r	Npr3
Mc5r	Npy1r
Mchr1	Npy2r
Met	Npy5r
Mpl	Nr3c1
Mrgprx2	Nrp1
Mst1r	Nrp2
Mtnr1b	Ntng1
Ncoa3	Ntng2
Ncor1	Ntrk1
Neo1	Ntrk2
Ngfr	Ntrk3
Notch1	Ntsr1
Notch2	Oprl1
Notch3	Osmr
Npffr1	Oxtr
Npffr2	Pdgfa
Npr1	Pdgfra
Npr2	Pdgfrb
Npr3	Pgr
Npy1r	Plaur
Npy2r	Plgrkt
Npy5r	Plxna1
Nr3c1	Plxna2
Nrp1	Plxna3
Nrp2	Plxna4
Ntng1	Plxnb1
Ntng2	Plxnc1
Ntrk1	Plxnd1
Ntrk2	Procr
Ntrk3	Prokr1
Ntsr1	Prokr2
Oprl1	Ptch1
Osmr	Ptch2
Oxtr	Pth1r
Pdgfa	Pth2r
Pdgfra	Ptprk
Pdgfrb	Ptprs
Pgr	Ptprz1
Plaur	Ret
Plgrkt	Robo3
Plxna1	Ror1
Plxna2	Ror2
Plxna3	Rorb
Plxna4	Rtn4r
Plxnb1	Rtn4rl1

(Continued)

Table 8: Continued

Microarrays	
DRGs (321)	SCGs (297)
Plxnc1	Rxrg
Plxnd1	Ryr1
Prlhr	Ryr2
Prlr	Sctr
Procr	Sdc4
Prokr1	Sfrp1
Prokr2	Sfrp2
Ptch1	Slc1a5
Ptch2	Sorcs3
Pth1r	Sort1
Pth2r	Sstr1
Ptprh	Sstr2
Ptprk	Sstr3
Ptprs	Sstr4
Ptprz1	Sstr5
Ret	Tek
Robo3	Tgfbr2
Ror1	Tgfbr3
Ror2	Thbd
Rorb	Thra
Rtn4r	Thrap3
Rtn4rl1	Tnfrsf10b
Rxfp1	Tnfrsf11a
Rxrg	Tnfrsf11b
Ryr1	Tnfrsf12a
Ryr2	Tnfrsf13c
Sctr	Tnfrsf14
Sdc4	Tnfrsf17
Sfrp1	Tnfrsf18
Sfrp2	Tnfrsf1a
Slc1a5	Tnfrsf1b
Sorcs3	Tnfrsf25
Sort1	Tnfrsf4
Sstr1	Tnfrsf8
Sstr2	Tnfrsf9
Sstr3	Tshr
Sstr4	Unc5b
Sstr5	Unc5c
Tek	Uts2r
Tgfbr2	Vipr1
Tgfbr3	Vldlr
Thbd	Vtn
Thra	Xcr1
Thrap3	
Tnfrsf10b	
Tnfrsf11a	
Tnfrsf11b	
Tnfrsf12a	
Tnfrsf13c	
Tnfrsf14	
Tnfrsf17	
Tnfrsf18	
Tnfrsf1a	
Tnfrsf1b	
Tnfrsf25	
Tnfrsf4	
Tnfrsf8	
Tnfrsf9	
Tshr	
Unc5b	
Unc5c	

(Continued)

Table 8: Continued

Microarrays	
DRGs (321)	SCGs (297)
Uts2r	
Vipr1	
Vipr2	
Vldlr	
Vtn	
Xcr1	

Gene symbols of proteins identified by mass spectrometry exclusively on sensory neurons (DRGs), exclusively on sympathetic neurons (SCGs), or on both neuron types, which were identified from the protein lists shown in Table 7. Also shown are receptor mRNAs identified by microarrays as expressed by DRG and SCG neurons, defined using the updated ligand-receptor database (modified from Yuzwa et al., 2016). Only receptor mRNAs that had expression exceeding the cutoffs for each neuron type (DRGs; *Itgam*, 87% and SCGs; *Sorcs3*, 81%) are included. The total numbers of receptors in each column are indicated.

proteins with the lowest mRNA expression on the microarray for each neuron type and used those as the cutoffs. For sensory and sympathetic neurons, these were *Itgam* and *Sorcs3* mRNAs, respectively (expressed at 87% and 81% of total mRNAs; Extended Data Fig. 5-1*D*). When these thresholds were applied to the microarray data, there were 321 and 297 receptor mRNAs in sensory and sympathetic neurons, respectively (Table 8). Importantly, there was good correspondence between the proteomics and microarray data; *TrkA*/*Ntrk1*, *Bmpr2*, *Ret*, and *Igf2r* mRNAs were similarly expressed in both populations of neurons; *Rtn4r*, *Gfra3*, and *Acvr2a* mRNAs were enriched in sensory neurons (2.8-, 10-, and 3.1-fold enriched, respectively); and *Alk* mRNA was 9-fold enriched in sympathetic neurons ($p < 0.05$ FDR for differences).

Computational modeling predicts that ligands deriving from multiple types of nerve cells, including mesenchymal cells, act on peripheral neurons

We performed computational modeling with the 143 injured nerve ligands and the sensory and sympathetic neuron receptors we had defined to predict how the injured nerve environment might regulate peripheral axon biology. This modeling predicted 122 and 125 potential unidirectional paracrine interactions between the injured nerve and sympathetic and sensory neurons, respectively (Fig. 5*C*,*D*; Table 9). Of these, cell-surface receptor protein expression was detected for 49 and 60 sympathetic and sensory neuron predicted interactions (Fig. 5*C*,*D*, blue boxes). Many predicted interactions involved known peripheral nerve ligands such as the neurotrophin and GDNF families. Notably, all but three ligands (GNRH1, CXCL1, and CXCL2) were predicted to act on both sympathetic and sensory neurons. The receptors for these predicted interactions were also largely the same, except for several sensory neuron receptors; the Erbb4 receptor for EGF/neuregulin family ligands, KDR for the VEGF family, ACVR1C for the activin/BMP family, and the CXCR5 chemokine receptor (Table 9). Thus, the injured nerve is predicted to produce ligands that act on both

Table 9: Ligand-receptor modeling between injured nerve ligands and sympathetic neurons (SCGs), sensory neurons (DRGs), motor neurons (MNs), and retinal ganglion cells (RGCs)

		SCGs	
Source cell	Ligand	Target cell	Receptor
Injured nerve	ADM	SCGs	CALCRL
Injured nerve	ANGPT1	SCGs	TEK
Injured nerve	ANGPT2	SCGs	TEK
Injured nerve	ANGPT4	SCGs	TEK
Injured nerve	APLN	SCGs	APLNR
Injured nerve	ARTN	SCGs	GFRA3
Injured nerve	ARTN	SCGs	RET
Injured nerve	BDNF	SCGs	NTRK2
Injured nerve	BDNF	SCGs	SORT1
Injured nerve	BDNF	SCGs	NGFR
Injured nerve	BMP2	SCGs	BMPR1A
Injured nerve	BMP2	SCGs	BMPR1B
Injured nerve	BMP2	SCGs	BMPR2
Injured nerve	BMP2	SCGs	ENG
Injured nerve	BMP2	SCGs	NEO1
Injured nerve	BMP4	SCGs	BMPR1A
Injured nerve	BMP4	SCGs	BMPR1B
Injured nerve	BMP4	SCGs	BMPR2
Injured nerve	BMP4	SCGs	NEO1
Injured nerve	BMP5	SCGs	BMPR1A
Injured nerve	BMP7	SCGs	ACVR1
Injured nerve	BMP7	SCGs	ACVR2A
Injured nerve	BMP7	SCGs	ACVR2B
Injured nerve	BMP7	SCGs	BMPR1A
Injured nerve	BMP7	SCGs	BMPR1B
Injured nerve	BMP7	SCGs	BMPR2
Injured nerve	BMP7	SCGs	NEO1
Injured nerve	BTC	SCGs	EGFR
Injured nerve	BTC	SCGs	ERBB2
Injured nerve	CCK	SCGs	CCKAR
Injured nerve	CCK	SCGs	CCKBR
Injured nerve	CCL11	SCGs	CXCR3
Injured nerve	CCL19	SCGs	CCR10
Injured nerve	CCL19	SCGs	CCR7
Injured nerve	CCL2	SCGs	CCR10
Injured nerve	CCL25	SCGs	CCR10
Injured nerve	CCL3	SCGs	CCR4
Injured nerve	CCL5	SCGs	CCR4
Injured nerve	CCL5	SCGs	CXCR3
Injured nerve	CCL5	SCGs	SDC4
Injured nerve	CCL7	SCGs	CCR10
Injured nerve	CCL7	SCGs	CXCR3
Injured nerve	CLCF1	SCGs	CNTFR
Injured nerve	CLCF1	SCGs	IL6ST
Injured nerve	CLCF1	SCGs	LIFR
Injured nerve	CRLF1	SCGs	CNTFR
Injured nerve	CRLF1	SCGs	IL6ST
Injured nerve	CRLF1	SCGs	LIFR
Injured nerve	CSF1	SCGs	CSF1R
Injured nerve	CX3CL1	SCGs	CX3CR1
Injured nerve	CXCL10	SCGs	CXCR3
Injured nerve	CXCL12	SCGs	CCR4
Injured nerve	CXCL12	SCGs	CXCR4
Injured nerve	CXCL13	SCGs	CCR10
Injured nerve	CXCL13	SCGs	CXCR3
Injured nerve	CXCL9	SCGs	CXCR3
Injured nerve	DHH	SCGs	PTCH1
Injured nerve	DHH	SCGs	PTCH2
Injured nerve	DLL1	SCGs	NOTCH1
Injured nerve	DLL1	SCGs	NOTCH2

(Continued)

Table 9: Continued

SCGs			
Source cell	Ligand	Target cell	Receptor
Injured nerve	DLL1	SCGs	NOTCH3
Injured nerve	DLL4	SCGs	NOTCH1
Injured nerve	EBI3	SCGs	IL27RA
Injured nerve	EDA	SCGs	EDAR
Injured nerve	EDN3	SCGs	EDNRA
Injured nerve	EDN3	SCGs	EDNRB
Injured nerve	EFNA1	SCGs	EPHA1
Injured nerve	EFNA1	SCGs	EPHA3
Injured nerve	EFNA2	SCGs	EPHA3
Injured nerve	EFNA4	SCGs	EPHA3
Injured nerve	EFNA4	SCGs	EPHA5
Injured nerve	EFNA5	SCGs	EPHA3
Injured nerve	EFNA5	SCGs	EPHA2
Injured nerve	EFNA5	SCGs	EPHA7
Injured nerve	EFNA5	SCGs	EPHA5
Injured nerve	EFNB1	SCGs	EPHB2
Injured nerve	EFNB2	SCGs	EPHB1
Injured nerve	EFNB2	SCGs	EPHA4
Injured nerve	EFNB2	SCGs	EPHA3
Injured nerve	EFNB2	SCGs	EPHB4
Injured nerve	EFNB2	SCGs	EPHB2
Injured nerve	FGF1	SCGs	FGFR1
Injured nerve	FGF1	SCGs	FGFR2
Injured nerve	FGF1	SCGs	FGFR3
Injured nerve	FGF1	SCGs	FGFR4
Injured nerve	FGF10	SCGs	FGFR2
Injured nerve	FGF18	SCGs	FGFR4
Injured nerve	FGF5	SCGs	FGFR1
Injured nerve	FGF5	SCGs	FGFR3
Injured nerve	FGF7	SCGs	FGFR2
Injured nerve	FGF7	SCGs	NRP1
Injured nerve	FIGF	SCGs	FLT4
Injured nerve	FIGF	SCGs	NRP1
Injured nerve	FIGF	SCGs	NRP2
Injured nerve	FSTL1	SCGs	CD14
Injured nerve	FSTL1	SCGs	DIP2A
Injured nerve	GAS6	SCGs	AXL
Injured nerve	GDF11	SCGs	ACVR1B
Injured nerve	GDF11	SCGs	ACVR2B
Injured nerve	GDNF	SCGs	GFRA2
Injured nerve	GDNF	SCGs	RET
Injured nerve	HBEGF	SCGs	EGFR
Injured nerve	HGF	SCGs	MET
Injured nerve	IGF1	SCGs	IGF1R
Injured nerve	IGF1	SCGs	IGFBP1
Injured nerve	IGF1	SCGs	IGFBP2
Injured nerve	IGF1	SCGs	IGFBP3
Injured nerve	IGF1	SCGs	IGFBP4
Injured nerve	IGF1	SCGs	IGFBP5
Injured nerve	IGF1	SCGs	IGFBP6
Injured nerve	IGF1	SCGs	IGFBP7
Injured nerve	IGF1	SCGs	INSR
Injured nerve	IGF2	SCGs	IGF1R
Injured nerve	IGF2	SCGs	IGF2R
Injured nerve	IGF2	SCGs	INSR
Injured nerve	IL15	SCGs	IL15RA
Injured nerve	IL15	SCGs	IL2RB
Injured nerve	IL15	SCGs	IL2RG
Injured nerve	IL16	SCGs	CD4
Injured nerve	IL16	SCGs	GRIN2A
Injured nerve	IL16	SCGs	GRIN2B

(Continued)

Table 9: Continued

SCGs			
Source cell	Ligand	Target cell	Receptor
Injured nerve	IL16	SCGs	GRIN2C
Injured nerve	IL16	SCGs	GRIN2D
Injured nerve	IL18	SCGs	IL18R1
Injured nerve	IL18	SCGs	IL18RAP
Injured nerve	IL1B	SCGs	IL1R1
Injured nerve	IL1B	SCGs	IL1R2
Injured nerve	IL1B	SCGs	IL1RAP
Injured nerve	IL33	SCGs	IL1RL1
Injured nerve	IL6	SCGs	IL6R
Injured nerve	IL6	SCGs	IL6ST
Injured nerve	INHA	SCGs	ACVR2A
Injured nerve	INHA	SCGs	TGFBR3
Injured nerve	INHBA	SCGs	ACVR1B
Injured nerve	INHBA	SCGs	ACVR2A
Injured nerve	INHBA	SCGs	ACVR2B
Injured nerve	INHBB	SCGs	ACVR1
Injured nerve	INHBB	SCGs	ACVR1B
Injured nerve	INHBB	SCGs	ACVR2A
Injured nerve	INHBB	SCGs	ACVR2B
Injured nerve	JAG1	SCGs	NOTCH1
Injured nerve	JAG1	SCGs	NOTCH2
Injured nerve	JAG1	SCGs	NOTCH3
Injured nerve	JAG2	SCGs	NOTCH1
Injured nerve	JAG2	SCGs	NOTCH2
Injured nerve	JAG2	SCGs	NOTCH3
Injured nerve	LIF	SCGs	IL6ST
Injured nerve	LIF	SCGs	LIFR
Injured nerve	LTB	SCGs	LTBR
Injured nerve	MDK	SCGs	ALK
Injured nerve	MDK	SCGs	LRP1
Injured nerve	MDK	SCGs	LRP2
Injured nerve	MDK	SCGs	PTPRZ1
Injured nerve	MIF	SCGs	CD74
Injured nerve	NGF	SCGs	NGFR
Injured nerve	NGF	SCGs	NTRK1
Injured nerve	NGF	SCGs	SORCS3
Injured nerve	NGF	SCGs	SORT1
Injured nerve	NOV	SCGs	NOTCH1
Injured nerve	NPPC	SCGs	NPR2
Injured nerve	NPPC	SCGs	NPR3
Injured nerve	NTF3	SCGs	NGFR
Injured nerve	NTF3	SCGs	NTRK1
Injured nerve	NTF3	SCGs	NTRK2
Injured nerve	NTF3	SCGs	NTRK3
Injured nerve	NTN1	SCGs	DCC
Injured nerve	NTN1	SCGs	NEO1
Injured nerve	NTN1	SCGs	UNC5B
Injured nerve	NTN1	SCGs	UNC5C
Injured nerve	OSM	SCGs	IL6ST
Injured nerve	OSM	SCGs	LIFR
Injured nerve	OSM	SCGs	OSMR
Injured nerve	PDGFA	SCGs	PDGFRA
Injured nerve	PDGFB	SCGs	PDGFRA
Injured nerve	PDGFB	SCGs	PDGFRB
Injured nerve	PDGFC	SCGs	PDGFRA
Injured nerve	PF4	SCGs	CXCR3
Injured nerve	PF4	SCGs	LDLR
Injured nerve	PF4	SCGs	THBD
Injured nerve	PGF	SCGs	FLT1
Injured nerve	PGF	SCGs	NRP1
Injured nerve	PGF	SCGs	NRP2

(Continued)

Table 9: Continued

SCGs			
Source cell	Ligand	Target cell	Receptor
Injured nerve	POMC	SCGs	MC1R
Injured nerve	POMC	SCGs	MC2R
Injured nerve	POMC	SCGs	MC3R
Injured nerve	POMC	SCGs	MC4R
Injured nerve	POMC	SCGs	MC5R
Injured nerve	PTHLH	SCGs	PTH1R
Injured nerve	PTN	SCGs	ALK
Injured nerve	PTN	SCGs	PTPRS
Injured nerve	PTN	SCGs	PTPRZ1
Injured nerve	RSPO1	SCGs	LGR5
Injured nerve	RTN4	SCGs	LINGO1
Injured nerve	RTN4	SCGs	RTN4R
Injured nerve	RTN4	SCGs	RTN4RL1
Injured nerve	SEMA3B	SCGs	PLXNA1
Injured nerve	SEMA3B	SCGs	PLXNA2
Injured nerve	SEMA3B	SCGs	PLXNA3
Injured nerve	SEMA3B	SCGs	PLXNA4
Injured nerve	SEMA3B	SCGs	PLXND1
Injured nerve	SEMA3C	SCGs	PLXNA1
Injured nerve	SEMA3C	SCGs	PLXNA2
Injured nerve	SEMA3C	SCGs	PLXNA3
Injured nerve	SEMA3C	SCGs	PLXNA4
Injured nerve	SEMA3C	SCGs	PLXND1
Injured nerve	SEMA3D	SCGs	PLXNA1
Injured nerve	SEMA3D	SCGs	PLXNA2
Injured nerve	SEMA3D	SCGs	PLXNA3
Injured nerve	SEMA3D	SCGs	PLXNA4
Injured nerve	SEMA3D	SCGs	PLXND1
Injured nerve	SEMA3E	SCGs	PLXNA1
Injured nerve	SEMA3E	SCGs	PLXNA2
Injured nerve	SEMA3E	SCGs	PLXNA3
Injured nerve	SEMA3E	SCGs	PLXNA4
Injured nerve	SEMA3E	SCGs	PLXND1
Injured nerve	SEMA3F	SCGs	PLXNA1
Injured nerve	SEMA3F	SCGs	PLXNA2
Injured nerve	SEMA3F	SCGs	PLXNA3
Injured nerve	SEMA3F	SCGs	PLXNA4
Injured nerve	SEMA3F	SCGs	PLXND1
Injured nerve	SEMA3G	SCGs	PLXNA1
Injured nerve	SEMA3G	SCGs	PLXNA2
Injured nerve	SEMA3G	SCGs	PLXNA3
Injured nerve	SEMA3G	SCGs	PLXNA4
Injured nerve	SEMA3G	SCGs	PLXND1
Injured nerve	SEMA4A	SCGs	PLXNB1
Injured nerve	SEMA4A	SCGs	PLXNC1
Injured nerve	SEMA4A	SCGs	PLXND1
Injured nerve	SEMA4B	SCGs	PLXNB1
Injured nerve	SEMA4B	SCGs	PLXNC1
Injured nerve	SEMA4C	SCGs	PLXNB1
Injured nerve	SEMA4C	SCGs	PLXNC1
Injured nerve	SEMA4D	SCGs	PLXNB1
Injured nerve	SEMA4D	SCGs	PLXNC1
Injured nerve	SEMA4F	SCGs	PLXNB1
Injured nerve	SEMA4F	SCGs	PLXNC1
Injured nerve	SEMA5A	SCGs	PLXNA3
Injured nerve	SEMA5A	SCGs	PLXNA4
Injured nerve	SEMA5A	SCGs	PLXNC1
Injured nerve	SEMA5B	SCGs	PLXNA3
Injured nerve	SEMA5B	SCGs	PLXNA4
Injured nerve	SEMA5B	SCGs	PLXNC1
Injured nerve	SEMA6A	SCGs	PLXNA1

(Continued)

Table 9: Continued

SCGs			
Source cell	Ligand	Target cell	Receptor
Injured nerve	SEMA6A	SCGs	PLXNA2
Injured nerve	SEMA6B	SCGs	PLXNA1
Injured nerve	SEMA6C	SCGs	PLXNA1
Injured nerve	SEMA6D	SCGs	PLXNA1
Injured nerve	SEMA7A	SCGs	PLXNC1
Injured nerve	SHH	SCGs	PTCH1
Injured nerve	SHH	SCGs	PTCH2
Injured nerve	TGFA	SCGs	EGFR
Injured nerve	TGFA	SCGs	ERBB2
Injured nerve	TGFB1	SCGs	ACVRL1
Injured nerve	TGFB1	SCGs	ENG
Injured nerve	TGFB1	SCGs	TGFBR2
Injured nerve	TGFB1	SCGs	TGFBR3
Injured nerve	TGFB2	SCGs	TGFBR2
Injured nerve	TGFB2	SCGs	TGFBR3
Injured nerve	TGFB3	SCGs	ACVRL1
Injured nerve	TGFB3	SCGs	TGFBR2
Injured nerve	TNF	SCGs	TNFRSF1A
Injured nerve	TNF	SCGs	TNFRSF1B
Injured nerve	TNFSF10	SCGs	TNFRSF10B
Injured nerve	TNFSF12	SCGs	TNFRSF12A
Injured nerve	TNFSF12	SCGs	TNFRSF25
Injured nerve	TNFSF14	SCGs	LTBR
Injured nerve	TNFSF14	SCGs	TNFRSF14
Injured nerve	TNFSF8	SCGs	TNFRSF8
Injured nerve	TNFSF9	SCGs	TNFRSF9
Injured nerve	TSLP	SCGs	CRLF2
Injured nerve	TSLP	SCGs	IL7R
Injured nerve	UCN2	SCGs	CRHR2
Injured nerve	VEGFA	SCGs	FLT1
Injured nerve	VEGFA	SCGs	NRP1
Injured nerve	VEGFA	SCGs	NRP2
Injured nerve	VEGFB	SCGs	FLT1
Injured nerve	VEGFB	SCGs	NRP1
Injured nerve	VEGFC	SCGs	FLT4
Injured nerve	VEGFC	SCGs	NRP1
Injured nerve	VEGFC	SCGs	NRP2
Injured nerve	WNT11	SCGs	FZD4
Injured nerve	WNT2	SCGs	FZD1
Injured nerve	WNT2	SCGs	FZD9
Injured nerve	WNT5A	SCGs	FZD2
Injured nerve	WNT5A	SCGs	FZD5
Injured nerve	WNT5A	SCGs	ROR1
Injured Nerve	WNT5A	SCGs	ROR2
DRGs			
Source cell	Ligand	Target cell	Receptor
Injured nerve	ADM	DRGs	CALCRL
Injured nerve	ANGPT1	DRGs	TEK
Injured nerve	ANGPT2	DRGs	TEK
Injured nerve	ANGPT4	DRGs	TEK
Injured nerve	APLN	DRGs	APLNR
Injured nerve	ARTN	DRGs	GFRA3
Injured nerve	ARTN	DRGs	RET
Injured nerve	BDNF	DRGs	NGFR
Injured nerve	BDNF	DRGs	NTRK2
Injured nerve	BDNF	DRGs	SORT1
Injured nerve	BMP2	DRGs	BMPR1A
Injured nerve	BMP2	DRGs	BMPR1B
Injured nerve	BMP2	DRGs	BMPR2
Injured nerve	BMP2	DRGs	ENG
Injured nerve	BMP2	DRGs	NEO1

(Continued)

Table 9: Continued

DRGs			
Source cell	Ligand	Target cell	Receptor
Injured nerve	BMP4	DRGs	BMPR1A
Injured nerve	BMP4	DRGs	BMPR1B
Injured nerve	BMP4	DRGs	BMPR2
Injured nerve	BMP4	DRGs	NEO1
Injured nerve	BMP5	DRGs	BMPR1A
Injured nerve	BMP7	DRGs	ACVR1
Injured nerve	BMP7	DRGs	ACVR2A
Injured nerve	BMP7	DRGs	ACVR2B
Injured nerve	BMP7	DRGs	BMPR1A
Injured nerve	BMP7	DRGs	BMPR1B
Injured nerve	BMP7	DRGs	BMPR2
Injured nerve	BMP7	DRGs	NEO1
Injured nerve	BTC	DRGs	EGFR
Injured nerve	BTC	DRGs	ERBB2
Injured nerve	BTC	DRGs	ERBB4
Injured nerve	CCK	DRGs	CCKAR
Injured nerve	CCK	DRGs	CCKBR
Injured nerve	CCL11	DRGs	CXCR3
Injured nerve	CCL19	DRGs	CCR10
Injured nerve	CCL19	DRGs	CCR7
Injured nerve	CCL2	DRGs	CCR10
Injured nerve	CCL25	DRGs	CCR10
Injured nerve	CCL3	DRGs	CCR4
Injured nerve	CCL5	DRGs	CCR4
Injured nerve	CCL5	DRGs	CXCR3
Injured nerve	CCL5	DRGs	SDC4
Injured nerve	CCL7	DRGs	CCR10
Injured nerve	CCL7	DRGs	CXCR3
Injured nerve	CLCF1	DRGs	CNTFR
Injured nerve	CLCF1	DRGs	IL6ST
Injured nerve	CLCF1	DRGs	LIFR
Injured nerve	CRLF1	DRGs	CNTFR
Injured nerve	CRLF1	DRGs	IL6ST
Injured nerve	CRLF1	DRGs	LIFR
Injured nerve	CSF1	DRGs	CSF1R
Injured nerve	CX3CL1	DRGs	CX3CR1
Injured nerve	CXCL1	DRGs	CXCR2
Injured nerve	CXCL10	DRGs	CXCR3
Injured nerve	CXCL12	DRGs	CCR4
Injured nerve	CXCL12	DRGs	CXCR4
Injured nerve	CXCL13	DRGs	CCR10
Injured nerve	CXCL13	DRGs	CXCR3
Injured nerve	CXCL13	DRGs	CXCR5
Injured nerve	CXCL2	DRGs	CXCR2
Injured nerve	CXCL9	DRGs	CXCR3
Injured nerve	DHH	DRGs	PTCH1
Injured nerve	DHH	DRGs	PTCH2
Injured nerve	DLL1	DRGs	NOTCH1
Injured nerve	DLL1	DRGs	NOTCH2
Injured nerve	DLL1	DRGs	NOTCH3
Injured nerve	DLL4	DRGs	NOTCH1
Injured nerve	EBI3	DRGs	IL27RA
Injured nerve	EDA	DRGs	EDAR
Injured nerve	EDN3	DRGs	EDNRA
Injured nerve	EDN3	DRGs	EDNRB
Injured nerve	EFNA1	DRGs	EPHA1
Injured nerve	EFNA1	DRGs	EPHA3
Injured nerve	EFNA2	DRGs	EPHA3
Injured nerve	EFNA4	DRGs	EPHA3
Injured nerve	EFNA4	DRGs	EPHA5
Injured nerve	EFNA5	DRGs	EPHA3

(Continued)

Table 9: Continued

DRGs			
Source cell	Ligand	Target cell	Receptor
Injured nerve	EFNA5	DRGs	EPHA2
Injured nerve	EFNA5	DRGs	EPHA7
Injured nerve	EFNA5	DRGs	EPHA5
Injured nerve	EFNB1	DRGs	EPHB2
Injured nerve	EFNB2	DRGs	EPHB1
Injured nerve	EFNB2	DRGs	EPHA4
Injured nerve	EFNB2	DRGs	EPHA3
Injured nerve	EFNB2	DRGs	EPHB4
Injured nerve	EFNB2	DRGs	EPHB2
Injured nerve	FGF1	DRGs	FGFR1
Injured nerve	FGF1	DRGs	FGFR2
Injured nerve	FGF1	DRGs	FGFR3
Injured nerve	FGF1	DRGs	FGFR4
Injured nerve	FGF10	DRGs	FGFR2
Injured nerve	FGF18	DRGs	FGFR4
Injured nerve	FGF5	DRGs	FGFR1
Injured nerve	FGF5	DRGs	FGFR3
Injured nerve	FGF7	DRGs	FGFR2
Injured nerve	FGF7	DRGs	NRP1
Injured nerve	FIGF	DRGs	FLT4
Injured nerve	FIGF	DRGs	KDR
Injured nerve	FIGF	DRGs	NRP1
Injured nerve	FIGF	DRGs	NRP2
Injured nerve	FSTL1	DRGs	CD14
Injured nerve	FSTL1	DRGs	DIP2A
Injured nerve	GAS6	DRGs	AXL
Injured nerve	GDF11	DRGs	ACVR1B
Injured nerve	GDF11	DRGs	ACVR1C
Injured nerve	GDF11	DRGs	ACVR2B
Injured nerve	GDNF	DRGs	GFRA2
Injured nerve	GDNF	DRGs	RET
Injured nerve	GNRH1	DRGs	GNRHR
Injured nerve	HBEGF	DRGs	EGFR
Injured nerve	HBEGF	DRGs	ERBB4
Injured nerve	HGF	DRGs	MET
Injured nerve	IGF1	DRGs	IGF1R
Injured nerve	IGF1	DRGs	IGFBP1
Injured nerve	IGF1	DRGs	IGFBP2
Injured nerve	IGF1	DRGs	IGFBP3
Injured nerve	IGF1	DRGs	IGFBP4
Injured nerve	IGF1	DRGs	IGFBP5
Injured nerve	IGF1	DRGs	IGFBP6
Injured nerve	IGF1	DRGs	IGFBP7
Injured nerve	IGF1	DRGs	INSR
Injured nerve	IGF2	DRGs	IGF1R
Injured nerve	IGF2	DRGs	IGF2R
Injured nerve	IGF2	DRGs	INSR
Injured nerve	IL15	DRGs	IL15RA
Injured nerve	IL15	DRGs	IL2RB
Injured nerve	IL15	DRGs	IL2RG
Injured nerve	IL16	DRGs	CD4
Injured nerve	IL16	DRGs	GRIN2A
Injured nerve	IL16	DRGs	GRIN2B
Injured nerve	IL16	DRGs	GRIN2C
Injured nerve	IL16	DRGs	GRIN2D
Injured nerve	IL18	DRGs	IL18R1
Injured nerve	IL18	DRGs	IL18RAP
Injured nerve	IL1B	DRGs	IL1R1
Injured nerve	IL1B	DRGs	IL1R2
Injured nerve	IL1B	DRGs	IL1RAP
Injured nerve	IL33	DRGs	IL1RL1

(Continued)

Table 9: Continued

DRGs			
Source cell	Ligand	Target cell	Receptor
Injured nerve	IL6	DRGs	IL6R
Injured nerve	IL6	DRGs	IL6ST
Injured nerve	INHA	DRGs	ACVR2A
Injured nerve	INHA	DRGs	TGFBR3
Injured nerve	INHBA	DRGs	ACVR1B
Injured nerve	INHBA	DRGs	ACVR2A
Injured nerve	INHBA	DRGs	ACVR2B
Injured nerve	INHBB	DRGs	ACVR1
Injured nerve	INHBB	DRGs	ACVR1B
Injured nerve	INHBB	DRGs	ACVR1C
Injured nerve	INHBB	DRGs	ACVR2A
Injured nerve	INHBB	DRGs	ACVR2B
Injured nerve	JAG1	DRGs	NOTCH1
Injured nerve	JAG1	DRGs	NOTCH2
Injured nerve	JAG1	DRGs	NOTCH3
Injured nerve	JAG2	DRGs	NOTCH1
Injured nerve	JAG2	DRGs	NOTCH2
Injured nerve	JAG2	DRGs	NOTCH3
Injured nerve	LIF	DRGs	IL6ST
Injured nerve	LIF	DRGs	LIFR
Injured nerve	LTB	DRGs	LTBR
Injured nerve	MDK	DRGs	ALK
Injured nerve	MDK	DRGs	LRP1
Injured nerve	MDK	DRGs	LRP2
Injured nerve	MDK	DRGs	PTPRZ1
Injured nerve	MIF	DRGs	CD74
Injured nerve	NGF	DRGs	NGFR
Injured nerve	NGF	DRGs	NTRK1
Injured nerve	NGF	DRGs	SORCS3
Injured nerve	NGF	DRGs	SORT1
Injured nerve	NOV	DRGs	NOTCH1
Injured nerve	NPPC	DRGs	NPR2
Injured nerve	NPPC	DRGs	NPR3
Injured nerve	NTF3	DRGs	NGFR
Injured nerve	NTF3	DRGs	NTRK1
Injured nerve	NTF3	DRGs	NTRK2
Injured nerve	NTF3	DRGs	NTRK3
Injured nerve	NTN1	DRGs	DCC
Injured nerve	NTN1	DRGs	NEO1
Injured nerve	NTN1	DRGs	UNC5B
Injured nerve	NTN1	DRGs	UNC5C
Injured nerve	OSM	DRGs	IL6ST
Injured nerve	OSM	DRGs	LIFR
Injured nerve	OSM	DRGs	OSMR
Injured nerve	PDGFA	DRGs	PDGFRA
Injured nerve	PDGFB	DRGs	PDGFRA
Injured nerve	PDGFB	DRGs	PDGFRB
Injured nerve	PDGFC	DRGs	PDGFRA
Injured nerve	PF4	DRGs	CXCR3
Injured nerve	PF4	DRGs	LDLR
Injured nerve	PF4	DRGs	THBD
Injured nerve	PGF	DRGs	FLT1
Injured nerve	PGF	DRGs	NRP1
Injured nerve	PGF	DRGs	NRP2
Injured nerve	POMC	DRGs	MC1R
Injured nerve	POMC	DRGs	MC2R
Injured nerve	POMC	DRGs	MC3R
Injured nerve	POMC	DRGs	MC4R
Injured nerve	POMC	DRGs	MC5R
Injured nerve	PTHLH	DRGs	PTH1R
Injured nerve	PTN	DRGs	ALK

(Continued)

Table 9: Continued

DRGs			
Source cell	Ligand	Target cell	Receptor
Injured nerve	PTN	DRGs	PTPRS
Injured nerve	PTN	DRGs	PTPRZ1
Injured nerve	RSPO1	DRGs	LGR5
Injured nerve	RTN4	DRGs	LINGO1
Injured nerve	RTN4	DRGs	RTN4R
Injured nerve	RTN4	DRGs	RTN4RL1
Injured nerve	SEMA3B	DRGs	PLXNA1
Injured nerve	SEMA3B	DRGs	PLXNA2
Injured nerve	SEMA3B	DRGs	PLXNA3
Injured nerve	SEMA3B	DRGs	PLXNA4
Injured nerve	SEMA3B	DRGs	PLXND1
Injured nerve	SEMA3C	DRGs	PLXNA1
Injured nerve	SEMA3C	DRGs	PLXNA2
Injured nerve	SEMA3C	DRGs	PLXNA3
Injured nerve	SEMA3C	DRGs	PLXNA4
Injured nerve	SEMA3C	DRGs	PLXND1
Injured nerve	SEMA3D	DRGs	PLXNA1
Injured nerve	SEMA3D	DRGs	PLXNA2
Injured nerve	SEMA3D	DRGs	PLXNA3
Injured nerve	SEMA3D	DRGs	PLXNA4
Injured nerve	SEMA3D	DRGs	PLXND1
Injured nerve	SEMA3E	DRGs	PLXNA1
Injured nerve	SEMA3E	DRGs	PLXNA2
Injured nerve	SEMA3E	DRGs	PLXNA3
Injured nerve	SEMA3E	DRGs	PLXNA4
Injured nerve	SEMA3E	DRGs	PLXND1
Injured nerve	SEMA3F	DRGs	PLXNA1
Injured nerve	SEMA3F	DRGs	PLXNA2
Injured nerve	SEMA3F	DRGs	PLXNA3
Injured nerve	SEMA3F	DRGs	PLXNA4
Injured nerve	SEMA3F	DRGs	PLXND1
Injured nerve	SEMA3G	DRGs	PLXNA1
Injured nerve	SEMA3G	DRGs	PLXNA2
Injured nerve	SEMA3G	DRGs	PLXNA3
Injured nerve	SEMA3G	DRGs	PLXNA4
Injured nerve	SEMA3G	DRGs	PLXND1
Injured nerve	SEMA4A	DRGs	PLXNB1
Injured nerve	SEMA4A	DRGs	PLXNC1
Injured nerve	SEMA4A	DRGs	PLXND1
Injured nerve	SEMA4B	DRGs	PLXNB1
Injured nerve	SEMA4B	DRGs	PLXNC1
Injured nerve	SEMA4C	DRGs	PLXNB1
Injured nerve	SEMA4C	DRGs	PLXNC1
Injured nerve	SEMA4D	DRGs	PLXNB1
Injured nerve	SEMA4D	DRGs	PLXNC1
Injured nerve	SEMA4F	DRGs	PLXNB1
Injured nerve	SEMA4F	DRGs	PLXNC1
Injured nerve	SEMA5A	DRGs	PLXNA3
Injured nerve	SEMA5A	DRGs	PLXNA4
Injured nerve	SEMA5A	DRGs	PLXNC1
Injured nerve	SEMA5B	DRGs	PLXNA3
Injured nerve	SEMA5B	DRGs	PLXNA4
Injured nerve	SEMA5B	DRGs	PLXNC1
Injured nerve	SEMA6A	DRGs	PLXNA1
Injured nerve	SEMA6A	DRGs	PLXNA2
Injured nerve	SEMA6B	DRGs	PLXNA1
Injured nerve	SEMA6C	DRGs	PLXNA1
Injured nerve	SEMA6D	DRGs	PLXNA1
Injured nerve	SEMA7A	DRGs	PLXNC1
Injured nerve	SHH	DRGs	PTCH1
Injured nerve	SHH	DRGs	PTCH2

(Continued)

Table 9: Continued

DRGs			
Source cell	Ligand	Target cell	Receptor
Injured nerve	TGFA	DRGs	EGFR
Injured nerve	TGFA	DRGs	ERBB2
Injured nerve	TGFB1	DRGs	ACVRL1
Injured nerve	TGFB1	DRGs	ENG
Injured nerve	TGFB1	DRGs	TGFBR2
Injured nerve	TGFB1	DRGs	TGFBR3
Injured nerve	TGFB2	DRGs	TGFBR2
Injured nerve	TGFB2	DRGs	TGFBR3
Injured nerve	TGFB3	DRGs	ACVRL1
Injured nerve	TGFB3	DRGs	TGFBR2
Injured nerve	TNF	DRGs	TNFRSF1A
Injured nerve	TNF	DRGs	TNFRSF1B
Injured nerve	TNFSF10	DRGs	TNFRSF10B
Injured nerve	TNFSF12	DRGs	TNFRSF12A
Injured nerve	TNFSF12	DRGs	TNFRSF25
Injured nerve	TNFSF14	DRGs	LTBR
Injured nerve	TNFSF14	DRGs	TNFRSF14
Injured nerve	TNFSF8	DRGs	TNFRSF8
Injured nerve	TNFSF9	DRGs	TNFRSF9
Injured nerve	TSLP	DRGs	CRLF2
Injured nerve	TSLP	DRGs	IL7R
Injured nerve	UCN2	DRGs	CRHR2
Injured nerve	VEGFA	DRGs	FLT1
Injured nerve	VEGFA	DRGs	KDR
Injured nerve	VEGFA	DRGs	NRP1
Injured nerve	VEGFA	DRGs	NRP2
Injured nerve	VEGFB	DRGs	FLT1
Injured nerve	VEGFB	DRGs	NRP1
Injured nerve	VEGFC	DRGs	FLT4
Injured nerve	VEGFC	DRGs	KDR
Injured nerve	VEGFC	DRGs	NRP1
Injured nerve	VEGFC	DRGs	NRP2
Injured nerve	WNT11	DRGs	FZD4
Injured nerve	WNT2	DRGs	FZD1
Injured nerve	WNT2	DRGs	FZD9
Injured nerve	WNT5A	DRGs	FZD2
Injured nerve	WNT5A	DRGs	FZD5
Injured nerve	WNT5A	DRGs	ROR1
Injured nerve	WNT5A	DRGs	ROR2
MNs			
Source cell	Ligand	Target cell	Receptor
Injured nerve	ADM	MNs	CALCRL
Injured nerve	ANGPT1	MNs	TEK
Injured nerve	ANGPT2	MNs	TEK
Injured nerve	ANGPT4	MNs	TEK
Injured nerve	APLN	MNs	APLNR
Injured nerve	ARTN	MNs	GFRA3
Injured nerve	ARTN	MNs	RET
Injured nerve	BDNF	MNs	NGFR
Injured nerve	BDNF	MNs	NTRK2
Injured nerve	BDNF	MNs	SORT1
Injured nerve	BMP2	MNs	BMPR1A
Injured nerve	BMP2	MNs	BMPR1B
Injured nerve	BMP2	MNs	BMPR2
Injured nerve	BMP2	MNs	ENG
Injured nerve	BMP2	MNs	NEO1
Injured nerve	BMP4	MNs	BMPR1A
Injured nerve	BMP4	MNs	BMPR1B
Injured nerve	BMP4	MNs	BMPR2
Injured nerve	BMP4	MNs	NEO1
Injured nerve	BMP5	MNs	BMPR1A

(Continued)

Table 9: Continued

MNs			
Source cell	Ligand	Target cell	Receptor
Injured nerve	BMP7	MNs	ACVR1
Injured nerve	BMP7	MNs	ACVR2A
Injured nerve	BMP7	MNs	ACVR2B
Injured nerve	BMP7	MNs	BMPR1A
Injured nerve	BMP7	MNs	BMPR1B
Injured nerve	BMP7	MNs	BMPR2
Injured nerve	BMP7	MNs	NEO1
Injured nerve	BTC	MNs	EGFR
Injured nerve	BTC	MNs	ERBB2
Injured nerve	BTC	MNs	ERBB4
Injured nerve	CCK	MNs	CCKAR
Injured nerve	CCK	MNs	CCKBR
Injured nerve	CCL11	MNs	CCR5
Injured nerve	CCL11	MNs	CXCR3
Injured nerve	CCL19	MNs	CCR10
Injured nerve	CCL2	MNs	CCR10
Injured nerve	CCL2	MNs	CCR2
Injured nerve	CCL25	MNs	CCR10
Injured nerve	CCL25	MNs	CCR9
Injured nerve	CCL3	MNs	CCR5
Injured nerve	CCL5	MNs	CCR5
Injured nerve	CCL5	MNs	CXCR3
Injured nerve	CCL5	MNs	SDC4
Injured nerve	CCL7	MNs	CCR10
Injured nerve	CCL7	MNs	CCR2
Injured nerve	CCL7	MNs	CCR5
Injured nerve	CCL7	MNs	CXCR3
Injured nerve	CLCF1	MNs	CNTFR
Injured nerve	CLCF1	MNs	IL6ST
Injured nerve	CLCF1	MNs	LIFR
Injured nerve	CRLF1	MNs	CNTFR
Injured nerve	CRLF1	MNs	IL6ST
Injured nerve	CRLF1	MNs	LIFR
Injured nerve	CSF1	MNs	CSF1R
Injured nerve	CX3CL1	MNs	CX3CR1
Injured nerve	CXCL10	MNs	CXCR3
Injured nerve	CXCL12	MNs	CXCR4
Injured nerve	CXCL13	MNs	CCR10
Injured nerve	CXCL13	MNs	CXCR3
Injured nerve	CXCL13	MNs	CXCR5
Injured nerve	CXCL9	MNs	CXCR3
Injured nerve	DHH	MNs	PTCH1
Injured nerve	DHH	MNs	PTCH2
Injured nerve	DLL1	MNs	NOTCH1
Injured nerve	DLL1	MNs	NOTCH2
Injured nerve	DLL1	MNs	NOTCH3
Injured nerve	DLL4	MNs	NOTCH1
Injured nerve	EBI3	MNs	IL27RA
Injured nerve	EDN3	MNs	EDNRA
Injured nerve	EDN3	MNs	EDNRB
Injured nerve	EFNA1	MNs	EPHA1
Injured nerve	EFNA1	MNs	EPHA3
Injured nerve	EFNA2	MNs	EPHA3
Injured nerve	EFNA4	MNs	EPHA3
Injured nerve	EFNA4	MNs	EPHA5
Injured nerve	EFNA5	MNs	EPHA3
Injured nerve	EFNA5	MNs	EPHA2
Injured nerve	EFNA5	MNs	EPHA7
Injured nerve	EFNA5	MNs	EPHA5
Injured nerve	EFNB1	MNs	EPHB2
Injured nerve	EFNB2	MNs	EPHB1

(Continued)

Table 9: Continued

MNs			
Source cell	Ligand	Target cell	Receptor
Injured nerve	EFNB2	MNs	EPHA4
Injured nerve	EFNB2	MNs	EPHA3
Injured nerve	EFNB2	MNs	EPHB4
Injured nerve	EFNB2	MNs	EPHB2
Injured nerve	FGF1	MNs	FGFR1
Injured nerve	FGF1	MNs	FGFR2
Injured nerve	FGF1	MNs	FGFR3
Injured nerve	FGF1	MNs	FGFR4
Injured nerve	FGF10	MNs	FGFR2
Injured nerve	FGF18	MNs	FGFR4
Injured nerve	FGF5	MNs	FGFR1
Injured nerve	FGF5	MNs	FGFR3
Injured nerve	FGF7	MNs	FGFR2
Injured nerve	FGF7	MNs	NRP1
Injured nerve	FIGF	MNs	FLT4
Injured nerve	FIGF	MNs	KDR
Injured nerve	FIGF	MNs	NRP1
Injured nerve	FIGF	MNs	NRP2
Injured nerve	FSTL1	MNs	CD14
Injured nerve	FSTL1	MNs	DIP2A
Injured nerve	GAS6	MNs	AXL
Injured nerve	GDF11	MNs	ACVR1B
Injured nerve	GDF11	MNs	ACVR1C
Injured nerve	GDF11	MNs	ACVR2B
Injured nerve	GDNF	MNs	GFRA1
Injured nerve	GDNF	MNs	GFRA2
Injured nerve	GDNF	MNs	RET
Injured nerve	GNRH1	MNs	GNRHR
Injured nerve	GRP	MNs	GRPR
Injured nerve	HBEGF	MNs	EGFR
Injured nerve	HBEGF	MNs	ERBB4
Injured nerve	HGF	MNs	MET
Injured nerve	IGF1	MNs	IGF1R
Injured nerve	IGF1	MNs	IGFBP1
Injured nerve	IGF1	MNs	IGFBP2
Injured nerve	IGF1	MNs	IGFBP3
Injured nerve	IGF1	MNs	IGFBP4
Injured nerve	IGF1	MNs	IGFBP5
Injured nerve	IGF1	MNs	IGFBP6
Injured nerve	IGF1	MNs	IGFBP7
Injured nerve	IGF1	MNs	INSR
Injured nerve	IGF2	MNs	IGF1R
Injured nerve	IGF2	MNs	IGF2R
Injured nerve	IGF2	MNs	INSR
Injured nerve	IL15	MNs	IL15RA
Injured nerve	IL15	MNs	IL2RB
Injured nerve	IL15	MNs	IL2RG
Injured nerve	IL16	MNs	CD4
Injured nerve	IL16	MNs	GRIN2A
Injured nerve	IL16	MNs	GRIN2B
Injured nerve	IL16	MNs	GRIN2C
Injured nerve	IL16	MNs	GRIN2D
Injured nerve	IL18	MNs	IL18R1
Injured nerve	IL18	MNs	IL18RAP
Injured nerve	IL1B	MNs	IL1R1
Injured nerve	IL1B	MNs	IL1R2
Injured nerve	IL1B	MNs	IL1RAP
Injured nerve	IL33	MNs	IL1RL1
Injured nerve	IL6	MNs	IL6ST
Injured nerve	INHA	MNs	ACVR2A
Injured nerve	INHA	MNs	TGFBR3

(Continued)

Table 9: Continued

MNs			
Source cell	Ligand	Target cell	Receptor
Injured nerve	INHBA	MNs	ACVR1B
Injured nerve	INHBA	MNs	ACVR2A
Injured nerve	INHBA	MNs	ACVR2B
Injured nerve	INHBB	MNs	ACVR1
Injured nerve	INHBB	MNs	ACVR1B
Injured nerve	INHBB	MNs	ACVR1C
Injured nerve	INHBB	MNs	ACVR2A
Injured nerve	INHBB	MNs	ACVR2B
Injured nerve	JAG1	MNs	NOTCH1
Injured nerve	JAG1	MNs	NOTCH2
Injured nerve	JAG1	MNs	NOTCH3
Injured nerve	JAG2	MNs	NOTCH1
Injured nerve	JAG2	MNs	NOTCH2
Injured nerve	JAG2	MNs	NOTCH3
Injured nerve	LIF	MNs	IL6ST
Injured nerve	LIF	MNs	LIFR
Injured nerve	LTB	MNs	LTBR
Injured nerve	MDK	MNs	ALK
Injured nerve	MDK	MNs	LRP1
Injured nerve	MDK	MNs	PTPRZ1
Injured nerve	MIF	MNs	CD74
Injured nerve	NGF	MNs	NGFR
Injured nerve	NGF	MNs	NTRK1
Injured nerve	NGF	MNs	SORCS3
Injured nerve	NGF	MNs	SORT1
Injured nerve	NOV	MNs	NOTCH1
Injured nerve	NPPC	MNs	NPR2
Injured nerve	NPPC	MNs	NPR3
Injured nerve	NTF3	MNs	NGFR
Injured nerve	NTF3	MNs	NTRK1
Injured nerve	NTF3	MNs	NTRK2
Injured nerve	NTF3	MNs	NTRK3
Injured nerve	NTN1	MNs	DCC
Injured nerve	NTN1	MNs	NEO1
Injured nerve	NTN1	MNs	UNC5B
Injured nerve	NTN1	MNs	UNC5C
Injured nerve	OSM	MNs	IL6ST
Injured nerve	OSM	MNs	LIFR
Injured nerve	OSM	MNs	OSMR
Injured nerve	PDGFA	MNs	PDGFRA
Injured nerve	PDGFB	MNs	PDGFRA
Injured nerve	PDGFB	MNs	PDGFRB
Injured nerve	PDGFC	MNs	PDGFRA
Injured nerve	PF4	MNs	CXCR3
Injured nerve	PF4	MNs	LDLR
Injured nerve	PF4	MNs	THBD
Injured nerve	PGF	MNs	FLT1
Injured nerve	PGF	MNs	NRP1
Injured nerve	PGF	MNs	NRP2
Injured nerve	POMC	MNs	MC1R
Injured nerve	POMC	MNs	MC2R
Injured nerve	POMC	MNs	MC3R
Injured nerve	POMC	MNs	MC5R
Injured nerve	PTHLH	MNs	PTH1R
Injured nerve	PTN	MNs	ALK
Injured nerve	PTN	MNs	PTPRS
Injured nerve	PTN	MNs	PTPRZ1
Injured nerve	RSPO1	MNs	LGR5
Injured nerve	RTN4	MNs	LINGO1
Injured nerve	RTN4	MNs	RTN4R
Injured nerve	RTN4	MNs	RTN4RL1

(Continued)

Table 9: Continued

		MNs	
Source cell	Ligand	Target cell	Receptor
Injured nerve	SEMA3B	MNs	PLXNA1
Injured nerve	SEMA3B	MNs	PLXNA2
Injured nerve	SEMA3B	MNs	PLXNA3
Injured nerve	SEMA3B	MNs	PLXNA4
Injured nerve	SEMA3B	MNs	PLXNB2
Injured nerve	SEMA3B	MNs	PLXND1
Injured nerve	SEMA3C	MNs	PLXNA1
Injured nerve	SEMA3C	MNs	PLXNA2
Injured nerve	SEMA3C	MNs	PLXNA3
Injured nerve	SEMA3C	MNs	PLXNA4
Injured nerve	SEMA3C	MNs	PLXNB2
Injured nerve	SEMA3C	MNs	PLXND1
Injured nerve	SEMA3D	MNs	PLXNA1
Injured nerve	SEMA3D	MNs	PLXNA2
Injured nerve	SEMA3D	MNs	PLXNA3
Injured nerve	SEMA3D	MNs	PLXNA4
Injured nerve	SEMA3D	MNs	PLXNB2
Injured nerve	SEMA3D	MNs	PLXND1
Injured nerve	SEMA3E	MNs	PLXNA1
Injured nerve	SEMA3E	MNs	PLXNA2
Injured nerve	SEMA3E	MNs	PLXNA3
Injured nerve	SEMA3E	MNs	PLXNA4
Injured nerve	SEMA3E	MNs	PLXNB2
Injured nerve	SEMA3E	MNs	PLXND1
Injured nerve	SEMA3F	MNs	PLXNA1
Injured nerve	SEMA3F	MNs	PLXNA2
Injured nerve	SEMA3F	MNs	PLXNA3
Injured nerve	SEMA3F	MNs	PLXNA4
Injured nerve	SEMA3F	MNs	PLXNB2
Injured nerve	SEMA3F	MNs	PLXND1
Injured nerve	SEMA3G	MNs	PLXNA1
Injured nerve	SEMA3G	MNs	PLXNA2
Injured nerve	SEMA3G	MNs	PLXNA3
Injured nerve	SEMA3G	MNs	PLXNA4
Injured nerve	SEMA3G	MNs	PLXNB2
Injured nerve	SEMA3G	MNs	PLXND1
Injured nerve	SEMA4A	MNs	PLXNB1
Injured nerve	SEMA4A	MNs	PLXNB2
Injured nerve	SEMA4A	MNs	PLXNC1
Injured nerve	SEMA4A	MNs	PLXND1
Injured nerve	SEMA4B	MNs	PLXNB1
Injured nerve	SEMA4B	MNs	PLXNB2
Injured nerve	SEMA4B	MNs	PLXNC1
Injured nerve	SEMA4C	MNs	PLXNB1
Injured nerve	SEMA4C	MNs	PLXNB2
Injured nerve	SEMA4C	MNs	PLXNC1
Injured nerve	SEMA4D	MNs	PLXNB1
Injured nerve	SEMA4D	MNs	PLXNB2
Injured nerve	SEMA4D	MNs	PLXNC1
Injured nerve	SEMA4F	MNs	PLXNB1
Injured nerve	SEMA4F	MNs	PLXNB2
Injured nerve	SEMA4F	MNs	PLXNC1
Injured nerve	SEMA5A	MNs	PLXNA3
Injured nerve	SEMA5A	MNs	PLXNA4
Injured nerve	SEMA5A	MNs	PLXNC1
Injured nerve	SEMA5B	MNs	PLXNA3
Injured nerve	SEMA5B	MNs	PLXNA4
Injured nerve	SEMA5B	MNs	PLXNC1
Injured nerve	SEMA6A	MNs	PLXNA1
Injured nerve	SEMA6A	MNs	PLXNA2
Injured nerve	SEMA6B	MNs	PLXNA1

(Continued)

Table 9: Continued

MNs			
Source cell	Ligand	Target cell	Receptor
Injured nerve	SEMA6C	MNs	PLXNA1
Injured nerve	SEMA6D	MNs	PLXNA1
Injured nerve	SEMA7A	MNs	PLXNC1
Injured nerve	SHH	MNs	PTCH1
Injured nerve	SHH	MNs	PTCH2
Injured nerve	TGFA	MNs	EGFR
Injured nerve	TGFA	MNs	ERBB2
Injured nerve	TGFB1	MNs	ACVRL1
Injured nerve	TGFB1	MNs	ENG
Injured nerve	TGFB1	MNs	TGFBR1
Injured nerve	TGFB1	MNs	TGFBR2
Injured nerve	TGFB1	MNs	TGFBR3
Injured nerve	TGFB2	MNs	TGFBR1
Injured nerve	TGFB2	MNs	TGFBR2
Injured nerve	TGFB2	MNs	TGFBR3
Injured nerve	TGFB3	MNs	ACVRL1
Injured nerve	TGFB3	MNs	TGFBR1
Injured nerve	TGFB3	MNs	TGFBR2
Injured nerve	TNF	MNs	TNFRSF1A
Injured nerve	TNF	MNs	TNFRSF1B
Injured nerve	TNFSF10	MNs	TNFRSF10B
Injured nerve	TNFSF12	MNs	TNFRSF12A
Injured nerve	TNFSF12	MNs	TNFRSF25
Injured nerve	TNFSF14	MNs	LTBR
Injured nerve	TNFSF14	MNs	TNFRSF14
Injured nerve	TNFSF8	MNs	TNFRSF8
Injured nerve	TNFSF9	MNs	TNFRSF9
Injured nerve	TSLP	MNs	CRLF2
Injured nerve	TSLP	MNs	IL7R
Injured nerve	UCN2	MNs	CRHR2
Injured nerve	VEGFA	MNs	FLT1
Injured nerve	VEGFA	MNs	KDR
Injured nerve	VEGFA	MNs	NRP1
Injured nerve	VEGFA	MNs	NRP2
Injured nerve	VEGFB	MNs	FLT1
Injured nerve	VEGFB	MNs	NRP1
Injured nerve	VEGFC	MNs	FLT4
Injured nerve	VEGFC	MNs	KDR
Injured nerve	VEGFC	MNs	NRP1
Injured nerve	VEGFC	MNs	NRP2
Injured nerve	WNT11	MNs	FZD4
Injured nerve	WNT2	MNs	FZD1
Injured nerve	WNT2	MNs	FZD9
Injured nerve	WNT5A	MNs	FZD2
Injured nerve	WNT5A	MNs	FZD5
Injured nerve	WNT5A	MNs	ROR1
Injured nerve	WNT5A	MNs	ROR2
RGCs			
Source cell	Ligand	Target cell	Receptor
Injured nerve	ADM	RGCs	CALCRL
Injured nerve	ANGPT1	RGCs	TEK
Injured nerve	ANGPT2	RGCs	TEK
Injured nerve	ANGPT4	RGCs	TEK
Injured nerve	APLN	RGCs	APLNR
Injured nerve	ARTN	RGCs	GFRA3
Injured nerve	ARTN	RGCs	RET
Injured nerve	BDNF	RGCs	NGFR
Injured nerve	BDNF	RGCs	NTRK2
Injured nerve	BDNF	RGCs	SORT1
Injured nerve	BMP2	RGCs	BMPR1A
Injured nerve	BMP2	RGCs	BMPR1B

(Continued)

Table 9: Continued

RGCs			
Source cell	Ligand	Target cell	Receptor
Injured nerve	BMP2	RGCs	BMPR2
Injured nerve	BMP2	RGCs	ENG
Injured nerve	BMP2	RGCs	NEO1
Injured nerve	BMP4	RGCs	BMPR1A
Injured nerve	BMP4	RGCs	BMPR1B
Injured nerve	BMP4	RGCs	BMPR2
Injured nerve	BMP4	RGCs	NEO1
Injured nerve	BMP5	RGCs	BMPR1A
Injured nerve	BMP7	RGCs	ACVR1
Injured nerve	BMP7	RGCs	ACVR2A
Injured nerve	BMP7	RGCs	ACVR2B
Injured nerve	BMP7	RGCs	BMPR1A
Injured nerve	BMP7	RGCs	BMPR1B
Injured nerve	BMP7	RGCs	BMPR2
Injured nerve	BMP7	RGCs	NEO1
Injured nerve	BTC	RGCs	EGFR
Injured nerve	BTC	RGCs	ERBB2
Injured nerve	BTC	RGCs	ERBB4
Injured nerve	CCK	RGCs	CCKAR
Injured nerve	CCK	RGCs	CCKBR
Injured nerve	CCL11	RGCs	CCR5
Injured nerve	CCL11	RGCs	CXCR3
Injured nerve	CCL19	RGCs	CCR10
Injured nerve	CCL2	RGCs	CCR1
Injured nerve	CCL2	RGCs	CCR10
Injured nerve	CCL2	RGCs	CCR2
Injured nerve	CCL2	RGCs	DARC
Injured nerve	CCL25	RGCs	CCR10
Injured nerve	CCL25	RGCs	CCR9
Injured nerve	CCL3	RGCs	CCR1
Injured nerve	CCL3	RGCs	CCR4
Injured nerve	CCL3	RGCs	CCR5
Injured nerve	CCL5	RGCs	CCR1
Injured nerve	CCL5	RGCs	CCR4
Injured nerve	CCL5	RGCs	CCR5
Injured nerve	CCL5	RGCs	CXCR3
Injured nerve	CCL5	RGCs	DARC
Injured nerve	CCL5	RGCs	SDC4
Injured nerve	CCL7	RGCs	CCR1
Injured nerve	CCL7	RGCs	CCR10
Injured nerve	CCL7	RGCs	CCR2
Injured nerve	CCL7	RGCs	CCR5
Injured nerve	CCL7	RGCs	CXCR3
Injured nerve	CCL7	RGCs	DARC
Injured nerve	CCL9	RGCs	CCR1
Injured nerve	CLCF1	RGCs	CNTFR
Injured nerve	CLCF1	RGCs	IL6ST
Injured nerve	CLCF1	RGCs	LIFR
Injured nerve	CRLF1	RGCs	CNTFR
Injured nerve	CRLF1	RGCs	IL6ST
Injured nerve	CRLF1	RGCs	LIFR
Injured nerve	CSF1	RGCs	CSF1R
Injured nerve	CX3CL1	RGCs	CX3CR1
Injured nerve	CXCL1	RGCs	CXCR2
Injured nerve	CXCL1	RGCs	DARC
Injured nerve	CXCL10	RGCs	CXCR3
Injured nerve	CXCL12	RGCs	CCR4
Injured nerve	CXCL12	RGCs	CXCR4
Injured nerve	CXCL13	RGCs	CCR10
Injured nerve	CXCL13	RGCs	CXCR3
Injured nerve	CXCL13	RGCs	CXCR5

(Continued)

Table 9: Continued

RGCs			
Source cell	Ligand	Target cell	Receptor
Injured nerve	CXCL16	RGCs	CXCR6
Injured nerve	CXCL2	RGCs	CXCR2
Injured nerve	CXCL9	RGCs	CXCR3
Injured nerve	DHH	RGCs	PTCH1
Injured nerve	DHH	RGCs	PTCH2
Injured nerve	DLL1	RGCs	NOTCH1
Injured nerve	DLL1	RGCs	NOTCH2
Injured nerve	DLL1	RGCs	NOTCH3
Injured nerve	DLL4	RGCs	NOTCH1
Injured nerve	EBI3	RGCs	IL27RA
Injured nerve	EDA	RGCs	EDAR
Injured nerve	EDN3	RGCs	EDNRA
Injured nerve	EDN3	RGCs	EDNRB
Injured nerve	EFNA1	RGCs	EPHA1
Injured nerve	EFNA1	RGCs	EPHA3
Injured nerve	EFNA2	RGCs	EPHA3
Injured nerve	EFNA4	RGCs	EPHA3
Injured nerve	EFNA4	RGCs	EPHA5
Injured nerve	EFNA5	RGCs	EPHA3
Injured nerve	EFNA5	RGCs	EPHA2
Injured nerve	EFNA5	RGCs	EPHA7
Injured nerve	EFNA5	RGCs	EPHA5
Injured nerve	EFNB1	RGCs	EPHB2
Injured nerve	EFNB2	RGCs	EPHB1
Injured nerve	EFNB2	RGCs	EPHA4
Injured nerve	EFNB2	RGCs	EPHA3
Injured nerve	EFNB2	RGCs	EPHB4
Injured nerve	EFNB2	RGCs	EPHB2
Injured nerve	FGF1	RGCs	FGFR1
Injured nerve	FGF1	RGCs	FGFR2
Injured nerve	FGF1	RGCs	FGFR3
Injured nerve	FGF1	RGCs	FGFR4
Injured nerve	FGF10	RGCs	FGFR2
Injured nerve	FGF18	RGCs	FGFR4
Injured nerve	FGF5	RGCs	FGFR1
Injured nerve	FGF5	RGCs	FGFR3
Injured nerve	FGF7	RGCs	FGFR2
Injured nerve	FGF7	RGCs	NRP1
Injured nerve	FIGF	RGCs	FLT4
Injured nerve	FIGF	RGCs	KDR
Injured nerve	FIGF	RGCs	NRP1
Injured nerve	FIGF	RGCs	NRP2
Injured nerve	FSTL1	RGCs	CD14
Injured nerve	FSTL1	RGCs	DIP2A
Injured nerve	GAS6	RGCs	AXL
Injured nerve	GDF11	RGCs	ACVR1B
Injured nerve	GDF11	RGCs	ACVR1C
Injured nerve	GDF11	RGCs	ACVR2B
Injured nerve	GDNF	RGCs	GFRA1
Injured nerve	GDNF	RGCs	GFRA2
Injured nerve	GDNF	RGCs	RET
Injured nerve	HBEGF	RGCs	EGFR
Injured nerve	HBEGF	RGCs	ERBB4
Injured nerve	HGF	RGCs	MET
Injured nerve	IGF1	RGCs	IGF1R
Injured nerve	IGF1	RGCs	IGFBP1
Injured nerve	IGF1	RGCs	IGFBP2
Injured nerve	IGF1	RGCs	IGFBP3
Injured nerve	IGF1	RGCs	IGFBP4
Injured nerve	IGF1	RGCs	IGFBP5
Injured nerve	IGF1	RGCs	IGFBP6

(Continued)

Table 9: Continued

RGCs			
Source cell	Ligand	Target cell	Receptor
Injured nerve	IGF1	RGCs	IGFBP7
Injured nerve	IGF1	RGCs	INSR
Injured nerve	IGF2	RGCs	IGF1R
Injured nerve	IGF2	RGCs	IGF2R
Injured nerve	IGF2	RGCs	INSR
Injured nerve	IL15	RGCs	IL15RA
Injured nerve	IL15	RGCs	IL2RB
Injured nerve	IL15	RGCs	IL2RG
Injured nerve	IL16	RGCs	CD4
Injured nerve	IL16	RGCs	GRIN2A
Injured nerve	IL16	RGCs	GRIN2B
Injured nerve	IL16	RGCs	GRIN2C
Injured nerve	IL16	RGCs	GRIN2D
Injured nerve	IL18	RGCs	IL18RAP
Injured nerve	IL1B	RGCs	IL1R1
Injured nerve	IL1B	RGCs	IL1RAP
Injured nerve	IL33	RGCs	IL1RL1
Injured nerve	IL6	RGCs	IL6ST
Injured nerve	INHA	RGCs	ACVR2A
Injured nerve	INHA	RGCs	TGFBR3
Injured nerve	INHBA	RGCs	ACVR1B
Injured nerve	INHBA	RGCs	ACVR2A
Injured nerve	INHBA	RGCs	ACVR2B
Injured nerve	INHBB	RGCs	ACVR1
Injured nerve	INHBB	RGCs	ACVR1B
Injured nerve	INHBB	RGCs	ACVR1C
Injured nerve	INHBB	RGCs	ACVR2A
Injured nerve	INHBB	RGCs	ACVR2B
Injured nerve	JAG1	RGCs	NOTCH1
Injured nerve	JAG1	RGCs	NOTCH2
Injured nerve	JAG1	RGCs	NOTCH3
Injured nerve	JAG2	RGCs	NOTCH1
Injured nerve	JAG2	RGCs	NOTCH2
Injured nerve	JAG2	RGCs	NOTCH3
Injured nerve	LIF	RGCs	IL6ST
Injured nerve	LIF	RGCs	LIFR
Injured nerve	LTB	RGCs	LTBR
Injured nerve	MDK	RGCs	ALK
Injured nerve	MDK	RGCs	LRP1
Injured nerve	MDK	RGCs	LRP2
Injured nerve	MDK	RGCs	PTPRZ1
Injured nerve	MIF	RGCs	CD74
Injured nerve	NGF	RGCs	NGFR
Injured nerve	NGF	RGCs	NTRK1
Injured nerve	NGF	RGCs	SORCS3
Injured nerve	NGF	RGCs	SORT1
Injured nerve	NOV	RGCs	NOTCH1
Injured nerve	NPPC	RGCs	NPR2
Injured nerve	NPPC	RGCs	NPR3
Injured nerve	NTF3	RGCs	NGFR
Injured nerve	NTF3	RGCs	NTRK1
Injured nerve	NTF3	RGCs	NTRK2
Injured nerve	NTF3	RGCs	NTRK3
Injured nerve	NTN1	RGCs	DCC
Injured nerve	NTN1	RGCs	NEO1
Injured nerve	NTN1	RGCs	UNC5B
Injured nerve	NTN1	RGCs	UNC5C
Injured nerve	OSM	RGCs	IL6ST
Injured nerve	OSM	RGCs	LIFR
Injured nerve	OSM	RGCs	OSMR
Injured nerve	PDGFA	RGCs	PDGFRA

(Continued)

Table 9: Continued

RGCs			
Source cell	Ligand	Target cell	Receptor
Injured nerve	PDGFB	RGCs	PDGFRA
Injured nerve	PDGFB	RGCs	PDGFRB
Injured nerve	PDGFC	RGCs	PDGFRA
Injured nerve	PF4	RGCs	CXCR3
Injured nerve	PF4	RGCs	DARC
Injured nerve	PF4	RGCs	LDLR
Injured nerve	PF4	RGCs	THBD
Injured nerve	PGF	RGCs	FLT1
Injured nerve	PGF	RGCs	NRP1
Injured nerve	PGF	RGCs	NRP2
Injured nerve	POMC	RGCs	MC1R
Injured nerve	POMC	RGCs	MC3R
Injured nerve	POMC	RGCs	MC4R
Injured nerve	POMC	RGCs	MC5R
Injured nerve	PTHLH	RGCs	PTH1R
Injured nerve	PTN	RGCs	ALK
Injured nerve	PTN	RGCs	PTPRS
Injured nerve	PTN	RGCs	PTPRZ1
Injured nerve	RSPO1	RGCs	LGR5
Injured nerve	RTN4	RGCs	LINGO1
Injured nerve	RTN4	RGCs	RTN4R
Injured nerve	RTN4	RGCs	RTN4RL1
Injured nerve	SEMA3B	RGCs	PLXNA1
Injured nerve	SEMA3B	RGCs	PLXNA2
Injured nerve	SEMA3B	RGCs	PLXNA3
Injured nerve	SEMA3B	RGCs	PLXNA4
Injured nerve	SEMA3B	RGCs	PLXNB2
Injured nerve	SEMA3B	RGCs	PLXND1
Injured nerve	SEMA3C	RGCs	PLXNA1
Injured nerve	SEMA3C	RGCs	PLXNA2
Injured nerve	SEMA3C	RGCs	PLXNA3
Injured nerve	SEMA3C	RGCs	PLXNA4
Injured nerve	SEMA3C	RGCs	PLXNB2
Injured nerve	SEMA3C	RGCs	PLXND1
Injured nerve	SEMA3D	RGCs	PLXNA1
Injured nerve	SEMA3D	RGCs	PLXNA2
Injured nerve	SEMA3D	RGCs	PLXNA3
Injured nerve	SEMA3D	RGCs	PLXNA4
Injured nerve	SEMA3D	RGCs	PLXNB2
Injured nerve	SEMA3D	RGCs	PLXND1
Injured nerve	SEMA3E	RGCs	PLXNA1
Injured nerve	SEMA3E	RGCs	PLXNA2
Injured nerve	SEMA3E	RGCs	PLXNA3
Injured nerve	SEMA3E	RGCs	PLXNA4
Injured nerve	SEMA3E	RGCs	PLXNB2
Injured nerve	SEMA3E	RGCs	PLXND1
Injured nerve	SEMA3F	RGCs	PLXNA1
Injured nerve	SEMA3F	RGCs	PLXNA2
Injured nerve	SEMA3F	RGCs	PLXNA3
Injured nerve	SEMA3F	RGCs	PLXNA4
Injured nerve	SEMA3F	RGCs	PLXNB2
Injured nerve	SEMA3F	RGCs	PLXND1
Injured nerve	SEMA3G	RGCs	PLXNA1
Injured nerve	SEMA3G	RGCs	PLXNA2
Injured nerve	SEMA3G	RGCs	PLXNA3
Injured nerve	SEMA3G	RGCs	PLXNA4
Injured nerve	SEMA3G	RGCs	PLXNB2
Injured nerve	SEMA3G	RGCs	PLXND1
Injured nerve	SEMA4A	RGCs	PLXNB1
Injured nerve	SEMA4A	RGCs	PLXNB2
Injured nerve	SEMA4A	RGCs	PLXNC1

(Continued)

Table 9: Continued

RGCs			
Source cell	Ligand	Target cell	Receptor
Injured nerve	SEMA4A	RGCs	PLXND1
Injured nerve	SEMA4B	RGCs	PLXNB1
Injured nerve	SEMA4B	RGCs	PLXNB2
Injured nerve	SEMA4B	RGCs	PLXNC1
Injured nerve	SEMA4C	RGCs	PLXNB1
Injured nerve	SEMA4C	RGCs	PLXNB2
Injured nerve	SEMA4C	RGCs	PLXNC1
Injured nerve	SEMA4D	RGCs	PLXNB1
Injured nerve	SEMA4D	RGCs	PLXNB2
Injured nerve	SEMA4D	RGCs	PLXNC1
Injured nerve	SEMA4F	RGCs	PLXNB1
Injured nerve	SEMA4F	RGCs	PLXNB2
Injured nerve	SEMA4F	RGCs	PLXNC1
Injured nerve	SEMA5A	RGCs	PLXNA3
Injured nerve	SEMA5A	RGCs	PLXNA4
Injured nerve	SEMA5A	RGCs	PLXNC1
Injured nerve	SEMA5B	RGCs	PLXNA3
Injured nerve	SEMA5B	RGCs	PLXNA4
Injured nerve	SEMA5B	RGCs	PLXNC1
Injured nerve	SEMA6A	RGCs	PLXNA1
Injured nerve	SEMA6A	RGCs	PLXNA2
Injured nerve	SEMA6B	RGCs	PLXNA1
Injured nerve	SEMA6C	RGCs	PLXNA1
Injured nerve	SEMA6D	RGCs	PLXNA1
Injured nerve	SEMA7A	RGCs	PLXNC1
Injured nerve	SHH	RGCs	PTCH1
Injured nerve	SHH	RGCs	PTCH2
Injured nerve	TGFA	RGCs	EGFR
Injured nerve	TGFA	RGCs	ERBB2
Injured nerve	TGFB1	RGCs	ACVRL1
Injured nerve	TGFB1	RGCs	ENG
Injured nerve	TGFB1	RGCs	TGFBR1
Injured nerve	TGFB1	RGCs	TGFBR2
Injured nerve	TGFB1	RGCs	TGFBR3
Injured nerve	TGFB2	RGCs	TGFBR1
Injured nerve	TGFB2	RGCs	TGFBR2
Injured nerve	TGFB2	RGCs	TGFBR3
Injured nerve	TGFB3	RGCs	ACVRL1
Injured nerve	TGFB3	RGCs	TGFBR1
Injured nerve	TGFB3	RGCs	TGFBR2
Injured nerve	TNF	RGCs	TNFRSF1A
Injured nerve	TNF	RGCs	TNFRSF1B
Injured nerve	TNFSF10	RGCs	TNFRSF10B
Injured nerve	TNFSF12	RGCs	TNFRSF12A
Injured nerve	TNFSF12	RGCs	TNFRSF25
Injured nerve	TNFSF14	RGCs	LTBR
Injured nerve	TNFSF14	RGCs	TNFRSF14
Injured nerve	TNFSF8	RGCs	TNFRSF8
Injured nerve	TNFSF9	RGCs	TNFRSF9
Injured nerve	TSLP	RGCs	CRLF2
Injured nerve	TSLP	RGCs	IL7R
Injured nerve	UCN2	RGCs	CRHR2
Injured nerve	VEGFA	RGCs	FLT1
Injured nerve	VEGFA	RGCs	KDR
Injured nerve	VEGFA	RGCs	NRP1
Injured nerve	VEGFA	RGCs	NRP2
Injured nerve	VEGFB	RGCs	FLT1
Injured nerve	VEGFB	RGCs	NRP1
Injured nerve	VEGFC	RGCs	FLT4
Injured nerve	VEGFC	RGCs	KDR
Injured nerve	VEGFC	RGCs	NRP1

(Continued)

Table 9: Continued

		RGCs	
Source cell	Ligand	Target cell	Receptor
Injured nerve	VEGFC	RGCs	NRP2
Injured nerve	WNT11	RGCs	FZD4
Injured nerve	WNT2	RGCs	FZD1
Injured nerve	WNT2	RGCs	FZD9
Injured nerve	WNT5A	RGCs	FZD2
Injured nerve	WNT5A	RGCs	FZD5
Injured nerve	WNT5A	RGCs	ROR1
Injured nerve	WNT5A	RGCs	ROR2

Predicted unidirectional ligand-receptor interactions between the injured sciatic nerve ligands and receptors on sympathetic (SCGs) neurons, sensory (DRGs) neurons, motor neurons (MNs), and retinal ganglion cells (RGCs). Directionality of predicted paracrine interactions are indicated by the source cell (ligand) and target cell (receptor) column designations. Some ligands are predicted to act on more than one receptor. The interactions shown here accompany the models presented in Figures 5-7 and Extended Data Figure 6-1.

sympathetic and sensory neurons, largely through the same receptors.

We then used the scRNA-seq data to define the nerve cell types that made the ligands involved in the predicted interactions (Figs. 5*C*,*D*, 6*A*,*B*; Extended Data Fig. 6-1*A*,*B*). Almost half (57) of 122 shared predicted sympathetic and sensory neuron interactions involved ligands that were expressed in the highest proportions in *Pdgfra*-positive mesenchymal cells including FGF10, FGF18, HGF, SEMA3D, BMP7, IL33, and PTHLH (asterisks in the models denote ligands made by 4-fold more of the indicated cell relative to all other cell types). Moreover, 33 of these were highest in the endoneurial mesenchymal cells. Another 22 ligands were highest in Schwann cells, including ARTN, BTC, DHH, FGF5, GDNF, SEMA3B, SHH, and UCN2. The remaining 43 predicted interactions were split almost equally between endothelial cells (17), VSM/pericyte cells (14), and immune cells (12), and included well-characterized nerve ligands such as NGF, NT3 (*Ntf3*), and IGF2. Notably, while some of these ligands were predicted to signal via dedicated receptors (Fig. 6*A*,*B*; Extended Data Fig. 6-1*A*,*B*; Table 9), many others shared receptors or coreceptors, suggesting the potential for convergent signaling. As examples, CLCF1, CRLF1, and LIF were all predicted to share the receptor components LIFR and gp130, and ANGPT1, ANGPT2, and ANGPT4 were all predicted to act by interacting with TEK.

Modeling predicts that many nerve ligands have the capacity to act on both PNS and CNS neurons

This analysis predicts that peripheral nerve cells produce ligands that could act on at least two populations of peripheral neurons. To test the idea that this might reflect a ligand environment that is generally supportive of axonal growth, we asked about motor neurons, which also project axons via the sciatic nerve, and RGCs, CNS neurons that normally do not regenerate in the CNS, but will regenerate into peripheral nerve grafts (Politis and Spencer, 1986; for review, see Benowitz et al., 2017).

For motor neurons, we analyzed previously published microarray data from microdissected P7 mouse lumbar motor neurons (Kaplan et al., 2014), identifying receptor mRNAs using the same thresholding cutoff as for the sensory neurons (top 87% of mRNAs). Of 322 receptor mRNAs defined in the motor neuron dataset using this approach, 272 were also expressed by sensory and sympathetic neurons (Table 10). Computational modeling with the motor neuron receptors and the 143 injured nerve ligands showed that of the 122 shared sympathetic and sensory neuron interactions, 121 were also predicted for motor neurons, with the endoneurial ligand EDA the only exception (Fig. 7*A*,*C*; Table 9). There were also two predicted nerve to motor neuron interactions involving GRP-GRPR and GNRH1-GNRHR that were not shared with both sympathetic and sensory neurons.

We obtained similar findings when we analyzed RGCs using a bulk RNA-seq dataset generated from P5–P7 rat RGCs that were cultured for 12 h (Blanco-Suarez et al., 2018). Using an FPKM of 1 as a threshold for expression, we found 320 receptors expressed by RGCs, with 258 of them also expressed by the three peripheral neuron types (Table 10). Modeling of the unidirectional paracrine interactions between the injured nerve and RGCs identified 126 predicted interactions that included all 122 shared sensory and sympathetic neuron interactions (Fig. 7*B*, shared interactions are outlined in purple; Table 9). There were also four interactions that were unique to the RGC model involving CCL9, CXCL1, CXCL2, and CXCL16. Thus, the injured peripheral nerve and in particular the Schwann cells and endoneurial mesenchymal cells are predicted to provide a ligand environment that acts on multiple populations of neurons.

The communication networks identify mesenchymal-derived ligands that regulate peripheral axon growth

These models predict that, in addition to Schwann cells, nerve mesenchymal cells are key growth factor sources in the injured nerve. To validate this concept, we focused on two predicted endoneurial ligands that have not previously been explored within a nerve context, ANGPT1 and CCL11 (Fig. 8*A*,*B*). We also analyzed VEGFC, which is expressed at a low level in injured nerve mesenchymal cells (Fig. 8*A*), but that had a coreceptor (NPR1) that was validated at the protein level in both sensory and sympathetic neurons.

We first asked whether these three ligands were secreted by nerve mesenchymal cells. To do this, we isolated mesenchymal cells from rat sciatic nerves using antibody-based

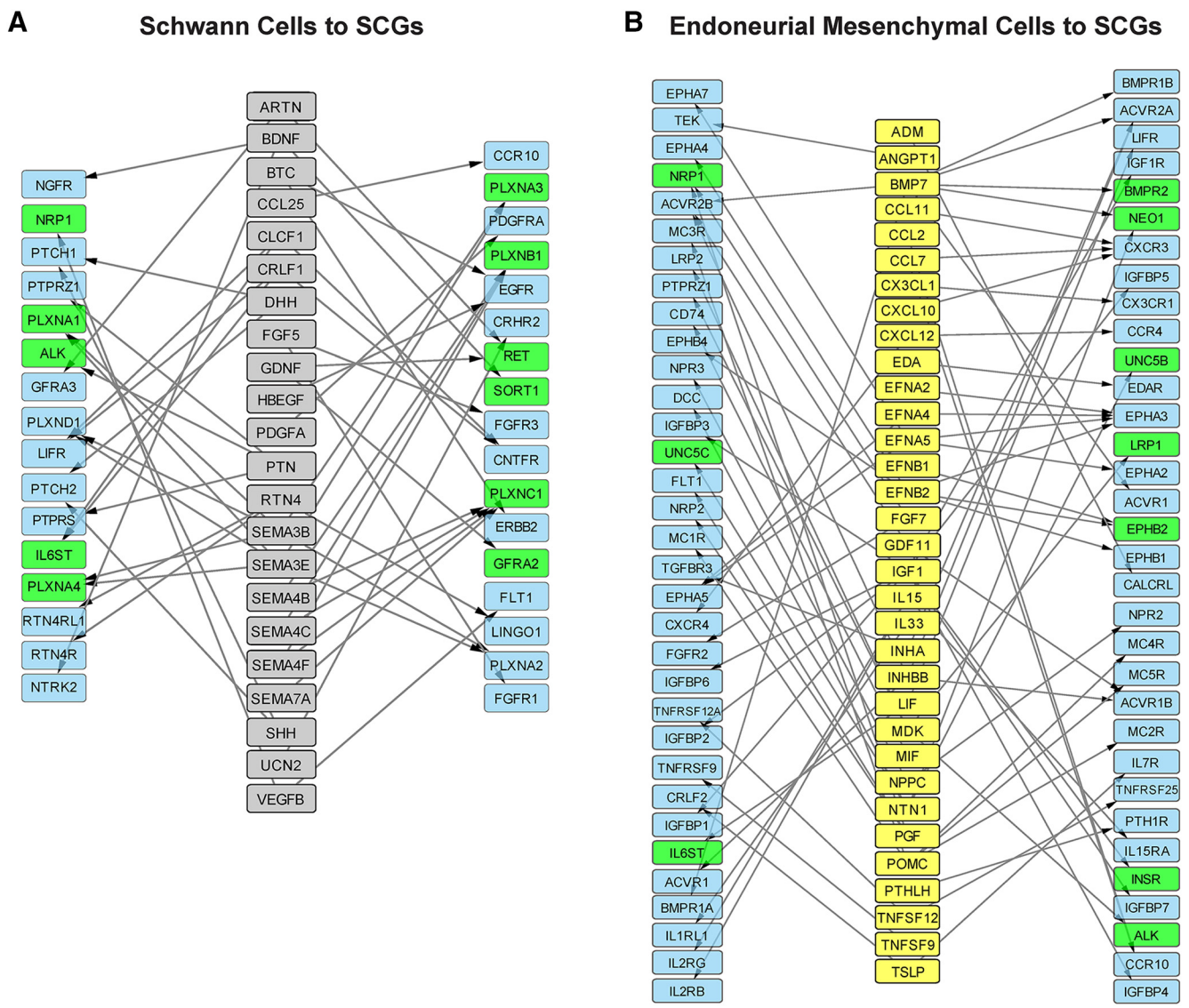

Figure 6. Predicted unidirectional ligand-receptor interactions between injured sciatic nerve Schwann cells or endoneurial mesenchymal cells and sympathetic neurons (see also Extended Data Fig. 6-1). Models showing predicted unidirectional interactions between the ligands most highly expressed by injured nerve Schwann cells (***A***) or endoneurial mesenchymal cells (***B***) and their receptors on cultured sympathetic neurons (SCGs). Ligands are shown in the central columns in ***A***, ***B*** and are color coded as in Figure 5 (Schwann cell ligands in gray and endoneurial mesenchymal cell ligands in yellow). Receptors are shown on either side of the ligand column and also include coreceptors that are well-characterized components of receptor complexes. Receptors that were observed at both the transcriptomic and proteomic levels are colored green while those defined only at the transcriptomic level are colored blue. Arrows indicate directionality of interactions. Note that many ligands interact with multiple receptors and, conversely, that multiple ligands are sometimes predicted to share receptors.

flow sorting for cell-surface PDGFRα. We cultured and expanded these sorted mesenchymal cells for 2.5–4 weeks, at which point the cultures were comprised of over 90% PDGFRα-positive mesenchymal cells, with the remaining cells being S100β-positive Schwann cells (Fig. 8*C*,*D*). After three further days in culture, we added defined, serum-free medium for 24–96 h, collected this conditioned medium, and performed ELISAs. ANGPT1, CCL11, and VEGFC were all detected in three independent preparations of nerve mesenchymal cell conditioned medium (Fig. 8*E*).

Having confirmed that these ligands were secreted by nerve mesenchymal cells in culture, we asked whether *Angpt1*, *Ccl11*, and *Vegfc* mRNAs were expressed in endoneurial cells of the injured nerve. To do this, we analyzed injured distal nerve sections from the *Pdgfra*$^{Egfp/+}$ mice. We resected sciatic nerves and at 9 DPI performed single molecule FISH. *Angpt1* and *Ccl11* mRNAs were detectable in many *Pdgfra*-EGFP-positive mesenchymal cells within the injured nerve endoneurium (Fig. 8*F*). Consistent with the scRNA-seq data, many but not all EGFP-positive cells were positive for these mRNAs (Fig. 8*A*,*B*; 24% and 87% of endoneurial cells express detectable *Angpt1* and *Ccl11* mRNAs, respectively). There were also some *Angpt1* or *Ccl11*-positive cells that were

Table 10: Receptors identified on motor neurons and RGCs using microarrays and RNA-seq

MNs (322)	DRGs. SCGs, and MNs (272)	RGCs (320)	DRGs, SCGs, MNs, and RGCs (258)
Acvr1	Acvr1	Acvr1	Acvr1
Acvr1b	Acvr1b	Acvr1b	Acvr1b
Acvr1c	Acvr2a	Acvr1c	Acvr2a
Acvr2a	Acvr2b	Acvr2a	Acvr2b
Acvr2b	Acvrl1	Acvr2b	Acvrl1
Acvrl1	Adcyap1r1	Acvrl1	Adcyap1r1
Adcyap1r1	Adipor1	Adcyap1r1	Adipor1
Adipor1	Adipor2	Adipor1	Adipor2
Adipor2	Adora2a	Adipor2	Adora2a
Adora2a	Adra1b	Adora2a	Adra1b
Adra1a	Adrb2	Adra1a	Adrb2
Adra1b	Ager	Adra1b	Ager
Adrb2	Alk	Adrb2	Alk
Ager	Amfr	Ager	Amfr
Alk	Aplnr	Alk	Aplnr
Amfr	Avpr1a	Amfr	Avpr1a
Amhr2	Axl	Amhr2	Axl
Aplnr	Bdkrb2	Aplnr	Bdkrb2
Ar	Bmpr1a	Ar	Bmpr1a
Avpr1a	Bmpr1b	Avpr1a	Bmpr1b
Avpr1b	Bmpr2	Avpr2	Bmpr2
Avpr2	C3ar1	Axl	C3ar1
Axl	C5ar1	Bdkrb2	C5ar1
Bdkrb2	Calcrl	Bmpr1a	Calcrl
Bmpr1a	Cckar	Bmpr1b	Cckar
Bmpr1b	Cckbr	Bmpr2	Cckbr
Bmpr2	Ccr10	Btn1a1	Ccr10
Btn1a1	Cd14	C3ar1	Cd14
C3ar1	Cd4	C5ar1	Cd4
C5ar1	Cd44	Calcr	Cd44
Calcr	Cd5l	Calcrl	Cd5l
Calcrl	Cd7	Cckar	Cd74
Cckar	Cd74	Cckbr	Cntfr
Cckbr	Cntfr	Ccr1	Crhr1
Ccr1	Crhr1	Ccr10	Crhr2
Ccr10	Crhr2	Ccr2	Crlf1
Ccr2	Crlf1	Ccr4	Crlf2
Ccr3	Crlf2	Ccr5	Csf1r
Ccr4	Csf1r	Ccr9	Csf2ra
Ccr5	Csf2ra	Cd14	Csf2rb
Ccr6	Csf2rb	Cd27	Csf3r
Ccr7	Csf3r	Cd33	Ctf1
Ccr8	Ctf1	Cd4	Cx3cr1
Ccr9	Cx3cr1	Cd40	Cxcr3
Cd14	Cxcr3	Cd44	Cxcr4
Cd27	Cxcr4	Cd5l	Dcc
Cd33	Dcc	Cd74	Ddr1
Cd4	Ddr1	Cntfr	Derl1
Cd40	Derl1	Cr2	Dip2a
Cd44	Dip2a	Crhr1	Ednra
Cd5l	Ednra	Crhr2	Ednrb
Cd7	Ednrb	Crlf1	Egfr
Cd74	Egfr	Crlf2	Eng
Cntfr	Eng	Csf1r	Epha1
Cr2	Epha1	Csf2ra	Epha2
Crhr1	Epha2	Csf2rb	Epha3
Crhr2	Epha3	Csf3r	Epha4
Crlf1	Epha4	Ctf1	Epha5
Crlf2	Epha5	Cx3cr1	Epha7

(Continued)

Table 10: Continued

MNs (322)	DRGs. SCGs, and MNs (272)	RGCs (320)	DRGs, SCGs, MNs, and RGCs (258)
Csf1r	Epha7	Cxcr2	Ephb1
Csf2ra	Ephb1	Cxcr3	Ephb2
Csf2rb	Ephb2	Cxcr4	Ephb3
Csf3r	Ephb3	Cxcr5	Ephb4
Ctf1	Ephb4	Cxcr6	Epor
Cx3cr1	Epor	Darc	Eps15l1
Cxcr2	Eps15l1	Dcc	Erbb2
Cxcr3	Erbb2	Ddr1	Erbb3
Cxcr4	Erbb3	Derl1	Esr2
Cxcr5	Esr2	Dip2a	F2r
Cxcr6	F2r	Dpp4	Fgfr1
Dcc	Fas	Edar	Fgfr2
Ddr1	Fgfr1	Ednra	Fgfr3
Derl1	Fgfr2	Ednrb	Fgfr4
Dip2a	Fgfr3	Egfr	Fgfrl1
Dpp4	Fgfr4	Eng	Flt1
Edar	Fgfrl1	Epha1	Flt3
Ednra	Flt1	Epha2	Flt4
Ednrb	Flt3	Epha3	Folr1
Egfr	Flt4	Epha4	Fzd1
Eng	Folr1	Epha5	Fzd2
Epha1	Fshr	Epha7	Fzd4
Epha2	Fzd1	Ephb1	Fzd5
Epha3	Fzd2	Ephb2	Fzd9
Epha5	Fzd4	Ephb3	Gabbr1
Ephb1	Fzd5	Ephb4	Galr2
Ephb2	Fzd9	Epor	Gcgr
Ephb3	Gabbr1	Eps15l1	Gfra2
Epor	Galr2	Erbb2	Gfra3
Eps15l1	Gcgr	Erbb3	Gfra4
Erbb2	Gfra2	Erbb4	Ghr
Erbb3	Gfra3	Esr1	Gipr
Erbb4	Gfra4	Esr2	Gosr1
Esr1	Ghr	F2r	Grik5
Esr2	Ghrhr	F2rl1	Grin2a
F2r	Gipr	F2rl3	Grin2b
F2rl1	Glp1r	Fgfr1	Grin2c
F2rl2	Gosr1	Fgfr2	Grin2d
F2rl3	Grik5	Fgfr3	Gucy2c
Fas	Grin2a	Fgfr4	Hcrtr1
Fgfr1	Grin2b	Fgfrl1	Hcrtr2
Fgfr2	Grin2c	Flt1	Hnf4a
Fgfr3	Grin2d	Flt3	Hpn
Fgfr4	Gucy2c	Flt4	Ifnar1
Fgfrl1	Hcrtr1	Folr1	Ifnar2
Flt1	Hcrtr2	Fzd1	Ifngr1
Flt3	Hnf4a	Fzd2	Ifngr2
Flt4	Hpn	Fzd4	Igf1r
Folr1	Ifnar1	Fzd5	Igf2r
Fshr	Ifnar2	Fzd8	Igfbp1
Fzd1	Ifngr1	Fzd9	Igfbp2
Fzd2	Ifngr2	Gabbr1	Igfbp3
Fzd4	Igf1r	Galr1	Igfbp4
Fzd5	Igf2r	Galr2	Igfbp5
Fzd8	Igfbp1	Gcgr	Igfbp6
Fzd9	Igfbp2	Gfra1	Igfbp7
Gabbr1	Igfbp3	Gfra2	Il10ra
Galr1	Igfbp4	Gfra3	Il10rb
Galr2	Igfbp5	Gfra4	Il12rb1
Gcgr	Igfbp6	Ghr	Il15ra

(Continued)

Table 10: Continued

MNs (322)	DRGs. SCGs, and MNs (272)	RGCs (320)	DRGs, SCGs, MNs, and RGCs (258)
Gfra1	Igfbp7	Ghsr	Il17ra
Gfra2	Il10ra	Gipr	Il17rc
Gfra3	Il10rb	Glp2r	Il18rap
Gfra4	Il12rb1	Gosr1	Il1r1
Ghr	Il15ra	Gpr151	Il1rap
Ghrhr	Il17ra	Grik5	Il1rl1
Ghsr	Il17rc	Grin2a	Il1rl2
Gipr	Il18r1	Grin2b	Il21r
Glp1r	Il18rap	Grin2c	Il27ra
Gnrhr	Il1r1	Grin2d	Il2rb
Gosr1	Il1r2	Gucy2c	Il2rg
Gpr151	Il1rap	Hcrtr1	Il3ra
Grik5	Il1rl1	Hcrtr2	Il6st
Grin2a	Il1rl2	Hnf4a	Il7r
Grin2b	Il21r	Hpn	Insr
Grin2c	Il22ra1	Ifnar1	Irs1
Grin2d	Il27ra	Ifnar2	Itga2
Grpr	Il2ra	Ifngr1	Itga2b
Gucy2c	Il2rb	Ifngr2	Itga5
Hcrtr1	Il2rg	Igf1r	Itga9
Hcrtr2	Il3ra	Igf2r	Itgal
Hnf4a	Il6st	Igfbp1	Itgav
Hpn	Il7r	Igfbp2	Itgb1
Hrh4	Insr	Igfbp3	Itgb3
Ifnar1	Irs1	Igfbp4	Itgb5
Ifnar2	Itga2	Igfbp5	Itgb6
Ifngr1	Itga2b	Igfbp6	Itgb8
Ifngr2	Itga5	Igfbp7	Itpr3
Igf1r	Itga9	Il10ra	Kit
Igf2r	Itgal	Il10rb	Ldlr
Igfbp1	Itgav	Il12rb1	Lgals3bp
Igfbp2	Itgb1	Il12rb2	Lgr5
Igfbp3	Itgb3	Il13ra1	Lifr
Igfbp4	Itgb5	Il15ra	Lingo1
Igfbp5	Itgb6	Il17ra	Lrp1
Igfbp6	Itgb8	Il17rb	Lrp5
Igfbp7	Itpr3	Il17rc	Lrp6
Il10ra	Kit	Il18rap	Lsr
Il10rb	Ldlr	Il1r1	Ltbr
Il12rb1	Lgals3bp	Il1rap	Mc1r
Il12rb2	Lgr5	Il1rl1	Mc3r
Il13ra1	Lifr	Il1rl2	Mc5r
Il13ra2	Lingo1	Il20ra	Mchr1
Il15ra	Lrp1	Il20rb	Met
Il17ra	Lrp5	Il21r	Mst1r
Il17rb	Lrp6	Il27ra	Ncoa3
Il17rc	Lsr	Il2rb	Ncor1
Il18r1	Ltbr	Il2rg	Neo1
Il18rap	Marco	Il3ra	Ngfr
Il1r1	Mc1r	Il6st	Notch1
Il1r2	Mc2r	Il7r	Notch2
Il1rap	Mc3r	Il9r	Notch3
Il1rl1	Mc5r	Insr	Npr1
Il1rl2	Mchr1	Irs1	Npr2
Il20ra	Met	Itga2	Npr3
Il20rb	Mpl	Itga2b	Npy1r
Il21r	Mst1r	Itga5	Npy5r
Il22ra1	Ncoa3	Itga9	Nr3c1
Il22ra2	Ncor1	Itgal	Nrp1
Il27ra	Neo1	Itgav	Nrp2

(Continued)

Table 10: Continued

MNs (322)	DRGs. SCGs, and MNs (272)	RGCs (320)	DRGs, SCGs, MNs, and RGCs (258)
Il2ra	Ngfr	Itgb1	Ntng1
Il2rb	Notch1	Itgb2	Ntng2
Il2rg	Notch2	Itgb3	Ntrk1
Il3ra	Notch3	Itgb5	Ntrk2
Il5ra	Npffr2	Itgb6	Ntrk3
Il6st	Npr1	Itgb8	Ntsr1
Il7r	Npr2	Itpr3	Oprl1
Il9r	Npr3	Kdr	Osmr
Insr	Npy1r	Kit	Oxtr
Irs1	Npy2r	Ldlr	Pdgfa
Itga2	Npy5r	Lepr	Pdgfra
Itga2b	Nr3c1	Lgals3bp	Pdgfrb
Itga5	Nrp1	Lgr5	Pgr
Itga9	Nrp2	Lhcgr	Plaur
Itgal	Ntng1	Lifr	Plgrkt
Itgav	Ntng2	Lingo1	Plxna1
Itgb1	Ntrk1	Loxl2	Plxna2
Itgb2	Ntrk2	Lrp1	Plxna3
Itgb3	Ntrk3	Lrp2	Plxna4
Itgb5	Ntsr1	Lrp5	Plxnb1
Itgb6	Oprl1	Lrp6	Plxnc1
Itgb8	Osmr	Lsr	Plxnd1
Itpr3	Oxtr	Ltbr	Procr
Kdr	Pdgfa	Mc1r	Prokr1
Kit	Pdgfra	Mc3r	Prokr2
Ldlr	Pdgfrb	Mc4r	Ptch1
Lepr	Pgr	Mc5r	Ptch2
Lgals3bp	Plaur	Mchr1	Pth1r
Lgr5	Plgrkt	Met	Ptprk
Lhcgr	Plxna1	Mst1r	Ptprs
Lifr	Plxna2	Ncoa3	Ptprz1
Lrp1	Plxna3	Ncor1	Ret
Lrp2	Plxna4	Neo1	Robo3
Lrp5	Plxnb1	Ngfr	Ror1
Lrp6	Plxnc1	Nmbr	Ror2
Lsr	Plxnd1	Nmur2	Rorb
Ltbr	Procr	Notch1	Rtn4r
Marco	Prokr1	Notch2	Rtn4rl1
Mc1r	Prokr2	Notch3	Rxrg
Mc2r	Ptch1	Npffr1	Ryr1
Mc3r	Ptch2	Npr1	Ryr2
Mc5r	Pth1r	Npr2	Sctr
Mchr1	Ptprk	Npr3	Sdc4
Met	Ptprs	Npy1r	Sfrp1
Mpl	Ptprz1	Npy5r	Sfrp2
Ncoa3	Ret	Nr3c1	Slc1a5
Ncor1	Robo3	Nrp1	Sorcs3
Ngfr	Ror1	Nrp2	Sort1
Nmbr	Ror2	Ntng1	Sstr1
Nmur2	Rorb	Ntng2	Sstr2
Notch1	Rtn4r	Ntrk1	Sstr3
Notch2	Rtn4rl1	Ntrk2	Sstr4
Notch3	Rxrg	Ntrk3	Sstr5
Npffr2	Ryr1	Ntsr1	Tek
Npr1	Ryr2	Oprl1	Tgfbr2
Npr2	Sctr	Osmr	Tgfbr3
Npr3	Sdc4	Oxtr	Thbd
Npy1r	Sfrp1	Pdgfa	Thra
Npy2r	Sfrp2	Pdgfra	Thrap3
Npy5r	Slc1a5	Pdgfrb	Tnfrsf10b

(Continued)

Table 10: Continued

MNs (322)	DRGs. SCGs, and MNs (272)	RGCs (320)	DRGs, SCGs, MNs, and RGCs (258)
Nr3c1	Sorcs3	Pgr	Tnfrsf11a
Nrp1	Sort1	Plat	Tnfrsf11b
Nrp2	Sstr1	Plaur	Tnfrsf12a
Ntrk1	Sstr2	Plgrkt	Tnfrsf13c
Ntrk2	Sstr3	Plxna1	Tnfrsf14
Ntrk3	Sstr4	Plxna2	Tnfrsf17
Ntsr1	Sstr5	Plxna3	Tnfrsf18
Oprl1	Tek	Plxna4	Tnfrsf1a
Osmr	Tgfbr2	Plxnb1	Tnfrsf1b
Oxtr	Tgfbr3	Plxnb2	Tnfrsf25
Pdgfa	Thbd	Plxnc1	Tnfrsf8
Pdgfra	Thra	Plxnd1	Tnfrsf9
Pdgfrb	Thrap3	Prlhr	Tshr
Pgr	Tnfrsf10b	Prlr	Unc5b
Plat	Tnfrsf11a	Procr	Unc5c
Plaur	Tnfrsf11b	Prokr1	Uts2r
Plgrkt	Tnfrsf12a	Prokr2	Vipr1
Plxnb2	Tnfrsf13c	Ptch1	Vldlr
Prlr	Tnfrsf14	Ptch2	Vtn
Procr	Tnfrsf17	Pth1r	
Prokr1	Tnfrsf18	Pth2r	
Prokr2	Tnfrsf1a	Ptprh	
Ptch1	Tnfrsf1b	Ptprk	
Ptch2	Tnfrsf25	Ptprs	
Pth1r	Tnfrsf8	Ptprz1	
Pth2r	Tnfrsf9	Ret	
Ptprk	Tshr	Robo3	
Ptprs	Unc5b	Ror1	
Ptprz1	Unc5c	Ror2	
Ret	Uts2r	Rorb	
Robo3	Vipr1	Rtn4r	
Ror1	Vldlr	Rtn4rl1	
Ror2	Vtn	Rxfp2	
Rorb		Rxfp4	
Rtn4r		Rxrg	
Rxfp1		Ryr1	
Rxfp2		Ryr2	
Rxrg		Sctr	
Ryr1		Sdc4	
Ryr2		Sfrp1	
Sctr		Sfrp2	
Sdc4		Slc1a5	
Sfrp1		Sorcs3	
Sfrp2		Sort1	
Slc1a5		Sstr1	
Sorcs3		Sstr2	
Sort1		Sstr3	
Sstr1		Sstr4	
Sstr2		Sstr5	
Sstr3		Tek	
Sstr4		Tgfbr1	
Sstr5		Tgfbr2	
Tek		Tgfbr3	
Tgfbr1		Thbd	
Tgfbr2		Thra	
Tgfbr3		Thrap3	
Thbd		Tnfrsf10b	
Thra		Tnfrsf11a	
Thrap3		Tnfrsf11b	
Tnfrsf10b		Tnfrsf12a	

(Continued)

Table 10: Continued

MNs (322)	DRGs. SCGs, and MNs (272)	RGCs (320)	DRGs, SCGs, MNs, and RGCs (258)
Tnfrsf11a		Tnfrsf13b	
Tnfrsf11b		Tnfrsf13c	
Tnfrsf12a		Tnfrsf14	
Tnfrsf13b		Tnfrsf17	
Tnfrsf13c		Tnfrsf18	
Tnfrsf14		Tnfrsf1a	
Tnfrsf17		Tnfrsf1b	
Tnfrsf18		Tnfrsf25	
Tnfrsf1a		Tnfrsf4	
Tnfrsf1b		Tnfrsf8	
Tnfrsf25		Tnfrsf9	
Tnfrsf4		Trhr	
Tnfrsf8		Tshr	
Tnfrsf9		Unc5b	
Trhr		Unc5c	
Tshr		Uts2r	
Unc5c		Vipr1	
Uts2r		Vipr2	
Vipr1		Vldlr	
Vipr2		Vtn	
Vldlr		Xcr1	
Vtn			
Xcr1			

Receptor mRNAs identified by microarray for motor neurons (MNs; column 1) and by RNA-seq for RGCs (column 3), as defined using the updated ligand-receptor database (modified from Yuzwa et al., 2016). Only included are receptor mRNAs that had expression levels exceeding a cutoff of the top 87% of mRNAs for motor neurons and FPKM of 1 for RGCs. Also shown are receptor mRNAs that overlap between sensory, sympathetic and motor neurons (column 2) or between all four populations of neurons (column 4). The sensory and sympathetic neuron receptor mRNAs are shown in Table 8. The total numbers of receptor mRNAs in each column are indicated.

Pdgfra-EGFP-negative. For *Angpt1* mRNA these are likely VSM/pericyte cells, while for *Ccl11* mRNA, they could be VSM/pericytes or immune cells (Fig. 8*B*). *Vegfc* mRNA was also detected in scattered endoneurial *Pdgfra*-EGFP-positive cells but consistent with the scRNA-seq analysis (Fig. 8*A*), there were fewer double-labeled cells and the FISH signal was low (Fig. 8*F*).

Having validated their expression, we asked whether ANGPT1, CCL11, or VEGFC could promote growth of peripheral axons. To do this, we used compartmented cultures of neonatal SCG sympathetic neurons (Campenot et al., 1991; Park et al., 2010). In these cultures, cell bodies are physically separated from axons so that ligands can be applied just to the axons, as would occur in the peripheral nerve (Fig. 8*G*). We established sympathetic neurons in these compartmented cultures with 10 ng/ml NGF, their obligate survival factor, in all compartments. Three days later, when axons had crossed into the side compartments, we replaced the side compartment medium with medium containing 0.5 ng/ml NGF plus 100 ng/ml of ANGPT1, CCL11, or VEGFC for three additional days. As a positive control, we added 50 ng/ml NGF into side compartments, and as a baseline control, we maintained axons in 0.5 ng/ml NGF alone. To quantify the density of axonal growth in these compartments, we drew a line perpendicular to the axis of the outgrowth within the furthest 1 mm of outgrowth where axons were maximally

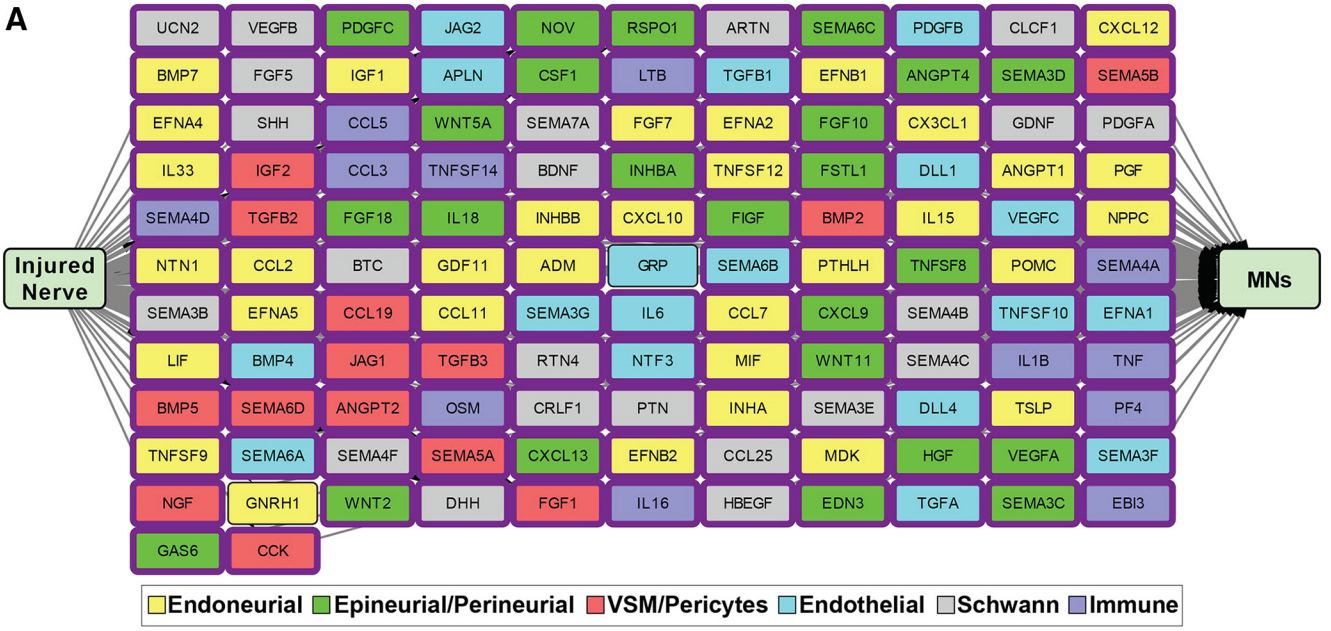

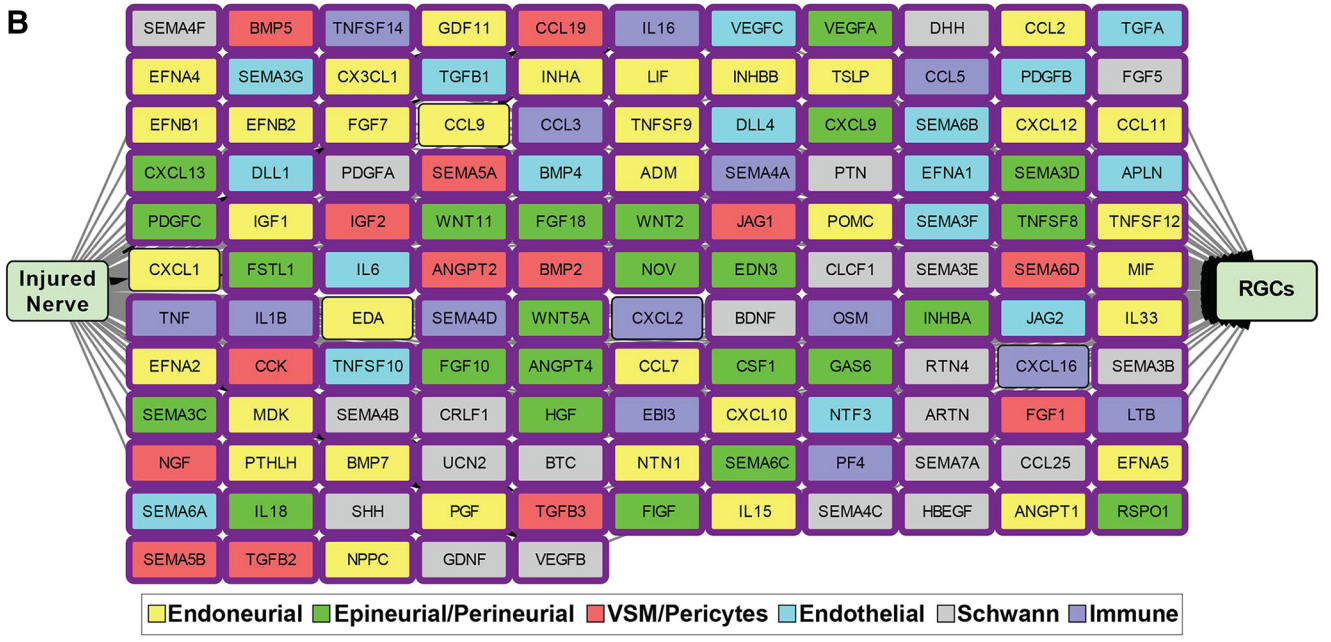

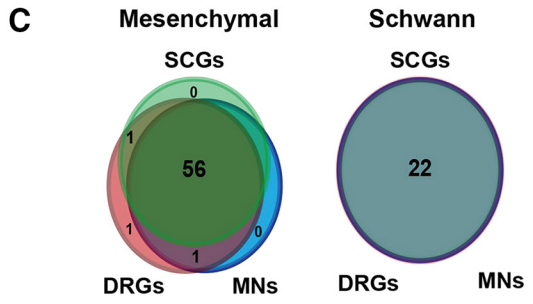

Figure 7. Modeling the potential paracrine interactions between ligands of the injured sciatic nerve and receptors on motor neurons and RGCs. ***A***, ***B***, Models showing predicted unidirectional paracrine interaction networks between the 143 injured nerve ligands and receptors expressed by motor neurons (***A***, MNs) and RGCs (***B***), as defined at the transcriptional level. Interactions were predicted

continued

by computational modeling using the ligand-receptor database, and then manually curated for well-validated interactions. Nodes represent ligands that are color coded to identify the injured nerve cell type with the highest expression of the ligand mRNA based on the scRNA-seq analysis. Arrows indicate directionality of interactions. Predicted interactions that were shared among all four injured nerve-neuron models are indicated by a purple box around the corresponding ligand nodes. ***C***, Venn diagrams showing the overlap of predicted ligand-receptor interactions between injured nerve mesenchymal cells (left) or Schwann cells (right) and sympathetic neurons (SCGs), sensory neurons (DRGs), and motor neurons (MNs).

defasciculated. This analysis showed that 50 ng/ml NGF caused a robust increase in the density of sympathetic axons relative to the 0.5 ng/ml NGF baseline control (Fig. 8*H*,*I*). Notably, all three mesenchymal ligands modestly but significantly enhanced axonal density, although to a lesser degree than maximal NGF (Fig. 8*H*,*I*). Thus, at least some of the mesenchymally derived ligands predicted in our models were bioactive on sympathetic axons.

Discussion

In the present study, we have characterized the ligand environment of the uninjured, injured, and developing sciatic nerves using bulk and single-cell transcriptional profiling. We have identified receptor proteins on the surface of two types of peripheral neurons (sensory and sympathetic) and made predictions of ligand-receptor paracrine interactions between the injured nerve and peripheral neurons. We then go on to show, based on these predictions, that mesenchymal cells express factors that are capable of augmenting growth of peripheral axons *in vitro*, indicating that at least some of these ligands may directly contribute to the positive axonal growth environment of the developing and regenerating peripheral nerves.

Peripheral nerves provide a highly supportive environment for axonal growth during development and following injury (Chen et al., 2007; Cattin and Lloyd, 2016; Fledrich et al., 2019) and promote the repair and regeneration of innervated tissues (Kumar and Brockes, 2012; Johnston et al., 2013, 2016; Mahmoud et al., 2015). Many nerve-derived growth factors have already been well studied, including NGF, BDNF, NTF3, GDNF, and cytokines of the LIF/CNTF family (for review, see Terenghi, 1999). These factors are generally assumed to be Schwann cell derived, although macrophages express factors like GAS6 that promote proper function of Schwann cells in the regenerating nerve (Stratton et al., 2018). To identify other important factors that might be involved in providing a supportive peripheral nerve environment, we used a modeling strategy based on transcriptomic analysis and cell-surface mass spectrometry, as has been previously done for embryonic cortical development and digit tip regeneration (Johnston et al., 2016; Yuzwa et al., 2016). However, while bulk transcriptomic profiling was used in these earlier studies, here we added single-cell transcriptional profiling, thereby providing a level of cellular resolution previously not possible for complex tissues. This approach allowed us to define a previously unappreciated role for mesenchymal cells in establishing the nerve paracrine environment, to identify new nerve ligands, and to predict that many nerve ligands will act on both PNS and CNS neurons, thereby potentially providing an explanation for why peripheral nerves can promote growth of CNS axons.

Our study defined many growth factor mRNAs induced in Schwann cells following nerve injury. Some of these encoded previously studied factors like *Artn*, *Bdnf*, *Gdnf*, *Pdgfa*, *Shh*, and *Lif*, while others encoded factors not well studied in this regard, including *Ucn2*, *Fgf5*, and the CNTF-like cytokines *Clcf1* and *Crlf1*. Previous studies have proposed that this ligand induction is part of a unique Schwann cell "repair" phenotype (Jessen and Mirsky, 2019) that is important for axonal regeneration in the case of ligands like BDNF, GDNF, and LIF, and for tissue repair, in the case of PDGFA (Johnston et al., 2016). What is this repair phenotype? Previous work has shown that following injury Schwann cells display altered morphology and gene expression that is thought to be conducive to promoting axonal regeneration (Gomez-Sanchez et al., 2017; Jessen and Mirsky, 2019). Repair Schwann cells have also been reported to have enhanced epithelial to mesenchymal transition gene expression and TGFβ signaling that contributes to the establishment of an invasive, "mesenchymal-like" phenotype (Arthur-Farraj et al., 2017; Clements et al., 2017). Our findings also show that following nerve injury, Schwann cells induce ligand genes that are not expressed at detectable levels in the uninjured neonatal or adult nerves. Moreover, our transcriptional comparisons expand on previous work and show that repair Schwann cells are more similar to neonatal than to adult uninjured nerve Schwann cells but that they are nonetheless distinct. In this regard, our developmental comparison was limited to the neonatal nerve when myelination is ongoing, and it would be interesting to use single-cell transcriptional profiling to see how similar repair Schwann cells are to embryonic nerve Schwann cells before myelination has commenced.

An important finding of this work is that *Pdgfra*-positive mesenchymal cells are a major source of ligands in the developing, adult, and injured nerves and that they express well-characterized nerve growth factors like NGF, HGF, and LIF. Of particular interest is the high ligand expression by endoneurial mesenchymal cells, which are neural crest derived (Joseph et al., 2004) and are scattered throughout the endoneurial space in close apposition to Schwann cells and axons. These endoneurial mesenchymal cells are thus ideally positioned to regulate axon and Schwann cell biology, and, like Schwann cells, they display increased expression of many ligand mRNAs following injury, including well-studied ligands like *Crlf1*, *Ngf*, and *Lif* and less-studied ligands such as *Angpt1*, *Ccl9*, and *Sema7a*. Equally intriguing was the observation that endoneurial cells express many little-studied ligands under homeostatic conditions, including *Adm*, *Bmp7*, *Il33*, *Pthlh*, and *Wnt5a*. Since mesenchymally derived

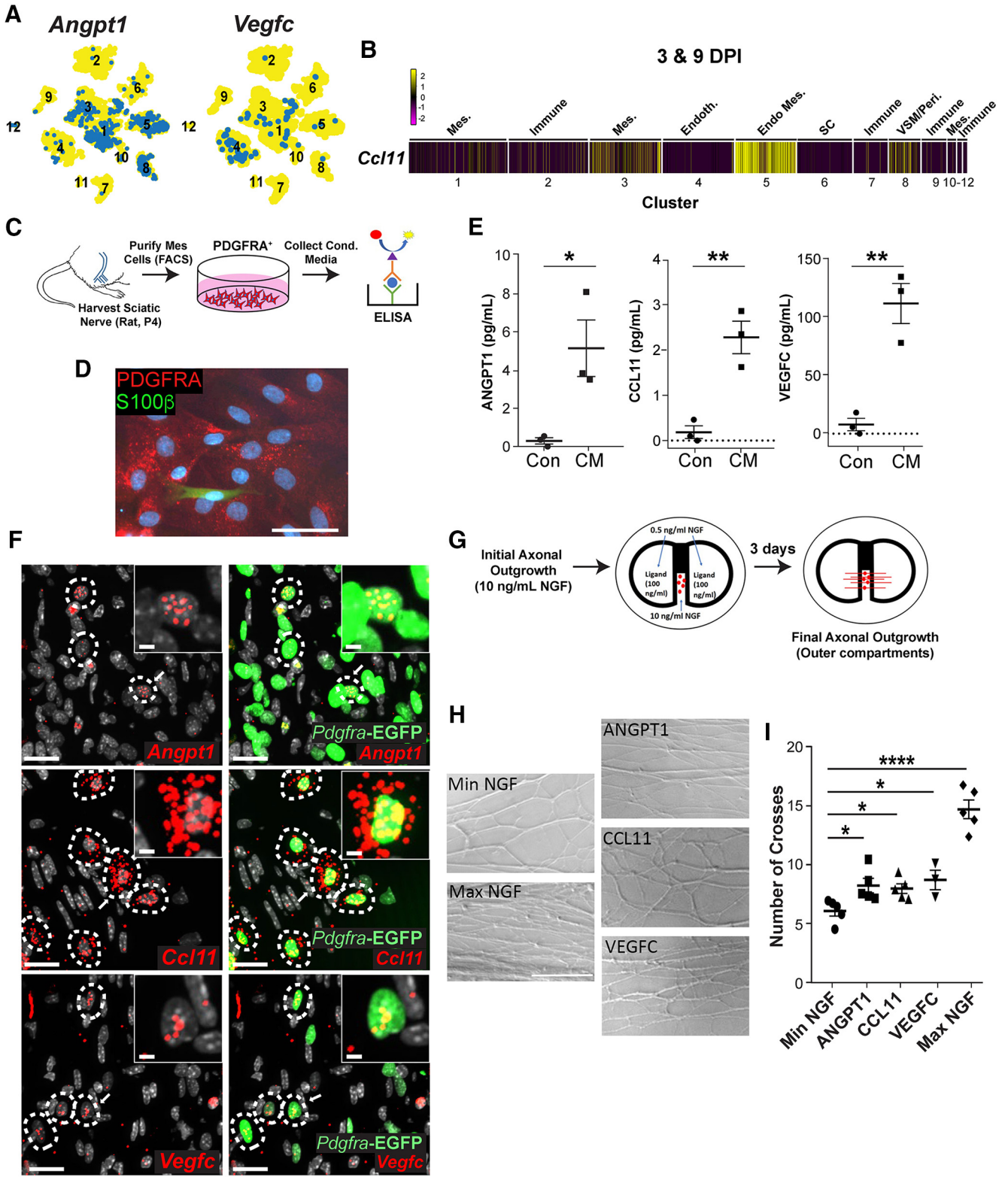

Figure 8. Identification and characterization of ligands expressed in nerve mesenchymal cells that locally promote sympathetic axon growth. ***A***, tSNE gene expression overlays of *Angpt1* and *Vegfc* on the combined 3 and 9 DPI nerve dataset shown in Figure 1*E*. Cells that detectably express the ligand are colored blue, and the numbers correspond to the clusters. ***B***, Heatmap showing expression of *Ccl11* mRNA in single cells within clusters of the combined injured nerve scRNA-seq dataset shown in Figure 1*E*. Each column line represents the level of expression in a single cell. Gene expression represents scaled expression values using Seurat's scaling function and is color coded as per the adjacent color key, where yellow indicates the highest expression. Cluster numbers are on the bottom, and the cell types in that cluster are annotated on the top. Mes. = mesenchymal, Endoth. = endothelial, Endo

continued

Mes. = endoneurial mesenchymal, SC = Schwann cell. ***C–E***, Neonatal (P4) rat sciatic nerve mesenchymal cells were sorted for cell-surface PDGFRα using FACS, cultured in defined growth medium, and medium was collected after 1–4 d of conditioning. ***C***, Schematic of the experiments. ***D***, Representative image of the mesenchymal cell cultures immunostained for PDGFRα and for the Schwann cell protein S100β to indicate the relative purity of the cultures. Scale bar = 50 μm. ***E***, Quantitative ELISA analysis of the nerve mesenchymal cell conditioned medium for ANGPT1, CCL11, and VEGFC (CM). Control growth medium was used as a negative control in each experiment (Con). Shown are the mean ± SEM from three independent experiments; $**p < 0.01$ (CCL11, $p = 0.0055$; VEGFC, $p = 0.0045$) and $*p < 0.05$ (ANGPT1, $p = 0.031$), two-tailed unpaired Student's *t* test. ***F***, Images of the 9-d injured distal sciatic nerve of an adult *Pdgfra*$^{Egfp/+}$ mouse analyzed by FISH for *Angpt1*, *Ccl11*, and *Vegfc* mRNAs. Hatched white lines outline EGFP-positive cells (green nuclei) that were also positive for the mRNA of interest (red dots). Also shown is Hoechst 33258 counterstaining (white/gray) to highlight cell nuclei. The arrows indicate cells that are shown at higher magnification in the insets. Scale bars = 20 μm. Scale bars in insets = 8.75 μm. ***G***, Schematic of the compartmented culture axon outgrowth experiments. Neonatal SCG sympathetic neurons were established in compartmented cultures in the presence of 10 ng/ml NGF. When their axons had crossed into the side compartments, the side compartment medium was replaced with medium containing 0.5 ng/ml NGF plus 100 ng/ml of ANGPT1, CCL11, or VEGFC for three additional days. As a positive control, 50 ng/ml NGF was added into side compartments and as a baseline control, axons were maintained in 0.5 ng/ml NGF alone. ***H***, Brightfield images of sympathetic axons in side compartments grown as described in ***G***, located within 1 mm of the furthest extent of axonal outgrowth. Positive control (Max NGF) = 50 ng/ml, negative control (Min NGF) = 0.5 ng/ml. Scale bar = 100 μm. ***I***, Scatter plots showing the density of outgrowth in response to the different ligands. A vertical line was drawn within the farthest 1 mm of axonal outgrowth, and the number of axons crossing the line was quantified. A maximum of eight separate lanes was scored per technical replicate, with three to four technical replicate cultures (i.e., cultures generated from sympathetic ganglia harvested from the same litter) scored per biological replicate (*n* values in plot). Individual points show mean ± SEM of individual biological replicates; $*p < 0.05$ ($p = 0.041$), $****p < 0.0001$, one-way ANOVA with Holm–Sidak's multiple comparison's test ($n = 5$ for all treatments except VEGFC, where $n = 3$).

ligands include both well-studied nerve growth factors such as NGF as well as many ligands with unknown roles in nerve biology, it is likely that mesenchymal cells express ligands that are critical components of the regenerative response of the injured nerve and/or the growth program of the developing nerve. Our validation studies indicate that at least some of these endoneurial cell ligands are active on axons, but they might be equally important for other nerve cell types and/or for the tissues they innervate. As one example, PTHLH and nerve innervation are both important for bone homeostasis and repair (Elefteriou et al., 2014; Ansari et al., 2018), and endoneurial cells, which express *Pthlh*, migrate into the injured bone where they directly contribute to bone repair (Carr et al., 2019). As a second example, the vasodilator peptide adrenomedullin (ADM) was previously shown to stimulate cAMP accumulation in endothelial cells and Schwann cells (Dumont et al., 2002), suggesting that endoneurial cell-derived ADM might be important for nerve vasculature and/or Schwann cell biology. As a final example, BMP7 inhibits myelin gene expression in Schwann cells (Liu et al., 2016) and promotes mammalian digit tip regeneration (Yu et al., 2010), suggesting that endoneurial cell-derived BMP7 might play multiple important roles.

Another important finding is that most injured nerve ligands are predicted to act on all three populations of PNS neurons as well as RGCs. In this regard, the nerve could promote axonal growth and regeneration in two somewhat disparate ways. In one model, Schwann cells and endoneurial mesenchymal cells would produce different ligands depending on the axons that they are currently or have previously interacted with, thereby tailoring the nerve environment to the axons that need to grow or regenerate. Support for this model comes from studies showing that denervated Schwann cells of motor versus sensory nerves provide ligands specific to different types of axons (Höke et al., 2006; Brushart et al., 2013). In a second model, during development or following nerve damage Schwann cells and mesenchymal cells could express a broad repertoire of ligands, thereby ensuring that growth of all types of PNS axons would be supported. Our findings support this latter model, since we find broad injury-induced ligand expression and a relatively broad repertoire of receptor expression on four different types of neurons, culminating in many similar predicted paracrine interactions. Such a mechanism would provide maximum flexibility and would explain why peripheral nerve grafts promote regeneration of multiple types of injured CNS neurons, which do not normally project in peripheral nerves. Nonetheless, our findings are still consistent with the finding of differential ligand expression in different nerve subtypes (Höke et al., 2006; Brushart et al., 2013), since we have only defined the ligand landscape in a mixed nerve.

How predictive are these models? Previous studies using bulk transcriptomics and/or cell-surface mass spectroscopy predicted three factors important for embryonic cortical neurogenesis (IFNγ, Neurturin, and GDNF; Yuzwa et al., 2016) and one for oligodendrogenesis (Fractalkine; Voronova et al., 2017), and two factors important for digit tip regeneration (PDGFA and OSM; Johnston et al., 2016). In those studies, the cell of origin for each ligand was identified either by isolating cells or by performing single-cell resolution morphologic approaches. Here, we have instead used single-cell transcriptional profiling to provide the necessary resolution, an approach with much broader applicability. The validity of the resultant models is attested to by our finding that almost all ligands previously shown to be important for peripheral nerve regeneration were independently assigned in our models, including many ligands known to be expressed in Schwann cells. Nonetheless, to ensure the validity of these models, we also examined three ligands that were predicted to be made by nerve mesenchymal cells, ANGPT1, CCL11, and VEGFC. Two of these factors, ANGPT1 and VEGFC, are well-known angiogenesis factors, while the third, CCL11 or eotaxin, is a chemokine involved in eosinophil recruitment (Jose et al., 1994). None

of the three has been studied as a positive factor within the context of the injured nerve, although ANGPT1 has been shown to promote growth of cultured sensory neurons (Kosacka et al., 2006), VEGFC promotes growth of developing motor neurons in zebrafish (Kwon et al., 2013), and CCL11 inhibits Schwann cell differentiation (Büttner et al., 2018). Based on our predictive models, we tested these ligands and found that all three (1) were expressed by endoneurial mesenchymal cells in the injured nerve, as shown by both scRNA-seq and FISH analyses; (2) were synthesized and secreted by cultured nerve-derived PDGFRα-positive mesenchymal cells; and (3) enhanced sympathetic axon outgrowth when applied locally in the presence of minimal NGF. While we recognize that additional studies will be required to show that these three ligands are secreted by mesenchymal cells *in vivo*, our data indicate that they are highly expressed following nerve injury, raising the possibility that they are important for nerve repair. In this regard, ANGPT1, CCL11, and VEGFC were not as potent as NGF in promoting growth of sympathetic axons in culture, but they did enhance growth and thus could be important factors for peripheral axon growth in a regenerating nerve context. We therefore feel that our studies validate the predictive value of the modeling approach and provide support for the idea that mesenchymal cells within the nerve are important ligand sources, particularly within the context of nerve repair and regeneration.

The data presented here reinforce the importance of Schwann cells as sources of growth promoting factors and provide evidence that mesenchymal cells also play an important role in determining the ligand environment of the developing and injured nerve. Notably, some well-known nerve regeneration ligands such as GDNF and BDNF were expressed at the highest levels in Schwann cells, while others, such as NGF and HGF, were instead highest in mesenchymal cells. In addition, both cell types express ligands that are not well-characterized as nerve injury ligands, including BTC and UCN2 for Schwann cells, and ANGPT1, CCL11, and VEGFC for mesenchymal cells. While the relative contributions of growth factors from these two cell types to nerve growth and repair remain unknown, our study does highlight mesenchymal cells as a previously overlooked reservoir of growth factors for axon growth and potentially for nerve tissue regeneration, an area we are only now starting to understand (for examples, see Parrinello et al., 2010; Cattin et al., 2015). The data presented here thus provide an important step toward defining nerve paracrine interactions not only with regard to axon growth and peripheral nerve regeneration, but also with regard to the paracrine roles of the nerve during repair and regeneration of target tissues.

References

Ansari N, Ho PW, Crimeen-Irwin B, Poulton IJ, Brunt AR, Forwood MR, Divieti Pajevic P, Gooi JH, Martin TJ, Sims NA (2018) Autocrine and paracrine regulation of the murine skeleton by osteocyte-derived parathyroid hormone-related protein. J Bone Miner Res 33:137–153.

Arthur-Farraj PJ, Morgan CC, Adamowicz M, Gomez-Sanchez JA, Fazal SV, Beucher A, Razzaghi B, Mirsky R, Jessen KR, Aitman TJ (2017) Changes in the coding and non-coding transcriptome and DNA methylome that define the Schwann cell repair phenotype after nerve injury. Cell Rep 20:2719–2734.

Benowitz LI, He Z, Goldberg JL (2017) Reaching the brain: advances in optic nerve regeneration. Exp Neurol 287:365–373.

Blanco-Suarez E, Liu TF, Kopelevich A, Allen NJ (2018) Astrocyte-secreted chordin-like 1 drives synapse maturation and limits plasticity by increasing synaptic GluA2 AMPA receptors. Neuron 100:1116–1132.

Brownell I, Guevara E, Bai CB, Loomis CA, Joyner AL (2011) Nerve-derived sonic hedgehog defines a niche for hair follicle stem cells capable of becoming epidermal stem cells. Cell Stem Cell 8:552–565.

Brushart TM, Aspalter M, Griffin JW, Redett R, Hameed H, Zhou C, Wright M, Vyas A, Höke A (2013) Schwann cell phenotype is regulated by axon modality and central-peripheral location, and persists in vitro. Exp Neurol 247:272–281.

Bunge MB (2016) Efficacy of Schwann cell transplantation for spinal cord repair is improved with combinatorial strategies. J Physiol 594:3533–3538.

Butler A, Hoffman P, Smibert P, Papalexi E, Satija R (2018) Integrating single-cell transcriptomic data across different conditions, technologies, and species. Nat Biotechnol 36:411–420.

Büttner R, Schulz A, Reuter M, Akula AK, Mindos T, Carlstedt A, Riecken LB, Baader SL, Bauer R, Morrison H (2018) Inflammaging impairs peripheral nerve maintenance and regeneration. Aging Cell 17:e12833.

Campenot RB, Walji AH, Draker DD (1991) Effects of sphingosine, staurosporine, and phorbol ester on neurites of rat sympathetic neurons growing in compartmented cultures. J Neurosci 11:1126–1139.

Carr MJ, Toma JS, Johnston APW, Steadman PE, Yuzwa SA, Mahmud N, Frankland PW, Kaplan DR, Miller FD (2019) Mesenchymal precursor cells in adult nerves contribute to mammalian tissue repair and regeneration. Cell Stem Cell 24:240–256.

Cattin AL, Burden JJ, Van Emmenis L, Mackenzie FE, Hoving JJ, Garcia Calavia N, Guo Y, McLaughlin M, Rosenberg LH, Quereda V, Jamecna D, Napoli I, Parrinello S, Enver T, Ruhrberg C, Lloyd AC (2015) Macrophage-induced blood vessels guide Schwann cell-mediated regeneration of peripheral nerves. Cell 162:1127–1139.

Cattin AL, Lloyd AC (2016) The multicellular complexity of peripheral nerve regeneration. Curr Opin Neurobiol 39:38–46.

Chen ZL, Yu WM, Strickland S (2007) Peripheral regeneration. Annu Rev Neurosci 30:209–233.

Clements MP, Byrne E, Camarillo Guerrero LF, Cattin AL, Zakka L, Ashraf A, Burden JJ, Khadayate S, Lloyd AC, Marguerat S, Parrinello S (2017) The wound microenvironment reprograms Schwann cells to invasive mesenchymal-like cells to drive peripheral nerve regeneration. Neuron 96:98–114.

David S, Aguayo AJ (1981) Axonal elongation into peripheral nervous system "bridges" after central nervous system injury in adult rats. Science 214:931–933.

Dumont CE, Muff R, Flühmann B, Fischer JA, Born W (2002) Paracrine/autocrine function of adrenomedullin in peripheral nerves of rats. Brain Res 955:64–71.

Elefteriou F, Campbell P, Ma Y (2014) Control of bone remodeling by the peripheral sympathetic nervous system. Calcif Tissue Int 94:140–151.

Feinberg K, Eshed-Eisenbach Y, Frechter S, Amor V, Salomon D, Sabanay H, Dupree JL, Grumet M, Brophy PJ, Shrager P, Peles E (2010) A glial signal consisting of gliomedin and NrCAM clusters axonal Na+ channels during the formation of nodes of Ranvier. Neuron 65:490–502.

Feinberg K, Kolaj A, Wu C, Grinshtein N, Krieger JR, Moran MF, Rubin LL, Miller FD, Kaplan DR (2017) A neuroprotective agent that inactivates prodegenerative TrkA and preserves mitochondria. J Cell Biol 216:3655–3675.

Fledrich R, Kungl T, Nave KA, Stassart RM (2019) Axo-glial interdependence in peripheral nerve development. Development 146: dev151704.

Gardiner NJ (2011) Integrins and the extracellular matrix: key mediators of development and regeneration of the sensory nervous system. Dev Neurobiol 71:1054–1072.

Gerber T, Murawala P, Knapp D, Masselink W, Schuez M, Hermann S, Gac-Santel M, Nowoshilow S, Kageyama J, Khattak S, Currie JD, Camp JG, Tanaka EM, Treutlein B (2018) Single-cell analysis uncovers convergence of cell identities during axolotl limb regeneration. Science 362:eaaq0681.

Gomez-Sanchez JA, Pilch KS, van der Lans M, Fazal SV, Benito C, Wagstaff LJ, Mirsky R, Jessen KR (2017) After nerve injury, lineage tracing shows that myelin and remak Schwann cells elongate extensively and branch to form repair Schwann cells, which shorten radically on remyelination. J Neurosci 37:9086–9099.

Hamilton TG, Klinghoffer RA, Corrin PD, Soriano P (2003) Evolutionary divergence of platelet-derived growth factor alpha receptor signaling mechanisms. Mol Cell Biol 23:4013–4025.

Höke A, Redett R, Hameed H, Jari R, Zhou C, Li ZB, Griffin JW, Brushart TM (2006) Schwann cells express motor and sensory phenotypes that regulate axon regeneration. J Neurosci 26:9646–9655.

Innes BT, Bader GD (2019) scClustViz – Single-cell RNAseq cluster assessment and visualization. F1000Res 7:1522.

Jessen KR, Mirsky R (2019) The success and failure of the Schwann cell response to nerve injury. Front Cell Neurosci 13:33.

Johnston APW, Naska S, Jones K, Jinno H, Kaplan DR, Miller FD (2013) Sox2-mediated regulation of adult neural crest precursors and skin repair. Stem Cell Reports 1:38–45.

Johnston AP, Yuzwa SA, Carr MJ, Mahmud N, Storer MA, Krause MP, Jones K, Paul S, Kaplan DR, Miller FD (2016) Dedifferentiated Schwann cell precursors secreting paracrine factors are required for regeneration of the mammalian digit tip. Cell Stem Cell 19:433–448.

Jose PJ, Griffiths-Johnson DA, Collins PD, Walsh DT, Moqbel R, Totty NF, Truong O, Hsuan JJ, Williams TJ (1994) Eotaxin: a potent eosinophil chemoattractant cytokine detected in a guinea pig model of allergic airways inflammation. J Exp Med 179:881–887.

Joseph NM, Mukouyama YS, Mosher JT, Jaegle M, Crone SA, Dormand EL, Lee KF, Meijer D, Anderson DJ, Morrison SJ (2004) Neural crest stem cells undergo multilineage differentiation in developing peripheral nerves to generate endoneurial fibroblasts in addition to Schwann cells. Development 131:5599–5612.

Kaplan A, Spiller KJ, Towne C, Kanning KC, Choe GT, Geber A, Akay T, Aebischer P, Henderson CE (2014) Neuronal matrix metalloproteinase-9 is a determinant of selective neurodegeneration. Neuron 81:333–348.

Korsunsky I, Millard N, Fan J, Slowikowski K, Zhang F, Wei K, Baglaenko Y, Brenner M, Loh PR, Raychaudhuri S (2019) Fast, sensitive and accurate integration of single-cell data with Harmony. Nat Methods 16:1289–1296.

Kosacka J, Nowicki M, Kacza J, Borlak J, Engele J, Spanel-Borowski K (2006) Adipocyte-derived angiopoietin-1 supports neurite outgrowth and synaptogenesis of sensory neurons. J Neurosci Res 83:1160–1169.

Kumar A, Brockes JP (2012) Nerve dependence in tissue, organ, and appendage regeneration. Trends Neurosci 35:691–699.

Kumar A, Godwin JW, Gates PB, Garza-Garcia AA, Brockes JP (2007) Molecular basis for the nerve dependence of limb regeneration in an adult vertebrate. Science 318:772–777.

Kwon HB, Fukuhara S, Asakawa K, Ando K, Kashiwada T, Kawakami K, Hibi M, Kwon YG, Kim KW, Alitalo K, Mochizuki N (2013) The parallel growth of motoneuron axons with the dorsal aorta depends on Vegfc/Vegfr3 signaling in zebrafish. Development 140:4081–4090.

Leibrock J, Lottspeich F, Hohn A, Hofer M, Hengerer B, Masiakowski P, Thoenen H, Barde YA (1989) Molecular cloning and expression of brain-derived neurotrophic factor. Nature 341:149–152.

Lindsay RM (1988) Nerve growth factors (NGF, BDNF) enhance axonal regeneration but are not required for survival of adult sensory neurons. J Neurosci 8:2394–2405.

Liu X, Zhao Y, Peng S, Zhang S, Wang M, Chen Y, Zhang S, Yang Y, Sun C (2016) BMP7 retards peripheral myelination by activating p38 MAPK in Schwann cells. Sci Rep 6:31049.

Lun AT, McCarthy DJ, Marioni JC (2016) A step-by-step workflow for low-level analysis of single-cell RNA-seq data with Bioconductor. F1000Res 5:2122.

Macosko EZ, Basu A, Satija R, Nemesh J, Shekhar K, Goldman M, Tirosh I, Bialas AR, Kamitaki N, Martersteck EM, Trombetta JJ, Weitz DA, Sanes JR, Shalek AK, Regev A, McCarroll SA (2015) Highly parallel genome-wide expression profiling of individual cells using nanoliter droplets. Cell 161:1202–1214.

Mahmoud AI, O'Meara CC, Gemberling M, Zhao L, Bryant DM, Zheng R, Gannon JB, Cai L, Choi W-Y, Egnaczyk GF, Burns CE, Burns CG, MacRae CA, Poss KD, Lee RT (2015) Nerves regulate cardiomyocyte proliferation and heart regeneration. Dev Cell 34:387–399.

McDonald CA, Yang JY, Marathe V, Yen TY, Macher BA (2009) Combining results from lectin affinity chromatography and glycocapture approaches substantially improves the coverage of the glycoproteome. Mol Cell Proteomics 8:287–301.

Micallef L, Rodgers P (2014) eulerAPE: drawing area-proportional 3-Venn diagrams using ellipses. PLoS One 9:e101717.

Muir D (2010) The potentiation of peripheral nerve sheaths in regeneration and repair. Exp Neurol 223:102–111.

Naveilhan P, ElShamy WM, Ernfors P (1997) Differential regulation of mRNAs for GDNF and its receptors Ret and GDNFR alpha after sciatic nerve lesion in the mouse. Eur J Neurosci 9:1450–1460.

Park KJ, Grosso CA, Aubert I, Kaplan DR, Miller FD (2010) p75NTR-dependent, myelin-mediated axonal degeneration regulates neural connectivity in the adult brain. Nat Neurosci 13:559-566.

Parrinello S, Napoli I, Ribeiro S, Wingfield Digby P, Fedorova M, Parkinson DB, Doddrell RD, Nakayama M, Adams RH, Lloyd AC (2010) EphB signaling directs peripheral nerve regeneration through Sox2-dependent Schwann cell sorting. Cell 143:145–155.

Politis MJ, Spencer PS (1986) Regeneration of rat optic axons into peripheral nerve grafts. Exp Neurol 91:52–59.

Schiess R, Mueller LN, Schmidt A, Mueller M, Wollscheid B, Aebersold R (2009) Analysis of cell surface proteome changes via label-free, quantitative mass spectrometry. Mol Cell Proteomics 8:624–638.

Storer MA, Mahmud N, Karamboulas K, Borrett MJ, Yuzwa SA, Gont A, Androschuk A, Sefton MV, Kaplan DR, Miller FD (2020) Acquisition of a unique mesenchymal precursor-like blastema state underlies successful adult mammalian digit tip regeneration. Dev Cell 52:509–524.

Stratton JA, Holmes A, Rosin NL, Sinha S, Vohra M, Burma NE, Trang T, Midha R, Biernaskie J (2018) Macrophages regulate Schwann cell maturation after nerve injury. Cell Rep 24:2561–2572.

Terenghi G (1999) Peripheral nerve regeneration and neurotrophic factors. J Anat 194:1–14.

Trupp M, Rydén M, Jörnvall H, Funakoshi H, Timmusk T, Arenas E, Ibáñez CF (1995) Peripheral expression and biological activities of GDNF, a new neurotrophic factor for avian and mammalian peripheral neurons. J Cell Biol 130:137–148.

Voronova A, Yuzwa SA, Wang BS, Zahr S, Syal C, Wang J, Kaplan DR, Miller FD (2017) Migrating interneurons secrete fractalkine to promote oligodendrocyte formation in the developing mammalian brain. Neuron 94:500–516.

Yamazaki S, Ema H, Karlsson G, Yamaguchi T, Miyoshi H, Shioda S, Taketo MM, Karlsson S, Iwama A, Nakauchi H (2011) Nonmyelinating Schwann cells maintain hematopoietic stem cell hibernation in the bone marrow niche. Cell 147:1146–1158.

Yu L, Han M, Yan M, Lee EC, Lee J, Muneoka K (2010) BMP signaling induces digit regeneration in neonatal mice. Development 137:551–559.

Yuzwa SA, Yang G, Borrett MJ, Clarke G, Cancino GI, Zahr SK, Zandstra PW, Kaplan DR, Miller FD (2016) Proneurogenic ligands defined by modeling developing cortex growth factor communication networks. Neuron 91:988–1004.

Yuzwa SA, Borrett MJ, Innes BT, Voronova A, Ketela T, Kaplan DR, Bader GD, Miller FD (2017) Developmental emergence of adult neural stem cells as revealed by single-cell transcriptional profiling. Cell Rep 21:3970–3986.